Limit

6906-01012

FINAL REPORT

STUDY AND DESIGN OF

LASER COMMUNICATIONS SYSTEM FOR SPACE SHUTTLE

ITT Gilfillan
7821 Orion Avenue
Van Nuys, California 91409

6906-01012

FINAL REPORT

STUDY AND DESIGN OF LASER COMMUNICATIONS SYSTEM FOR SPACE SHUTTLE

Contract NAS8-26245
Line Item 2

Submitted to

George C. Marshall Space Flight Center
National Aeronautics and Space Agency
Marshall Space Flight Center
Huntsville, Alabama 35812

21 September 1973

ITT GILFILLAN
7821 Orion Avenue
Van Nuys, California 91409

TABLE OF CONTENTS

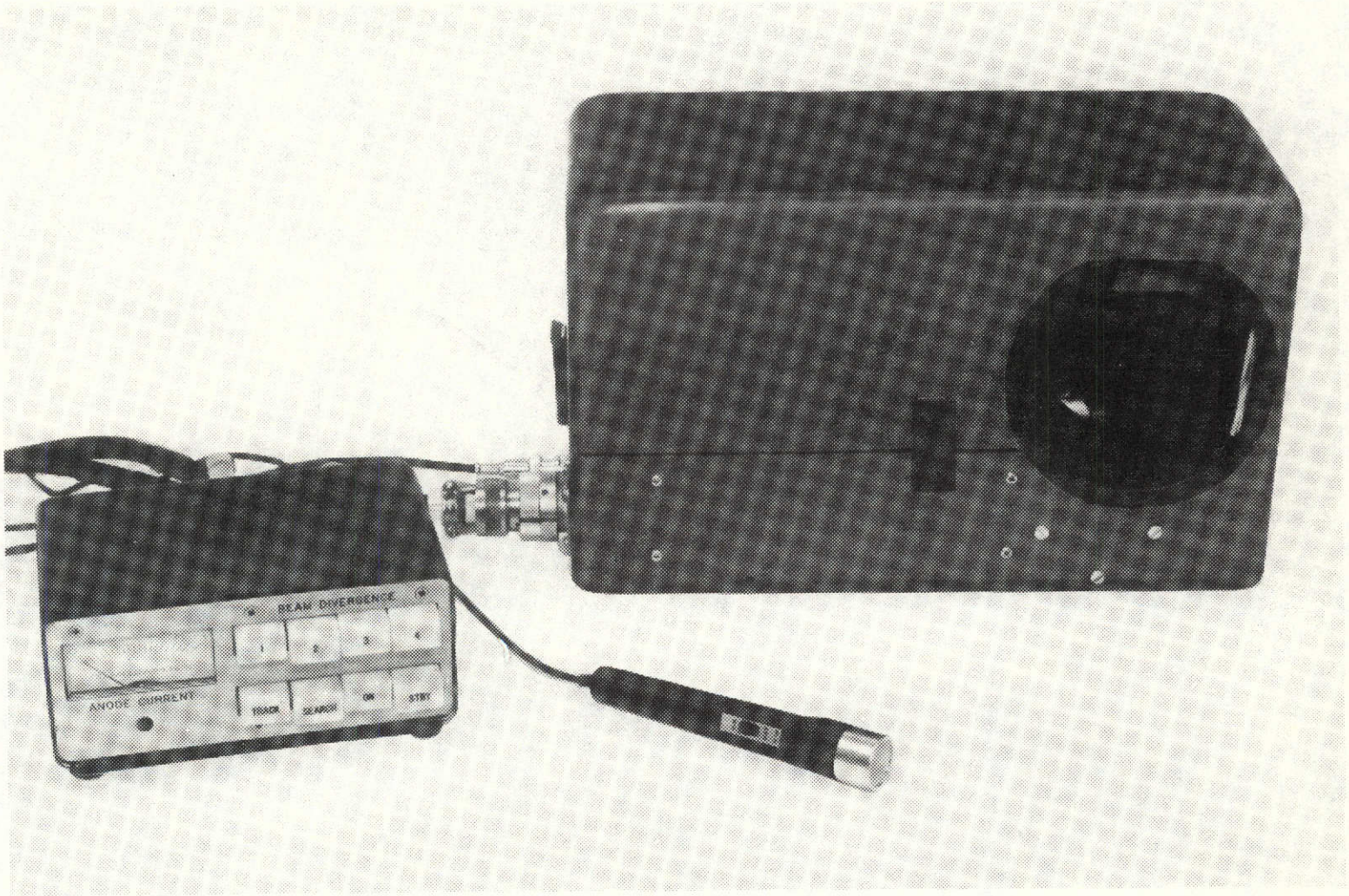

Laser Communications Transceiver

1. INTRODUCTION

This document constitutes the final report on contract NAS 8-26245. The purpose of this report is to describe the design, development and operation of the Laser Communications System developed for potential Space Shuttle application. A brief study was conducted early in this contract to identify the need, if any, for narrow bandwidth space-to-space communication on the shuttle vehicles. None have been specifically identified that could not be accommodated with existing equipments. However, future needs for orbiting and docking spacecraft would benefit from this development of compact laser transceiver having an automatic acquisition, tracking and pointing capability.

The key technical features developed in this hardware are the conically scanned tracker for optimized track while communicating with a single detector, and the utilization of a common optical carrier frequency for both transmission and detection. This latter feature permits a multiple access capability so that several transceivers can communicate with one another.

The conically scanned tracker technique allows the received signal energy to be efficiently divided between the tracking and communications functions within a common detector. Previous tracking techniques used a scan type which either interrupted the received signal to optimize tracking or compromised both tracking and communications by effecting a partial track scan.

Another goal of this development was to utilize available state-of-the-art components assembled as compactly as feasible within the constraints of program schedule and funding.

ITTG wishes to acknowledge the extreme cooperativeness of NASA for allowing a demonstration of this system prior to its delivery to other government agencies who are potential users.

2. BACKGROUND

This program has gone through several phases of redirection and delay during its long history. The initial program (awarded June 1970) concerned the development of a high data rate, 1.06 micron, communications link in a laboratory breadboard configuration. The primary task was to evaluate certain critical systems components. In late December of 1970 a recommendation was made by NASA/Hdqtrs for consideration of redirection of this contract to produce hardware more suitable to a near term space shuttle application.

A meeting in January of 1971 between ITT and NASA/MSFC technical personnel established new program guidelines, still within the general framework of the initial statement of work. The tasks resulting included a survey of Space Shuttle communications needs with the objective of configuring system concepts for meeting selected applications. Following a period of 60-day plant shut down resulting from an earthquake in February 1971, several system concepts were formulated and submitted to NASA/MSFC for approval. A system design approach was approved in October 1971 and a detailed hardware design phase was initiated. The formal modification to the contract SOW was signed on 26 May 1972. Further no-cost extension in the period of performance were granted to incorporate improvements and to allow for demonstration of the completed hardware to other government agencies. Although this program has gone through these modification and schedule stretches (from 12 months to 36 months) it is noteworthy that the original contract dollar was not exceeded.

3. SURVEY OF REQUIREMENTS

A survey of the Space Shuttle communications requirements was conducted for the purpose of identifying those needs that might benefit from laser techniques. The two prime contractors for the shuttle were contacted in January of 1971 and working interfaces were established. The shuttle mission's communications needs were not fully identified at this time nor were they expected to be determined sufficiently to be of value in configuring communications hardware on this contract. At NASA's request, communications links other than those of the normal mission were considered for laser communications such as Booster and Orbiter vehicles to ATS-G satellite and Data Relay Satellite.

During this survey period, numerous system configurations were proposed and analyzed with the initial goal of utilizing as much advanced technology as possible. This philosophy was later modified or discussed in Section 2 to one of using primarily immediately available, proven technology. In order to facilitate rapid system parametric analysis for the many system options, and to permit parametric performance trade-offs during design reviews, a set of design nomographs were prepared. These nomographs have proven to be very helpful in making first order system design trades to an accuracy of better than 10 percent. The error rate predictions are based on Poisson statistics with optimum decision thresholding. A complete set of design nomographs is included with this report as Appendix A.

Table 1 summarizes the various communications modes identified or postulated for this mission.

TABLE 1. OPTCOM APPLICATION FOR THE SPACE SHUTTLE

Communi-cations Mode	Range Extremes Statute Miles	Pointing Uncertainty (Degrees)	Field Angle Field	Angle Track Rate (Degrees/Sec)	Point Ahead (sec)	Receiver Bandwidth	Receiver Wavelengths (Probable)	Comments
Booster/Gnd. Station	0 - 150 - 0	$.5^{\circ}/.1^{\circ}$	$<2\pi$ (Hemis-pher.)	$>5^{\circ}$/sec	N.R.	20 KC/10^6	Open	OPTCOMM Not competitive with Microwave
Orbiter/ Ground	0 - 600 - 0	$.2^{\circ}/.1^{\circ}$	$<2\pi$ (Hemis-pher.)	$>5^{\circ}$/sec	N.R.	20 KC/10^6	Open	OPTCOMM Not competitive with Microwave
Booster/ Orbiter	0 - 1500	---	$90^{\circ} \times 60^{\circ}$	$>5^{\circ}$/sec	N.R.	20 KC/20 KC	Open	OPTCOMM Size/Power advantage Long Range Acq. Problem
Booster/ ATS-G	23,000	$.3^{\circ}/.1^{\circ}$	$120^{\circ} \times 60^{\circ}$	$>.3^{\circ}$/sec	<15	Unspecified	HeNe/YAG^2	Range and Point Ahead Requirements necessitate a sophisticated system
Orbiter/ ATS-G	23,000	$.2^{\circ}/.1^{\circ}$	$150^{\circ} \times 90^{\circ}$	$>.3^{\circ}$/sec	<15	20 KC/10^6	HeNe/YAG^2	
Booster/Data Relay Satellite	22,300	$.3^{\circ}/.1^{\circ}$	$120^{\circ} \times 60^{\circ}$	$>.3^{\circ}$/sec	<15	Unspecified	YAG^2/YAG	
Orbiter/Data Relay Satellite	22,300	$.2^{\circ}/.1^{\circ}$	$150^{\circ} \times 150^{\circ}$	$>.3^{\circ}$/sec	<15	20 KC/10^6	YAG^2/YAG	
Orbiter/Space Station	3000 - 0	$.1^{\circ}/.1^{\circ}$	$90^{\circ} \times 90^{\circ}$	$>1^{\circ}$/sec	N.R.	20 KC/20 KC	Open	OPTCOMM Size/ Power advantage Long range Acq. problem.

Ground rules for selection of a communication link to be implemented under this contract included:

- Laser techniques offer clear advantage in size, weight and power
- Laser system could be reduced to hardware within the cost limitations of this contract.

It was determined that for normal communication with the ground, the conventional microwave systems were superior and that the longer range communications required design sophistication or devices that outride the scope of the contract. This process of elimination left the intermediate range relatively low-data-rate links as possibilities. For these needs, the laser system indeed does offer significant advantage in terms of system size, weight and power.

A set of hardware specifications were derived to satisfy the conditions for communicating between Booster and Orbiter and Orbiter and Space Station. A detailed description of this system is presented in Section 4.0 of this report.

4. TECHNICAL DISCUSSION

4.1 System Description

Laser communication systems need a tracking and pointing capability as well as a communication modulation and demodulation scheme because of the narrow beamwidths involved. The primary necessity of an effective laser communication system is an ability to track the position of its communicating mate and to point its outgoing beam toward that other unit. The tracker should have a narrow field-of-view to limit the effect of background illumination. Also, the tracking and the pointing loop should have an accuracy which is a fraction of the outgoing beam diameter.

A block diagram of a communicator is shown in Figure 1. The system will be described in the sequence of optical energy entering the system and propagating to the tracker through the beamsteering and optical system. This will be followed by a discussion of the communication impressed upon that beam.

Light entering the transceiver is deflected by the steering mirror, filtered and focused by a lens onto the photocathode of the image dissector. The purpose of the mirror is to move the field-of-view of the image dissector sensor when the system is searching for the beacon transceiver unit. Upon acquisition, this mirror will move to point the outgoing beam toward the other system. The beamsteer is a two axis gimbaled mirror controlled by either a programmed search scan or, in the track mode, by the tracker outputs. The optical filter passes only a narrow band (20A) around the 0.63 micron Helium-Neon Laser to reduce the background radiation level to the tracker. The lense images the field-of-view onto the photocathode of the image dissector so that the field can be sampled sequentially in a raster type scan for acquisition.

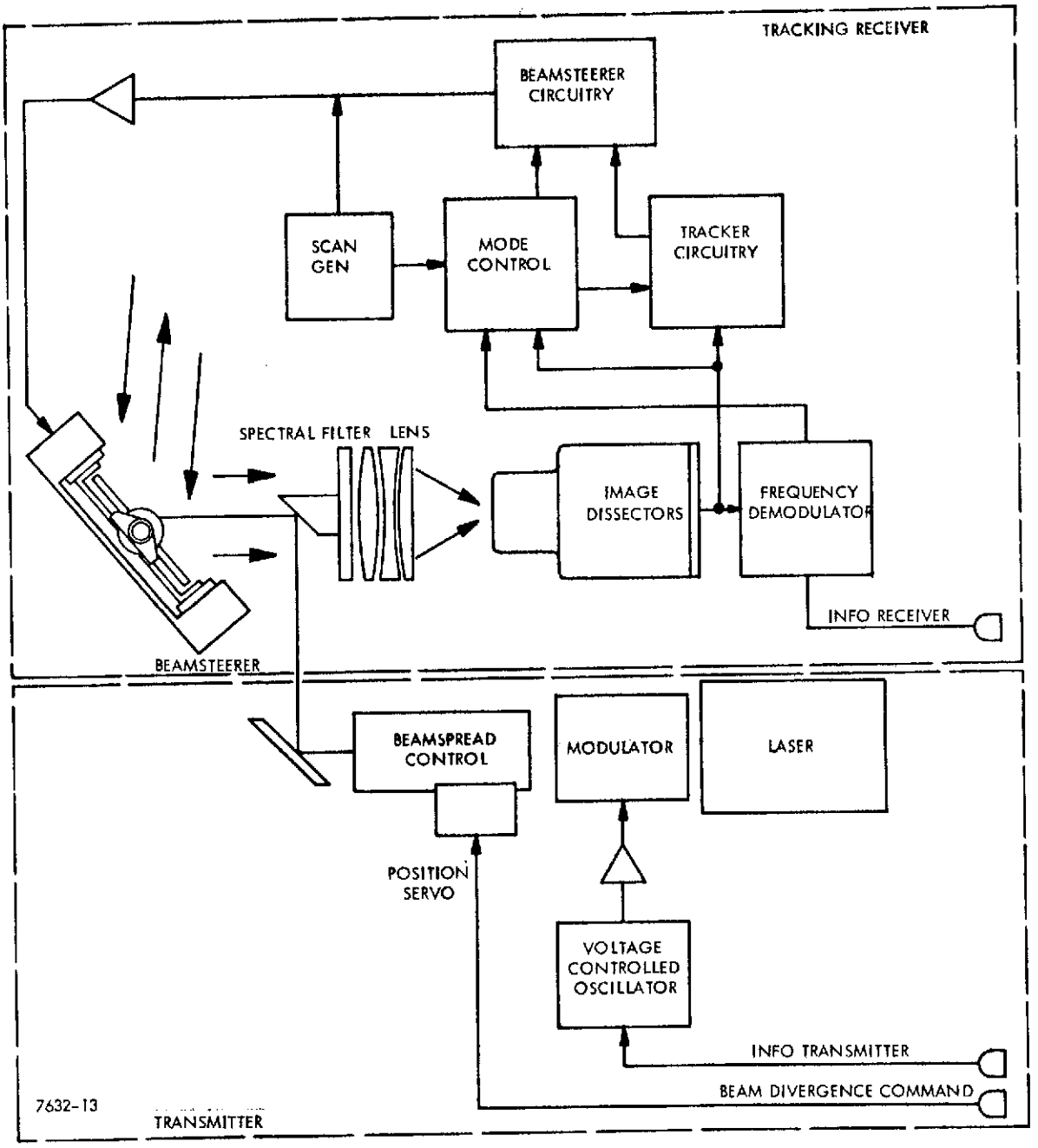

Figure 1. Communicator Block Diagram

The operation of the image dissector (ID) will be discussed later. At this point, it is sufficient to say that the ID sensor provides a high degree of spatial filtering of the acquisition scene. This sampling area (instantaneous field-of-view) can be moved (electronically) over the entire field-of-view and can be made to move in a pattern around the beacon image to enable tracking that image. A second part of this sensor is an electron multiplier section which provides a low noise high gain to the signal.

The output of this sensor is divided between the tracking and communications functions. The high frequency components of the signal are supplied to the communication receiver to be processed and detected. The lower frequencies containing the track scan and average power components are processed in the tracker circuitry. The mode control contains the logic that decides if the signal detected is the proper transceiver beacon or if it is simply an object in the background. If an object appears to be the proper transceiver, the mode control will enable the tracker to begin tracking that image. If the image continues to appear to be the appropriate beacon, it will enable the beamsteering system to operate and point the outgoing laser toward that transceiver. Assuming that a similar sequence is occurring in that other transceiver, when the beam of the second transceiver impinges on the first, the sequence will lead to both systems tracking and pointing to each other.

4.2 Communications

The next major task in developing a tracking communicator is to impress the information onto the laser output. The communication subsystem is shown in Figure 2. In the transmitter, the output of the Helium-Neon gas laser is amplitude modulated by the optical modulator at a frequency F3. (Note that each unit transmits on a frequency different

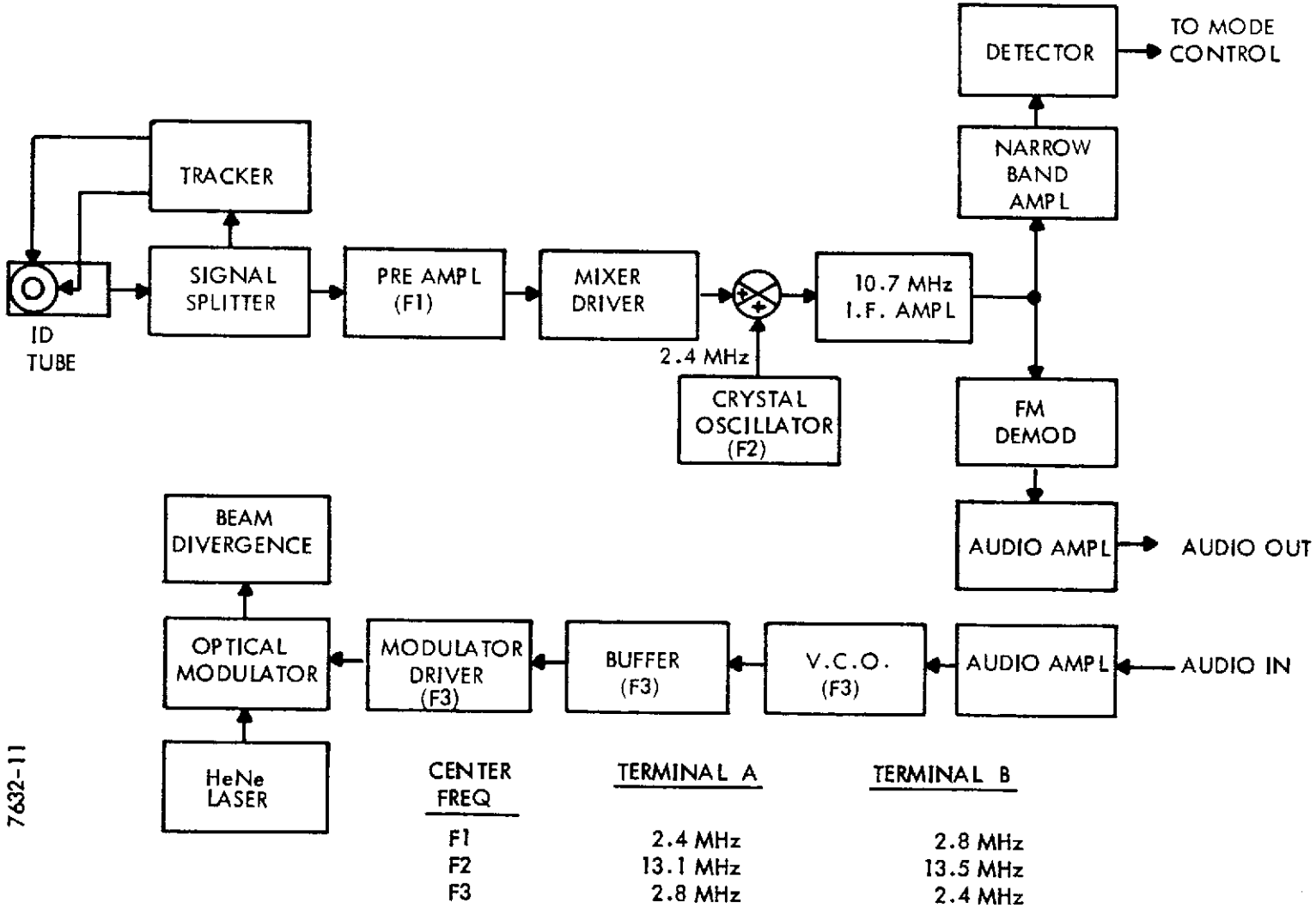

Figure 2. Shuttle Communications Link

from that received. This allows improved isolation between the high voltages necessary for modulation and the high impedance receiver within the same unit.) The frequency of the modulation is changed by the vocal communication by the voltage controlled oscillator (VCO). This is a standard frequency modulation technique. To summarize, the laser output is intensity modulated by a subcarrier which is frequency modulated.

At the receiver end, the subcarrier frequency intensity modulation is detected by the tracker. In the receiver circuitry, the signal is amplified and mixed to produce a convenient new 10.7 MHz IF frequency. The signal can now continue to be processed using well developed, off-the-shelf FM receiver components. The signal is amplified and then limited to minimize the effect of amplitude noise. The signal at this point is divided into two channels. In one, the FM signal is demodulated using standard FM techniques; and the vocal communication is amplified to drive a speaker. In the other channel, the 10.7 MHz is amplified and filtered and detected. The purpose of this latter channel is to simply detect the presence of subcarrier modulation. This information is sent to the mode control circuitry which uses it to decide whether the detected signal, that is the proper transceiver or simply a bright object in the field-of-view. (i.e., a simple bright object will not have modulation on it.)

4.3 Physical Layout

The major elements of the block diagrams are shown in Figure 3. This is a see-through drawing of the physical layout. In Figures 4 through 8, the blocks are shown on actual photographs of the equipment.

4.4 System Theory

The system theory of operation will be described in four sections: first, the radiometry; second, the acquisition sequence; third, the image

FOLDOUT FRAME

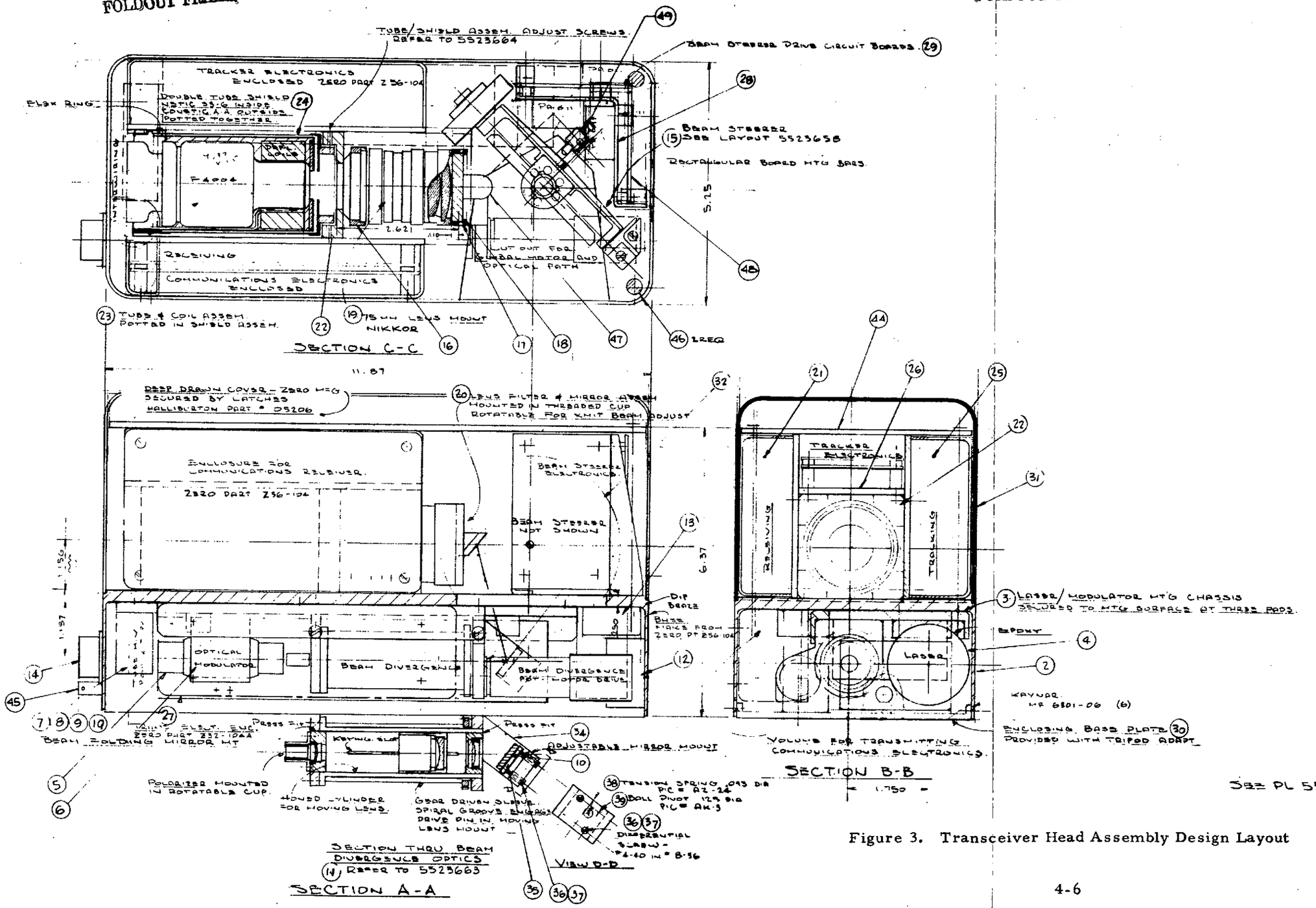

Figure 3. Transceiver Head Assembly Design Layout

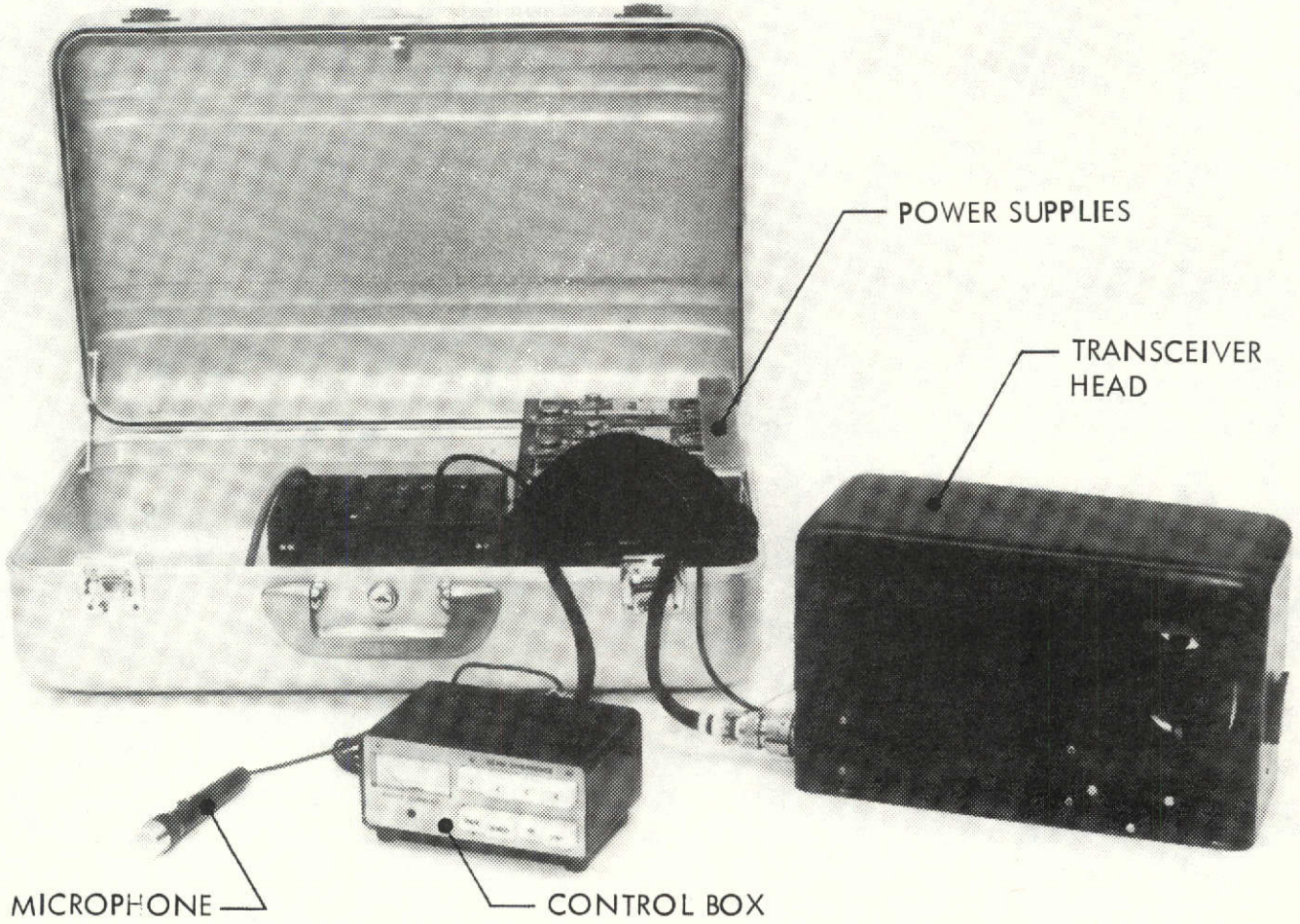

Figure 4. Shuttle Transceiver

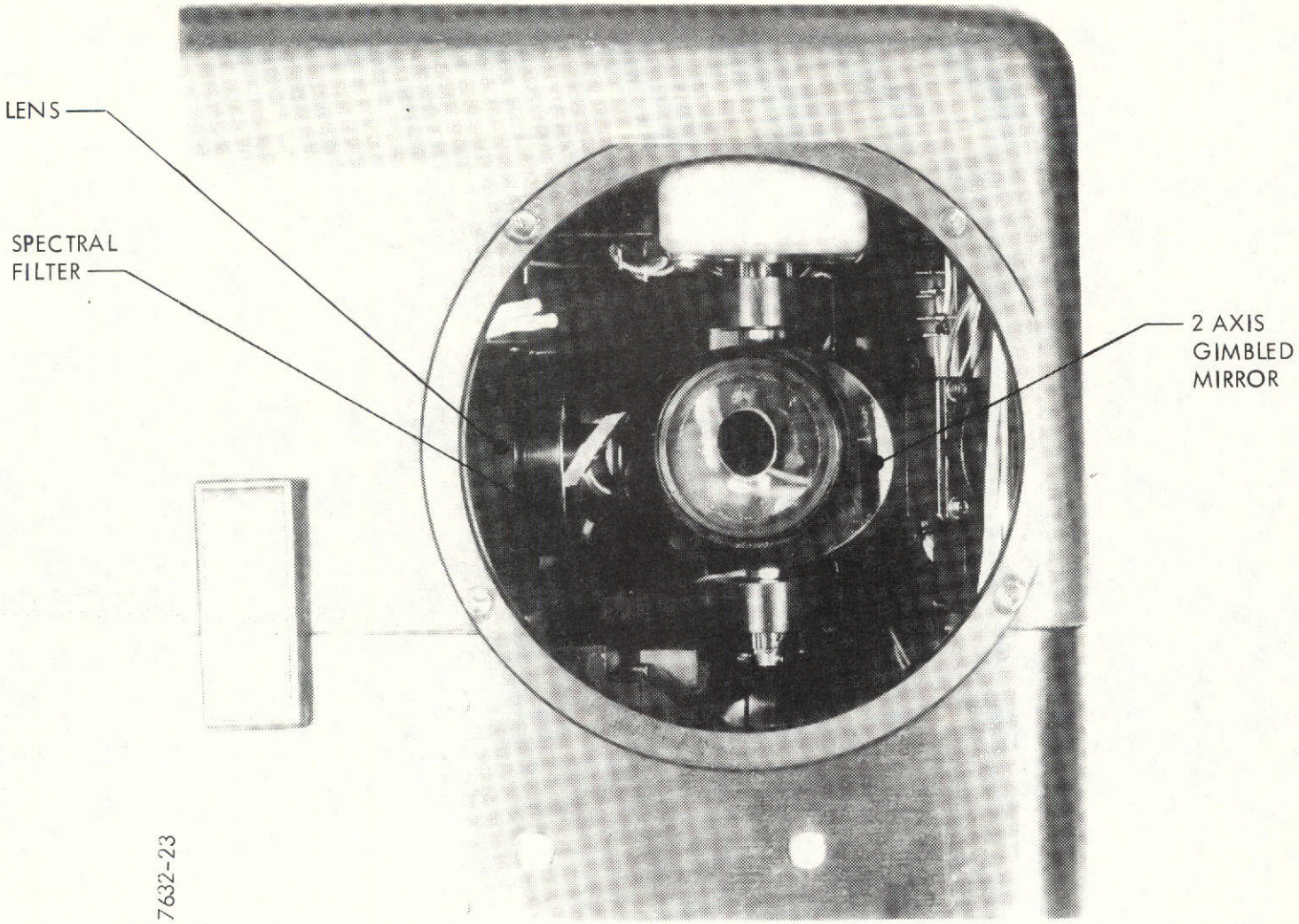

Figure 5. Optical Components of Communicator Head

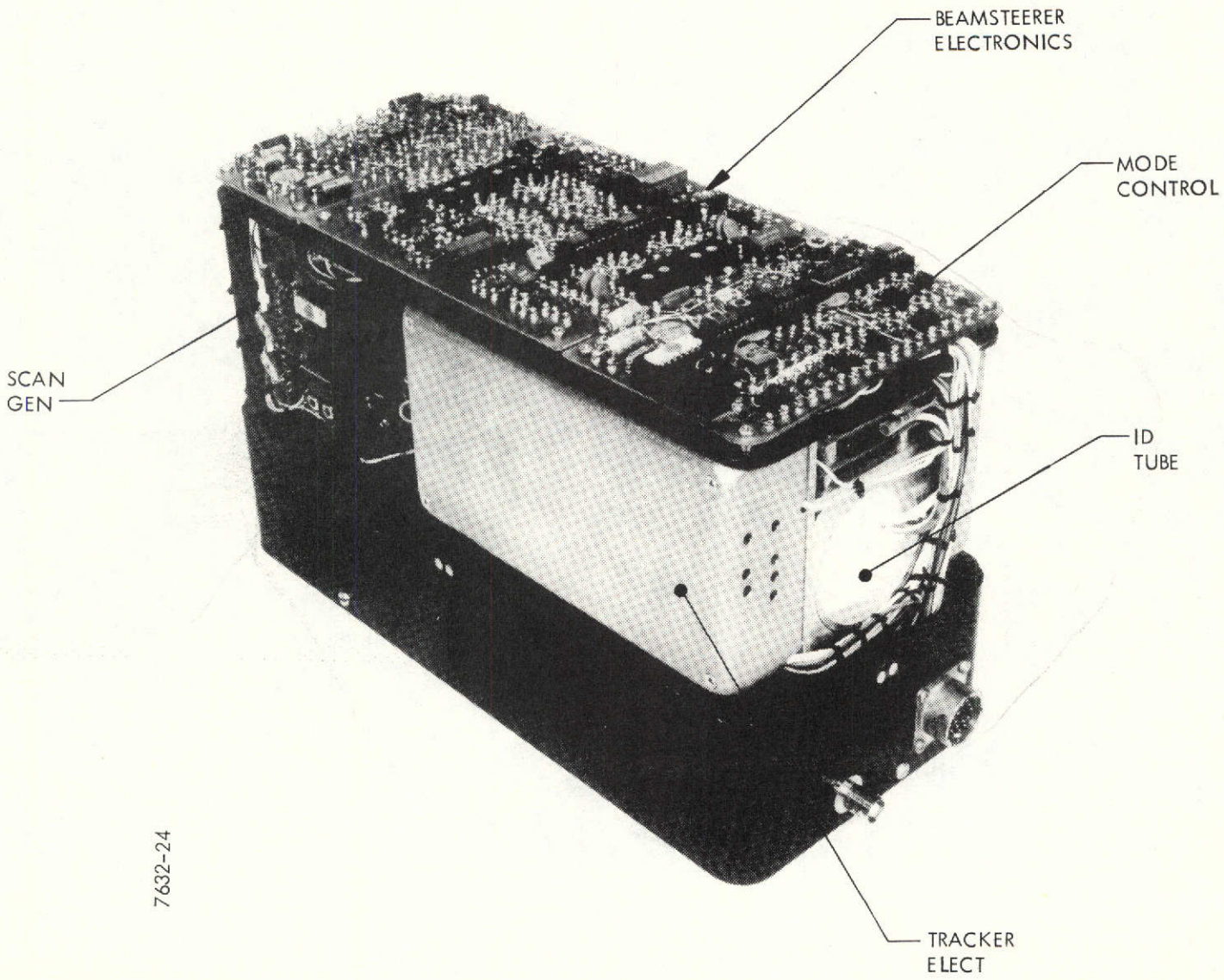

Figure 6. Transceiver Head, Rear View

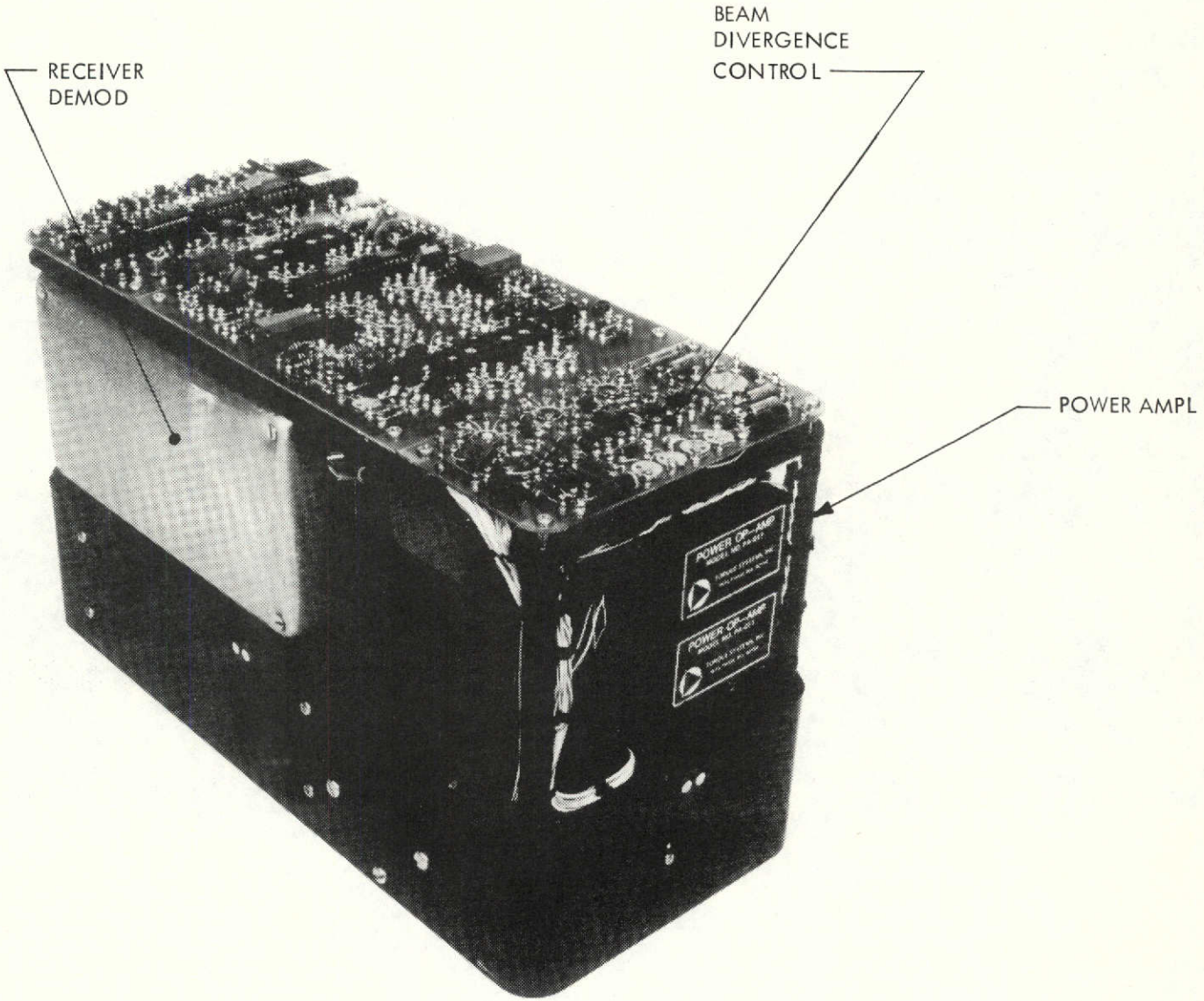

7632-25

Figure 7. Transceiver Head, Front View

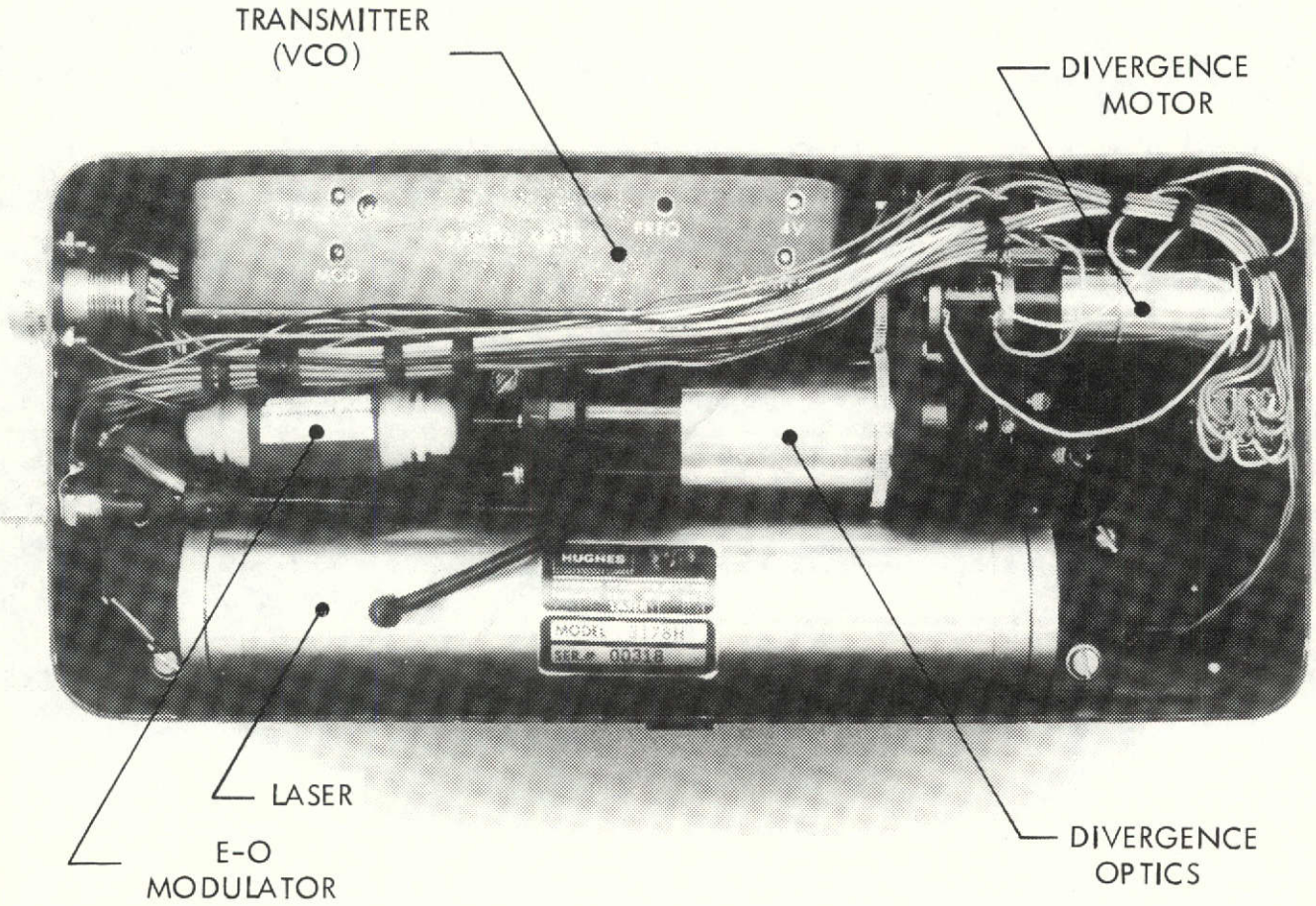

Figure 8. Transceiver Head, Bottom View

dissector and tracker; and fourth, the pointing mirror servo loop. These sections will discuss the principles of operation and also the mathematical relationships of its parameters.

The major estimates obtained through radiometric analysis are the power level received from the laser in the other communicator and the power level due to background illumination. The power at the receiver due to the other communicator is given by:

$$P_d = \frac{P_t L_t L_r A_r \quad (4)}{\pi \theta^2 R^2}$$

where

P_d - power at receiver detector

P_t - power of transmitter laser (watts)

L_t - losses in the transmitter

L_r - losses in the receiver optical path

A_r - area of receiving aperture (input lens)

θ - transmitter beam divergence (full angle)

R - range of receiver from transmitter meters

Substituting the appropriate values for these factors

$P_t = .001$

$L_t = .05$

$L_r = .25$

$A_r = 11.6 \text{ cm}^2$

$$P_d = \frac{1.85 \times 10^{-8}}{\theta^2 R^2} \text{ watts}$$

This relationship clearly shows the trade-off between beam divergence and range. Before we can solve for range, if given a specification for beam divergence, we must decide what is a reasonable minimum value for power at the receiving detector. A preliminary criteria is that this power at the detector should not be less than the power due to background illumination. A worse case background considered here is that which is due to a white cloud. Each square cm of cloud surface emits 0.014 watts into a steradian in a spectral band of 1 micron centered around 0.63 micron region.

The total power is obtained, therefore, by calculating the cloud area, the solid angle, and the optical bandwidth. The area of the cloud viewed is limited by the aperture within the image dissector. This will be discussed in more detail in following section. The size of this aperture is 2.5×10^{-3} radians in radius. The cloud area is, therefore

$$\pi (2.5 \times 10^{-3})^2 R^2 = \text{area of cloud}$$

The steradian size of the lens is its area divided by the range (R).

$$\text{solid angle} = \frac{11.6 \text{ cm}^2}{R^2}$$

The spectral bandwidth used in this system is 20 Å, which is 2×10^{-3} microns, with a center value of 0.6328 microns. The losses within the receiver optics, as before, are 0.25. Putting this all together, power at the detector due to background, (BkGd) P_d:

$$(\text{BkGd})\ P_d = (\text{Area of Cloud})\ (\text{Solid Angle})\ (\text{Losses})\ (\text{Bandwidth})$$

$$(0.014\ \text{W/cm}^2 \cdot \text{sr} \cdot \mu) = (3.14)\ (2.5 \times 10^{-3})^2$$

$$R^2 \frac{(11.6)}{R^2}\ (0.25)\ (2 \times 10^{-3})\ (0.014)$$

$$(\text{BkGd})\ P_d = 1.6 \times 10^{-9}\ \text{watts.}$$

We now have a level above which the power due to another communicator should be maintained. Using this criteria, therefore, a 1 milliradian beam can be used to communicate.

$$1.6 \times 10^{-9} = \frac{1.85 \times 10^{-8}}{\theta^2 R^2}$$

$$R = 3.4 \times 10^3\ \text{meters}$$

It should be noted that the criteria used here is only a "ballpark" criteria. Much improvement, for example, can be obtained by allowing only modulated targets to be tracked, thus distinguishing between other communicators and background. In many space applications, it may not be necessary to acquire and track against sunlit cloud background at great ranges. For any application, therefore, the limits of operation must be arrived by considering the particular characteristics of that environment. Figure 9 shows the envelope of system operation. The plot shows range of operation vs beam divergence, at various levels of power receiver in the detector. The minimum level of 1×10^{-11} watts is not a theoretical lower limit, but is a reasonable one for this equipment.

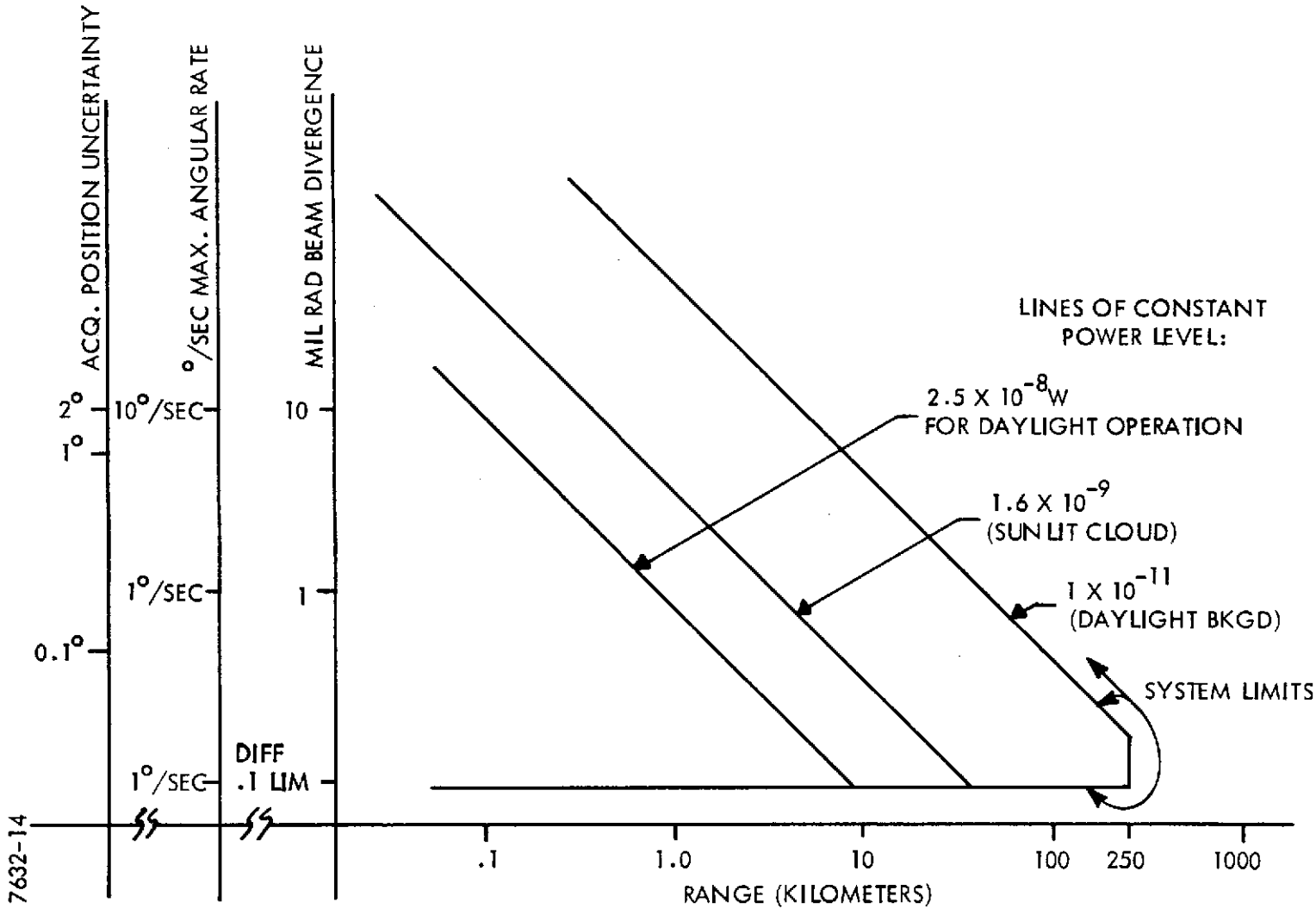

Figure 9. Beam Divergence vs Range Envelope for Various Choices of AGC Threshold

4.4.1 Acquisition Sequence. - Each communicator searches over a $2^{o} \times 2^{o}$ field-of-view with a transmitted beam that fills a $1/4^{o}$ wide cone (figure 10). This is done by the image dissector scanning the photocathode onto which the field-of-view has been imaged. Each $2^{o} \times 2^{o}$ field is scanned for 50 milliseconds, by each receiver. After 0.1 second (or two scans), the outgoing beam and also the field-of-view is moved $1/4^{o}$. This movement continues in a raster pattern with 8 steps horizontally and 8 lines vertically to form overlapping $2^{o} \times 2^{o}$ scans. The same action, continuing for 6.4 seconds, causes the outgoing beam to completely "paint" a two-degree field in space.

If the outgoing beam of system (System A) illuminates another system (System B) and if the B is looking in the correct direction, then within 50 milliseconds (at the maximum) System B will acquire and begin to track the image of System A (1, figure 11). Once the track is secure, the beamsteerers of System B automatically turn on and cause its outgoing beam to move and begin pointing accurately at System A (2, figure 11). This will take a maximum of 35 milliseconds. Now that System A is being illuminated by System B, it will acquire and begin to track System B. Its beamsteerers will be likewise turned on and will cause its outgoing beam to remain accurately pointed at System B. Thus, the two systems are tracking and pointing at each other. The total acquisition sequence will require an average of 85 milliseconds.

4.4.2 Tracker Principles and Theory. - The principles used in the tracking part of the system are similar to those used in conical scan radar trackers. The tracker must have a narrow beam in which sensitivity is greatest at the center, decreasing at the sides of the beam. This beam is then scanned around the target in a conical pattern (figure 12). The apparent intensity of the target, as the beam scans around it, is the

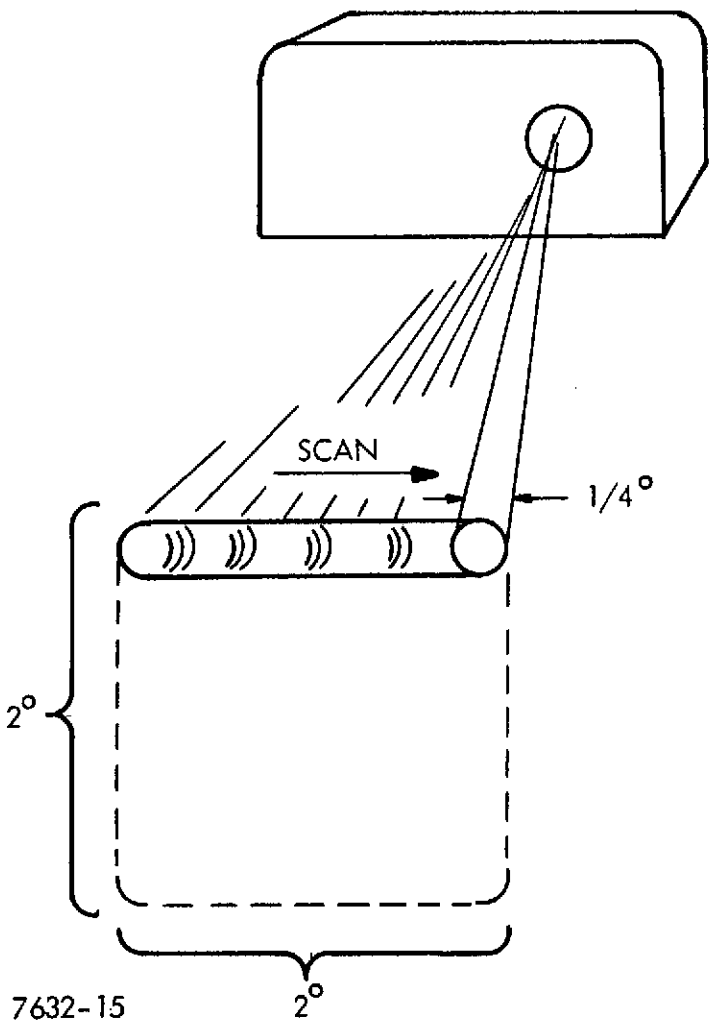

Figure 10. Acquisition Scan Pattern

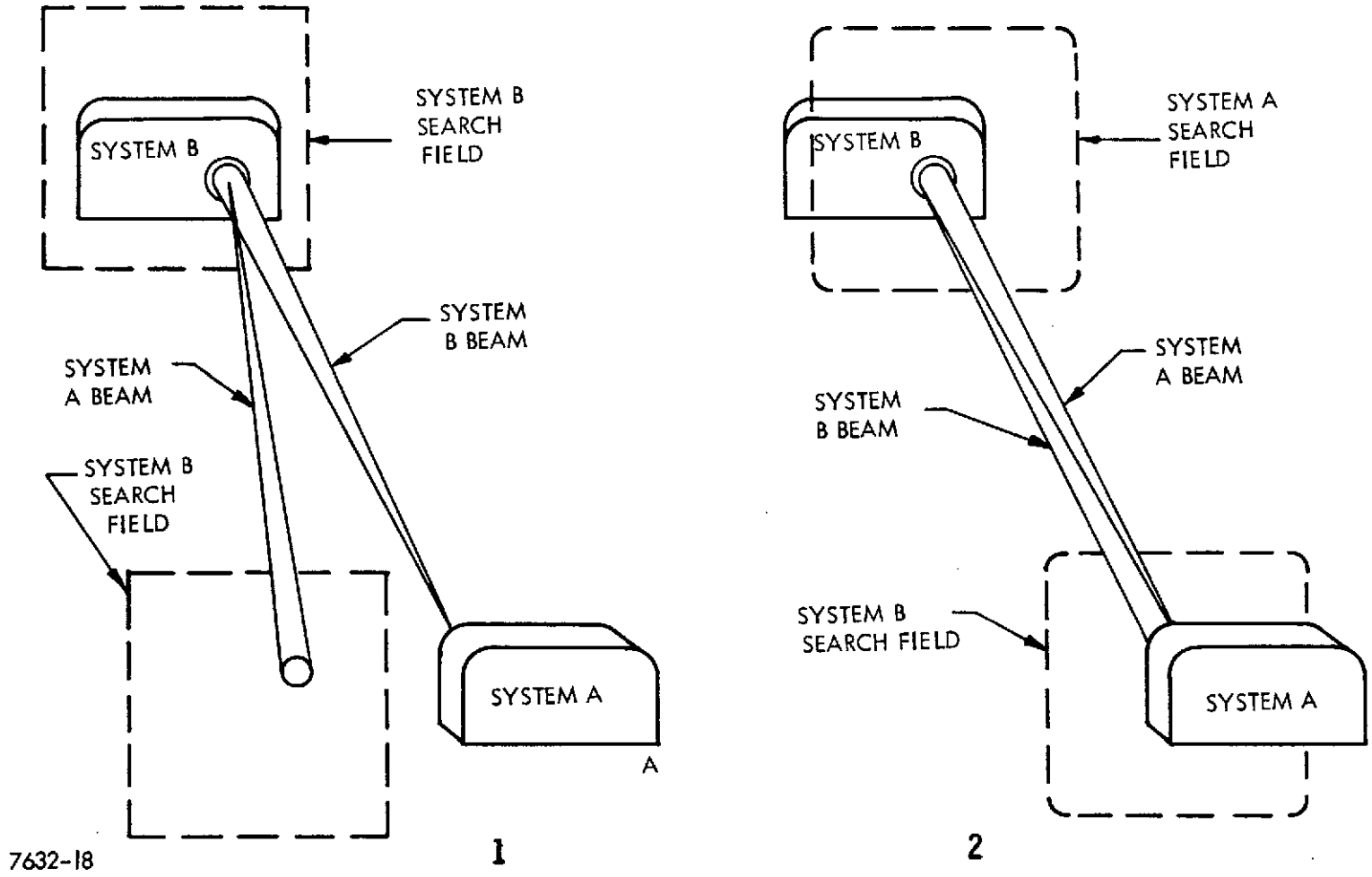

Figure 11. System Acquisition Sequence

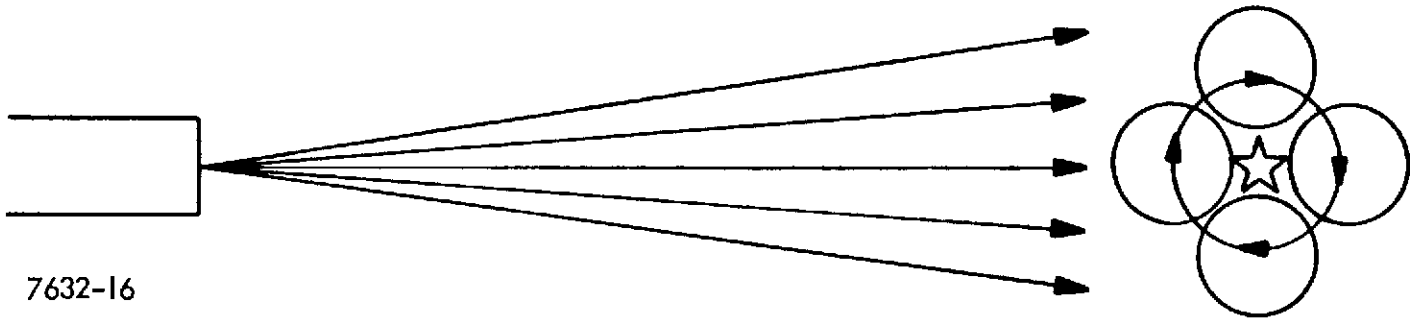

Figure 12. Conical Scanning

information that is processed to allow tracking. For example, referring to Figure 13, if the target is to the right of the center of the scan, then the intensity observed will have a maximum at point 2 during the scan and a minimum at point 4.

If there is no horizontal error, the intensity of the return will be constant. A horizontal error to the left (c, figure 13) will produce an intensity pattern opposite to the right. A similar process causes characteristic patterns for vertical errors. These intensity patterns are processed in phase sensitive detectors, and the resulting information is used to move the scan pattern such that it centers itself around the target.

To summarize, the basic elements of a sensor suitable for use in tracking system are a shaped sensitivity pattern and a method for moving that pattern. The remainder of the tracking system are error detectors and servo loop amplifiers and processors.

The image dissector is a sensor that fits the requirements of a tracking sensor. Figure 14 shows the basic parts of the optical and electron focusing components. Light passing through the lens is focused onto the photocathode where it produces a flow of electrons. The electrons accelerate in an electrostatic field and also are focused by means of an electrostatic focusing structure. These focused electrons fall on a metal plate in which there is only one small opening, or aperture, through which they can pass. Only electrons from one small area on the photocathode will enter this aperture and be amplified in the electron multiplier amplifier. Thus, light from only one small cone in space can cause electrons that will pass through the aperture and will be amplified and can be detected at the tube output.

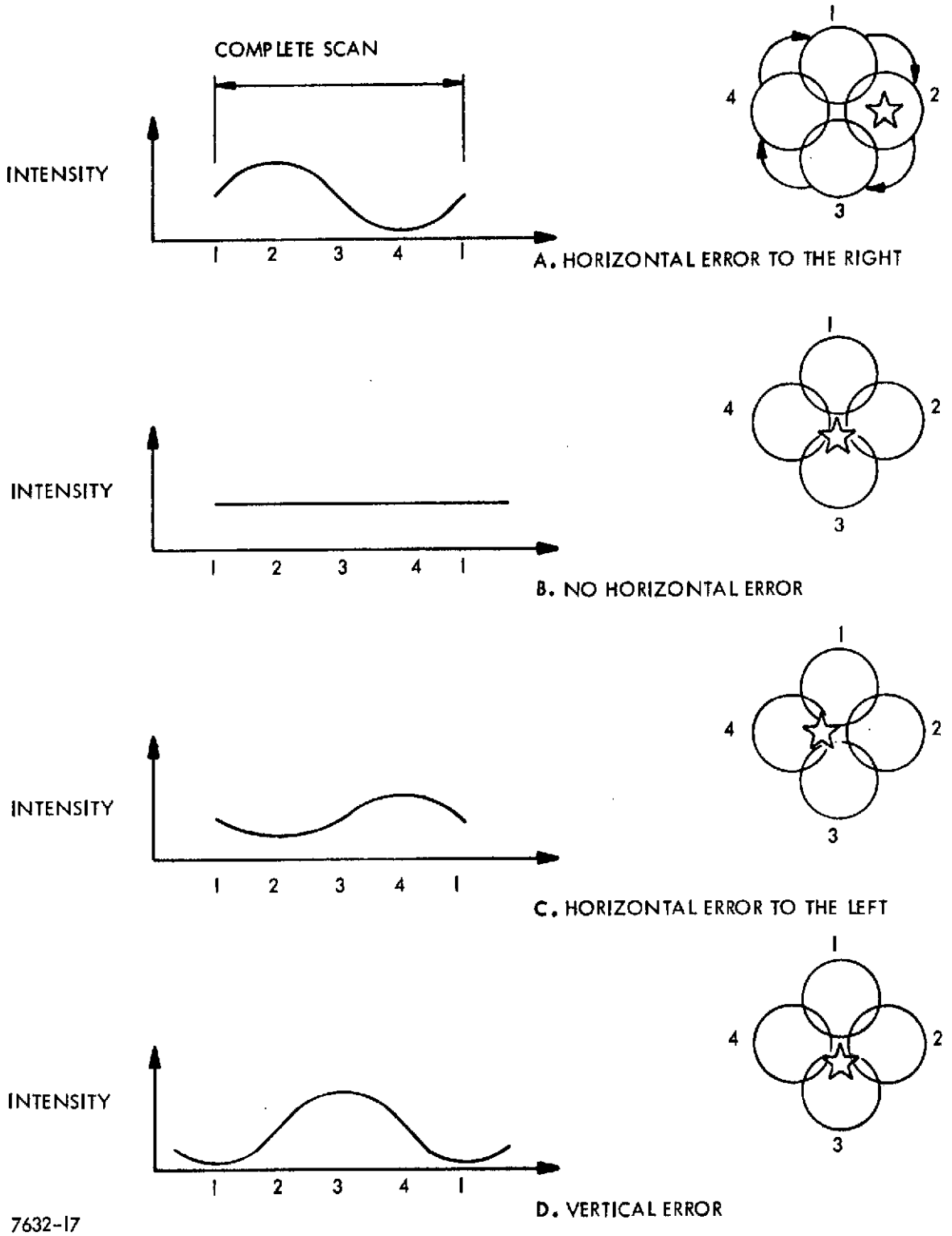

Figure 13. Intensity Patterns During Conical Scan

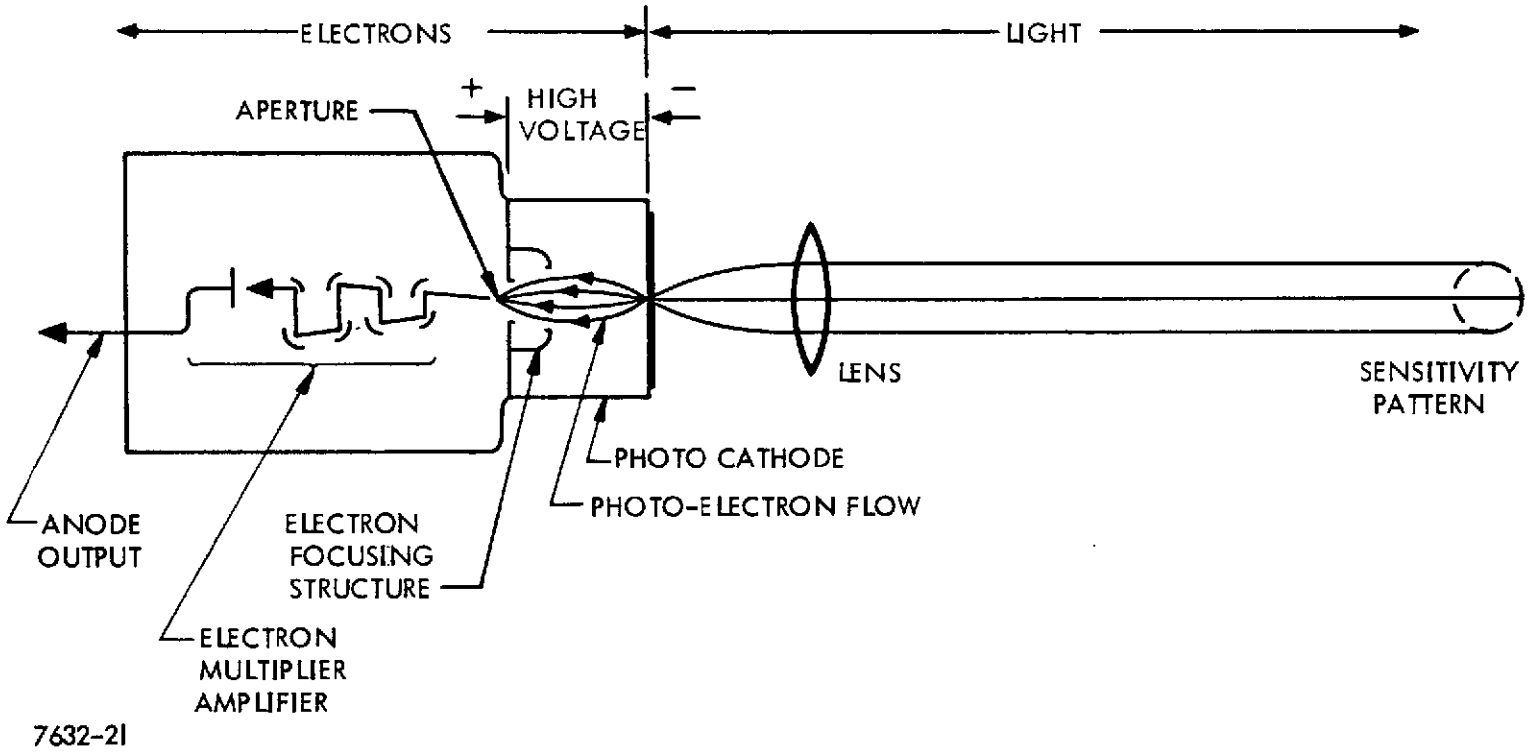

Figure 14. Image Dissector Tube

The second requirement of a tracker sensor is that the cone of sensitivity can be moved. The image dissector does this through the action of a magnetic field on the electron flow between the photocathode, and the aperture plane (figure 15). The magnetic field causes a force such that the electrons have a side-ways component to their drift. Electrons from the center of the photocathode no longer pass through the aperture. For each magnitude and direction of magnetic field, there is a unique area on the photocathode from which electrons will be detected. Thus a controlled magnetic field can cause the cone of sensitivity to move, to scan any image, and to move the whole scan pattern such that it is centered on the target. It therefore qualifies as a sensor for a tracking loop.

The remainder of the components necessary for a tracking loop are amplifiers, error detectors and scan generators. Figure 16 is a block diagram of a tracker. The system will be described by following the path of signal flow from the scan generator through to the power amplifier. The scan generates a high frequency (32 kHz) signal and provides it to both horizontal and vertical coils such that the image dissector is scanned in a circular pattern, as shown in figure 13. If a target is near the scan, an error signal, which is called a video signal, will be generated within the image dissector. The internal electron multiplier, which can have a gain of one million, amplifies the signal enough so that the noise figure is established (thermal noise of other components is unimportant). The output of the image dissector tube is ac coupled to a video amplifier which amplifies the 32 kHz to the desired level. The error detector is an analog multiplier which multiples a reference signal from the scan generator to the video error signal. Using two multipliers, one for each axis, and by using the proper phase in this multiplication, the up-down and left-right components of the error can be ascertained. This information will be fed back to correct the scan pattern position.

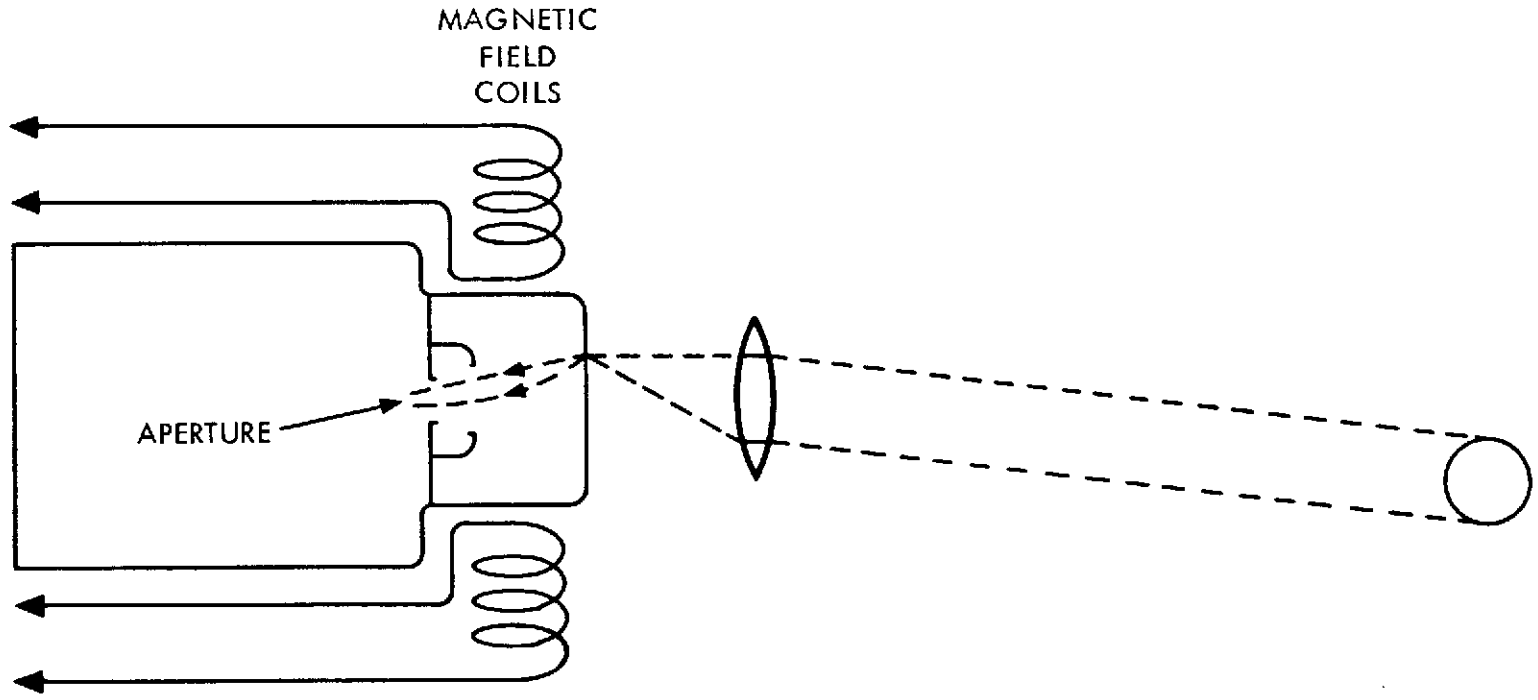

7632-4

Figure 15. Effect of Magnetic Field

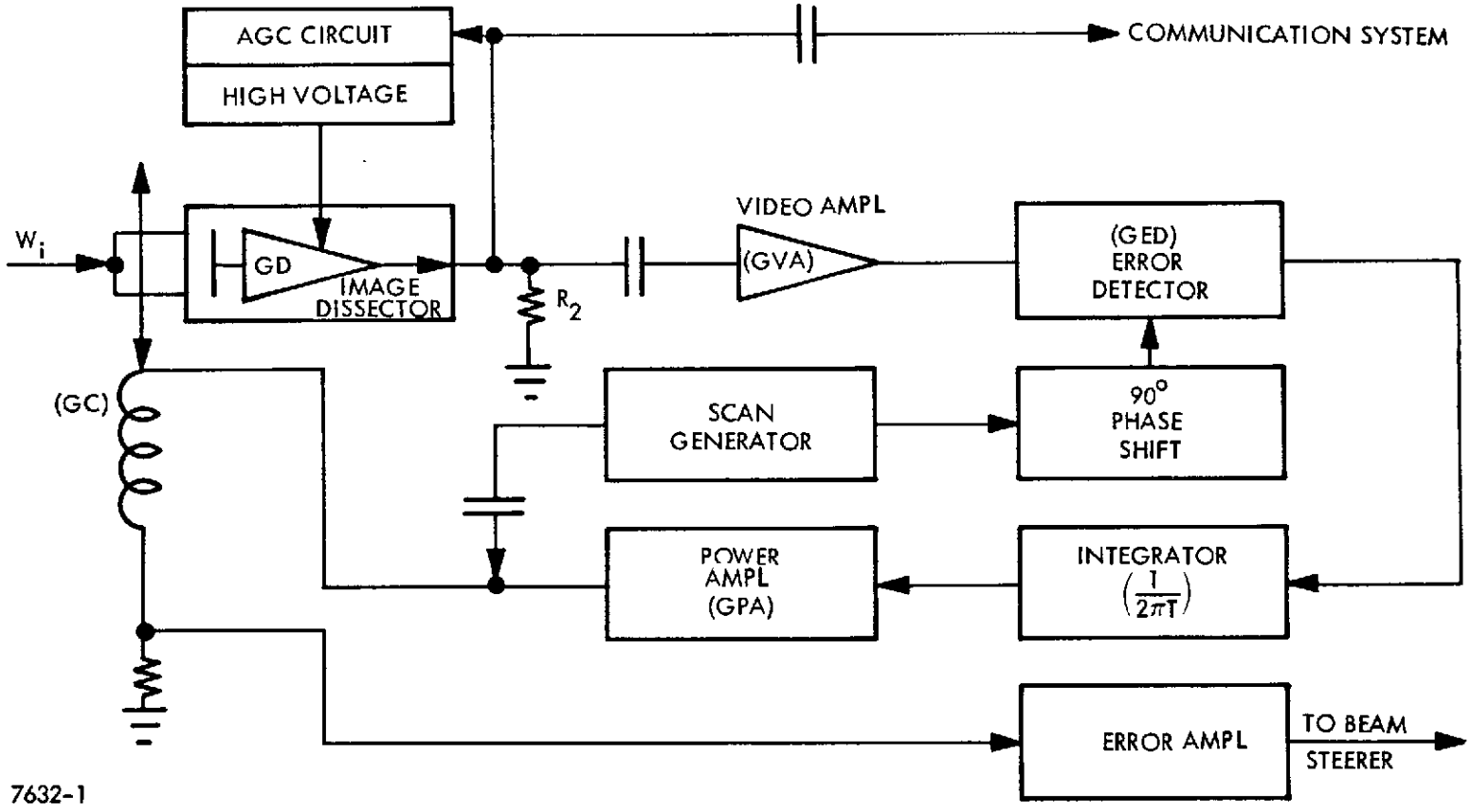

Figure 16. Tracker Block Diagram

The exact design of the feedback circuitry is arrived at through servo loop analysis. Two restraints limit the choice. The tracker should have as little tracking position error as possible. This requires one or more integrators to be in the feedback loop. Second, the system should be stable over a wide variation of optical target brightness. Since the tracker loop gain depends on the target brightness, two integrators within the loop cannot be used. Thus one integrator is used within the feedback path. The output of the integrator is amplified with a high current drive and supplied to the image dissector coil. To summarize, an error produces a video signal, is analyzed in the detector, and a low frequency current is supplied to the coils to push the scan pattern to reduce the error.

As was touched on above, analysis shows that the gain within the tracking loop depends on the intensity of the target. One can see that this is true by referring to figure 13. In A of figure 13 for example, suppose the target in this position were ten times brighter. Then the video error signal would be ten times as high. When this is processed, the error detectors would indicate ten times as much error, and would call for ten times as much movement of the scan pattern. The bandwidth of the tracker, then, will be ten times as high. The relationship describing this is:

$$BW \simeq \frac{1}{2\pi T} \times GDC$$

$$BW \simeq \frac{1}{2\pi T} \quad \frac{2\,(Wi)\,(APW)\,(GD)\,(R_L)\,(GVA)\,(GED)\,(GPA)\,(GC)}{\pi\,(DS)}$$

where

Wi - Image intensity (watts)

DS - Diameter of the image (meters)

APW - Photocathode sensitivity (amps per watt)

GD - Gain electron multiplier (dynode amp)

R_L - Tube load resistor (volts per amp)

GVA - Gain video amp

GED - Gain of error detector

GPA - Gain of power amp (amps per volt)

(GC) - Coil deflection (meters per amp)

T - Integrator time constant

GDC - Total loop gain

To keep the bandwidth from becoming too high, which may cause the loop to be unstable, a gain somewhere in the system must be decreased as the light image intensity becomes greater. In this system the gain that is reduced is that of the electron multiplier amplifier - also called the dynode amplifier. This amplifier gain depends upon the high voltage supplied to it. Thus, the output of the tube is sensed by the AGC circuitry, and the high voltage is controlled accordingly. The intensity level at which control begins is called the AGC threshold.

An additional purpose prompted the decision to control this amplifier. The tube should not be allowed to have more than 300 micro amps of current flowing from the anode. Because this communication system can be operated at close ranges during demonstrations, the potential current could well exceed this limit. By decreasing the dynode amplifier gain as an automatic control, however, at high light levels the gain will be reduced and the output current maintained at safe levels.

4.4.3 Tracker Performance. - The two important parameters of tracker performance are the bandwidth and the noise. The bandwidth is held to a maximum of 500 Hz. The noise level is dominated by the shot noise inherent in the optical detector. The interrelationship of noise, optical power

in the target image, and the bandwidth are shown in Figure 17. For image intensities greater than 2.5×10^{-8} watts, the system operates along a 500 Hz constant bandwidth line. As power increases the noise becomes less. Noise here is shown as a percentage of the size of the image, 1.0 milliradian. As the power becomes less than 2.5×10^{-8} watts, the AGC no longer holds the bandwidth constant and the system operates at a constant noise level and the effective bandwidth becomes less. From these curves, the noise on the outgoing beam can be predicted by using the 10 Hz constant bandwidth curve. The beamsteerers in other words, are influenced by the same noise source, but at a lower bandwidth. When the tracker bandwidth drops below 20 Hz, however, the beamsteerers loop is disconnected to prevent an oscillatory interaction between tracker and beamsteerer.

4.4.4 Beamsteerer Principles and Theory. - The purpose of the gimballed mirror is to move the field-of-view and move the outgoing beam such that the beam is pointed at the object it is tracking. Figure 18 shows the interrelationship of the tracker, mirror, and pointing. In A of Figure 18, if the tracker is tracking an object not in its center of view, the outgoing beam is not pointing correctly at the object. As the mirror rotates, B of Figure 18, the tracked image moves toward the center of the photocathode; and the outgoing beam becomes more accurate. If the outgoing beam is correctly "boresighted" with the center of the tube (a mechanical adjustment) when the tracker is tracking in the center of the tube, the outgoing beam will point exactly at the object.

The center of the tube is where no residual magnetic field is needed to have the scan pattern centered on the target. No magnetic field implies that the tracker is causing no residual current through the deflection coils. Therefore, the beamsteering loop acts to null out the current in the tube

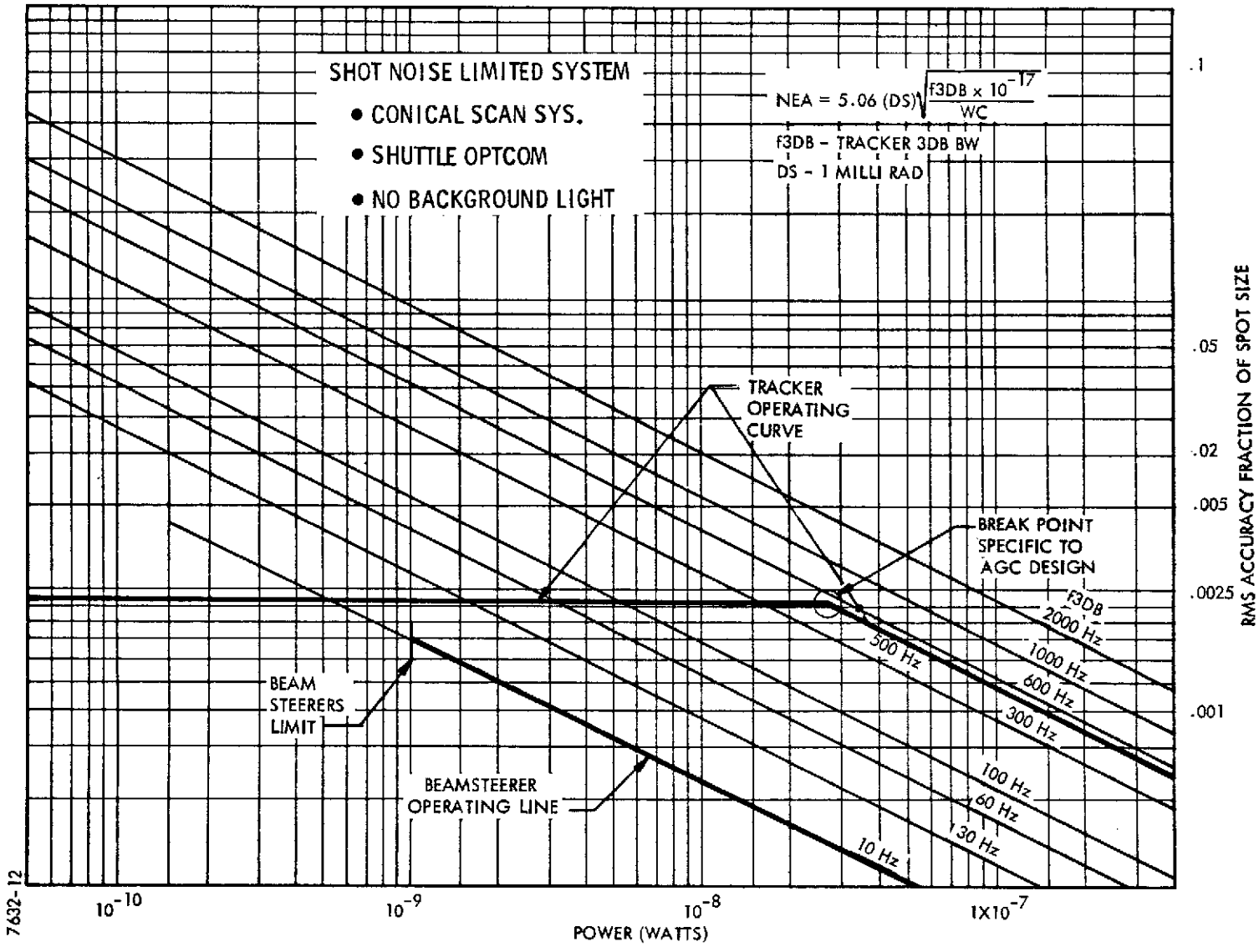

Figure 17. Interrelationship of Noise, Optical Power, and Beamwidth

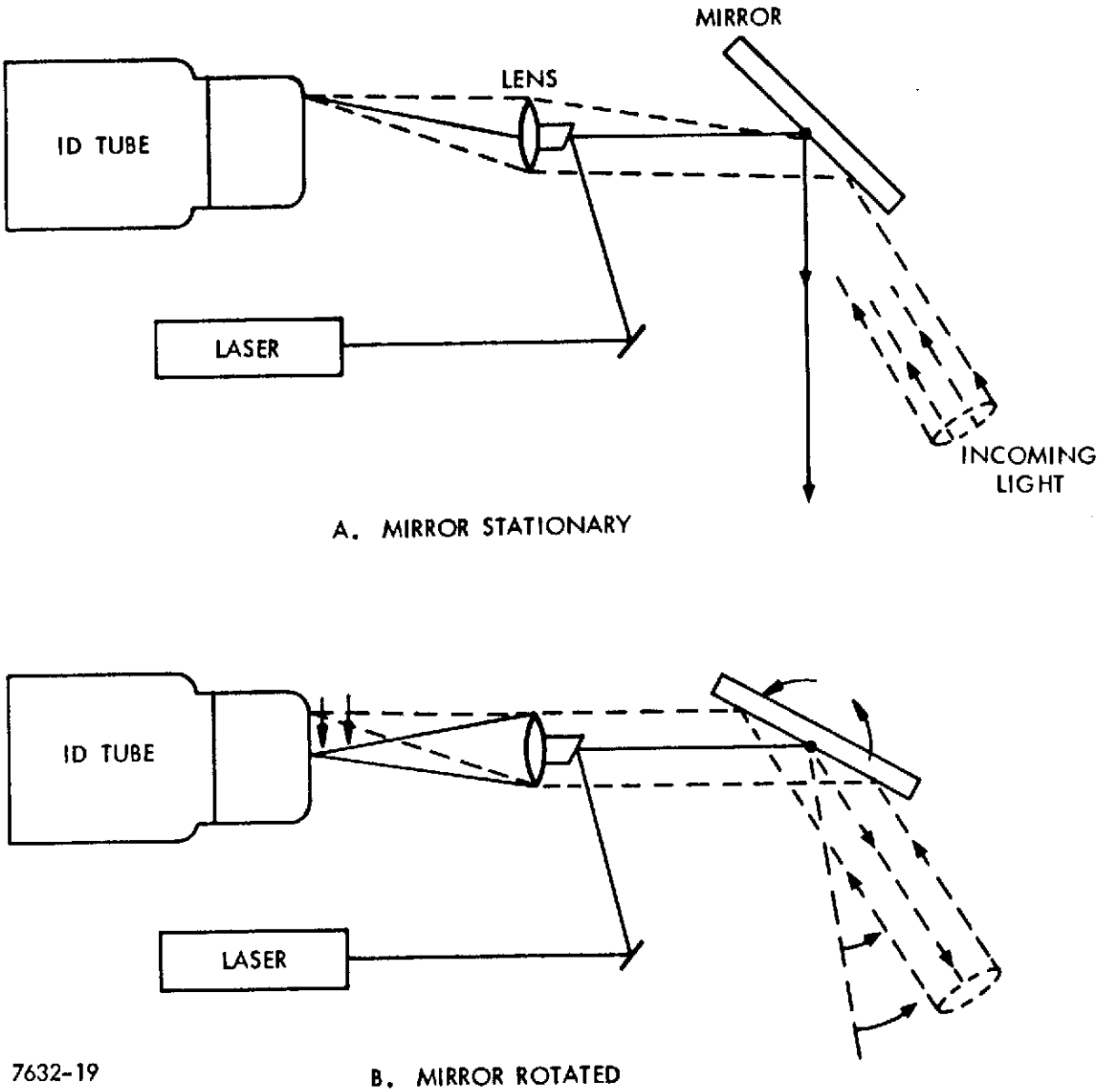

Figure 18. Alignment of Outgoing Beam and Image

deflection coils. The current is sensed by using a resistor in series with the coils (figure 16). The resulting voltage is amplified in a low frequency amplifier and is called the tracker error output.

The mirror itself is gimballed in two axes. The inside axis, called X, is a vertical axis for scanning horizontal movements. This frame, motors and pivots are as lightweight as possible to reduce high speed dynamic problem for the second axis. The second axis, Y, is horizontal and allows vertical movement of the beam. The motor on this axis has a high torque to enable swinging the inner axis structure. The pivots used in both axes are Bendix flexurals. This device is designed such that a moving axis is held in a crossed spring structure. They are quite rigid with respect to lateral movement, but allow friction-free rotational movement. Because of their construction, they offer a spring-like rotational torque against rotation from the null position. Each pivot in this system, for example, offers 1.312 ounce-inch of torque per radian of rotation. This null position quality of these pivots is the reason for their use in the system. When the motors are not powered, the mirror structure will return to viewing one certain field-of-view. If the mirror, on the other hand, were allowed to rotate freely, complex measuring devices would be needed to determine and control the field-of-view. On each shaft there are two motors. In the present design, one motor will be driven, and the other will be used as a tachometer. At this point, all of the mechanical characteristics are defined. The remainder is servo loop design. Table 2 lists the electro-mechanical parameters of the motor.

Servo Loop Design. - The first problem is to stabilize the motor - inertia - spring system. When the tracker is operating, it could effectively be used to stabilize the mirror. However, during acquisition and loss-of-target, the mirror would be free to bounce at its natural frequency. Thus, it is

TABLE 2. MOTOR SYSTEM PARAMETERS				
ITEM		AXIS X	AXIS Y	UNITS
Torque	K_t	2.4	6.5	Oz. - in/amp
Back Emf	K_a	.01	.05	V/rad/sec
Max. Torque		1.5	4	Oz. - in
Shaft Inertia	J	1.6	7.8	x 10^{-3} Oz - in sec^2/rad
Spring Torque	K_s	1.312	.66	Oz. - in/rad
Resultant Natural Freq	F_R	4.5	1.0	Hertz
Motor Resis.	R_1	50	55	Ohms
Motor Inductance	L	5	11	x 10^{-3} Henrie
Track Output		.01	.01	V/rad/sec
Max Accel.	α	545	278	rad/sec^2

best to dampen the mirror independent of the tracker. For this purpose, the tachometer output is fed back to the motor driver amp. The root locus plot, Figure 19, shows the operating point. The Tracker-mirror loop, which will form the final pointing loop, contains two main functions: Add one zero to cause stability, and a double integrator to increase low frequency gain and thereby decrease position error. The system is designed to allow two different zero locations. The low speed mode will allow the tracker to have a bandwidth of 10 Hz and the high speed mode bandwidth can be an under damped 30 Hz. The two integrators are needed because the spring pivot causes the inherent integration nature of the motor-inertia system to stop at the natural frequency, i.e., 1 Hz for the Y axis. Table 3 summarizes the control loop parameters. A root locus plot of the low speed mode total loop is shown in Figure 20. At the present time, only the low speed mode has been enabled.

Mode Control. - The mode control is the logic that controls the acquisition sequence and signal drop-out. The mode control consists of a set of threshold detector, timing elements, and logic gates to cause outputs that are appropriate to the sequence pattern of events. The circuitry also incorporates information from the communication receiver in its decision-making process. The outputs of this unit control acquisition scanning, enable tracking and close the beam-steering loop. The main information used in doing this is the current level coming from the image dissector.

The current from the tube is sensed in three threshold detectors: one high speed, low level; one low speed, low level; and one high speed, high level. The high speed, low level detector is used to detect a quick and low level "blip" which could be a target during acquisition scan. This immediately stops the scan and enables the tracker to try to track it. If the "blip" was due to noise, the tracker will not have anything to track,

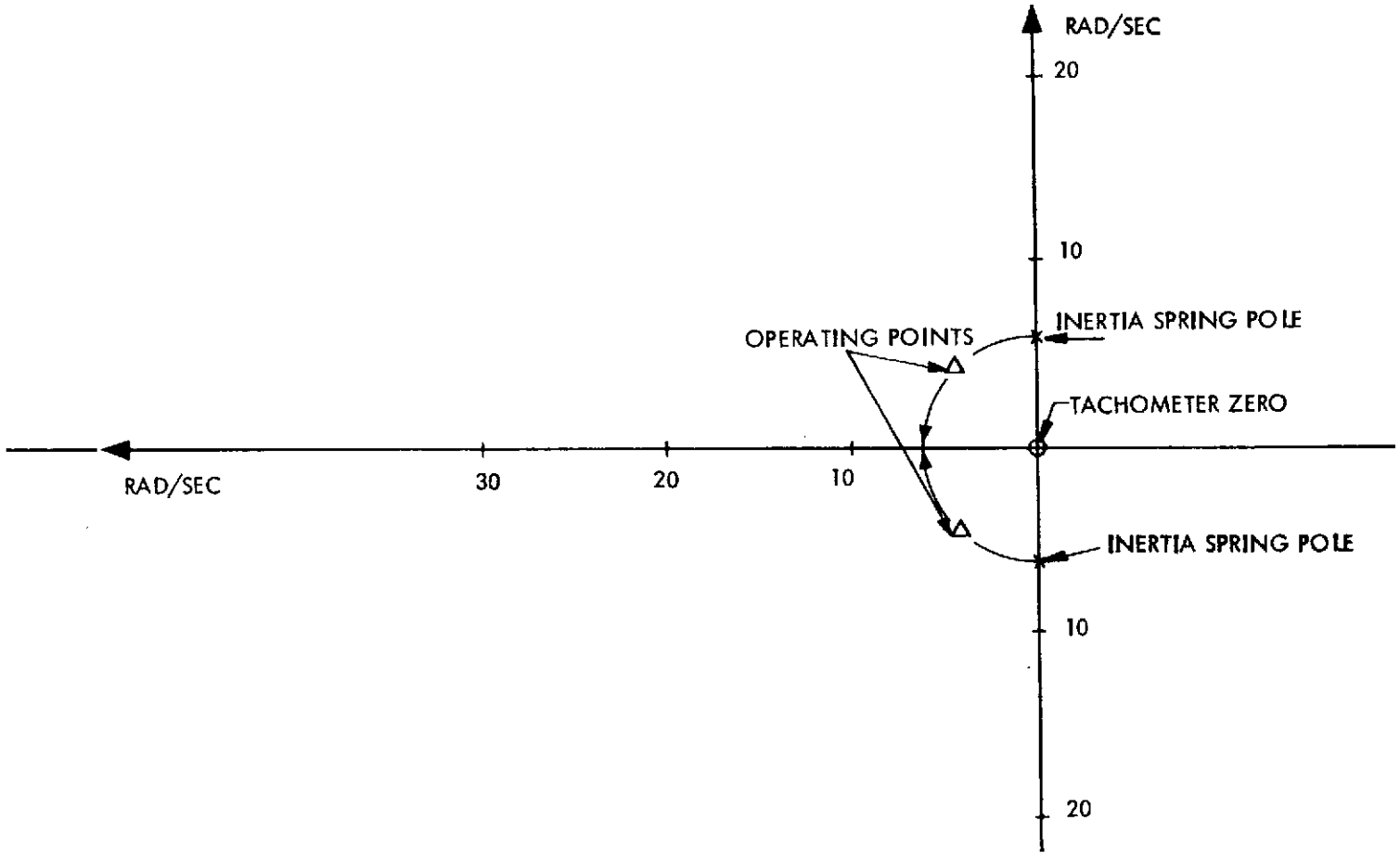

7632-2

Figure 19. Y Axis Tachometer-Stabilizes Root-Locus Plot

TABLE 3. CONTROL LOOP PARAMETERS

ITEM	DESCRIPTION			
	X Axis		Y Axis	
	Rad/sec	Hertz	Rad/sec	Hertz
TRACKER	29.5 V/rad 10.0 V/in		29.5 V/rad 10.0 V/in	
$\frac{K_6'(S+A')}{10}$ LEAD (A') = SLOW MODE	41.6	6.6	31	5.0 6.6
K_6' (S+A) LEAD (A) = FAST MODE	225	36	207	33
$K_6 \times 10 = K_6'$ =	0.024		0.07	
$\frac{S+B}{S+C}$ FIRST INTEG	B = 10 C = 1	1.59 .159	B = 3 C = 0.3	.475 .0475
$\frac{1}{10}\ \frac{S+B}{S+C}$ SECOND INTEG	"	"	"	"
DRIFT SCALE FACTOR AT POINT 1 (LIGHT ANGLE)	3.05 Rad/volt		4.95 Rad/volt	

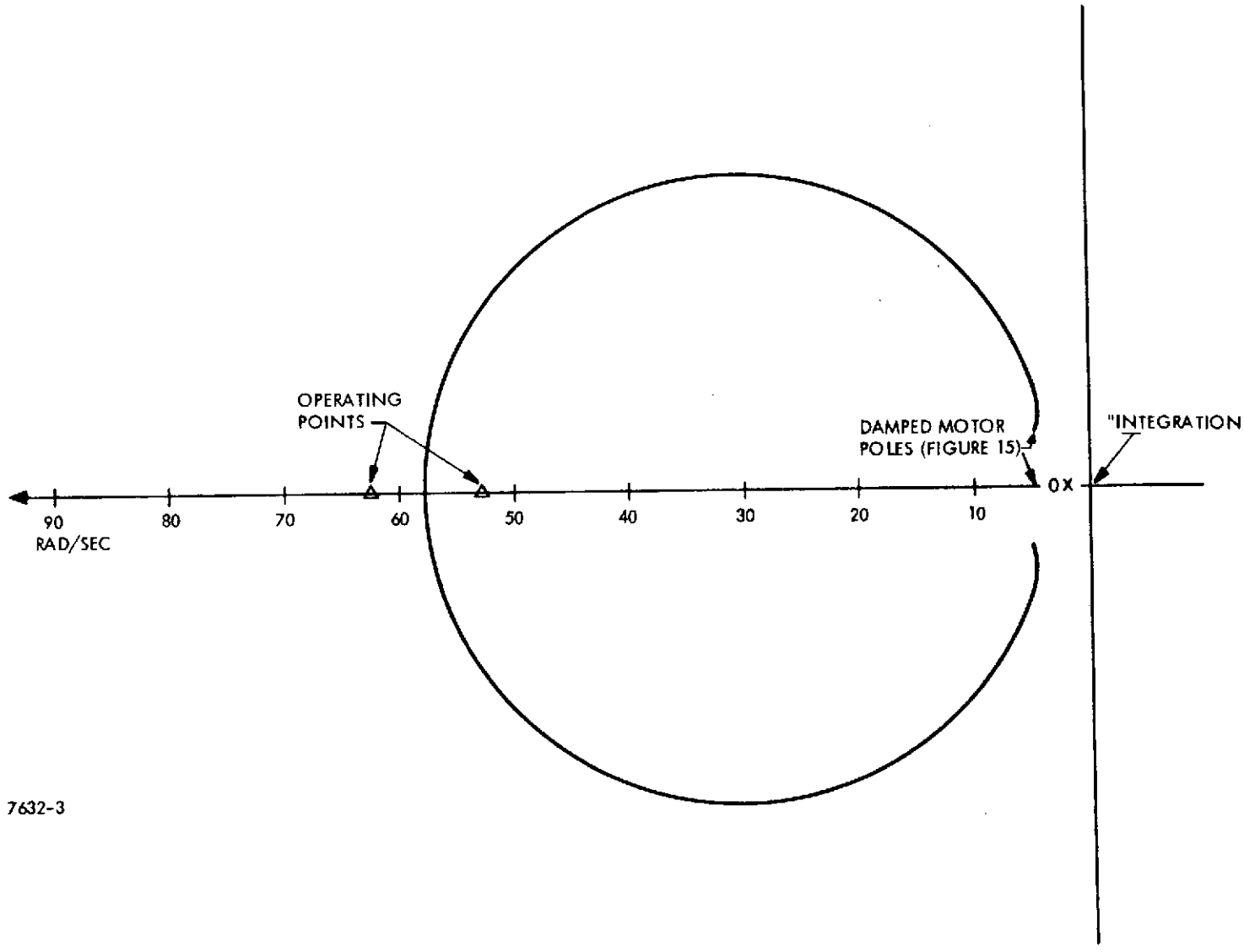

Figure 20. Total Loop, Low Speed Mode

and in 20 milliseconds the scan will be resumed. If the "blip" was a target, it will be tracked, and the low speed, low level threshold detector will be crossed, which will hold the unit in track mode. The beamsteerers will also be connected if this low level threshold is crossed. The purpose of the high level threshold was to change the beamsteering loop from 10 Hz to 30 Hz. Because this higher bandwidth mode was not enabled, this threshold is being ignored at the present stage of operation.

If the target level drops for a few milliseconds, the low speed, low level threshold will ignore it. If the fade is more than a few but less than 0.5 seconds, the beamsteerer is disconnected so that it will not be influenced by erroneous tracker output. Also, this will prevent the servo loop from oscillating in the event the tracker is continuing to track a very weak target. If the fade continues beyond one-half second, the tracker will be disabled, the beamsteerers will be relaxed, and a search scan and the slow sweeping scan of the outgoing beam will begin. The total operation is summarized in Figure 21.

There is built into the mode control a 16 second delay. This was intended for use in holding the mirrors in the position that they held when the target was last seen. This would enable a sweeping scan of that section of space before the mirrors would be relaxed and thereby returned to the neutral field-of-view. The holding technique is the difficult part of this procedure. A completely successful one has not been achieved at this time; and this mode is not used.

A second feature that adds to the growth potential of this system is a method for stabilizing the beamsteering loop in the event of a fade of the target intensity. This technique would decrease the beamsteerer bandwidth as a function of the optical intensity. This would allow the system to

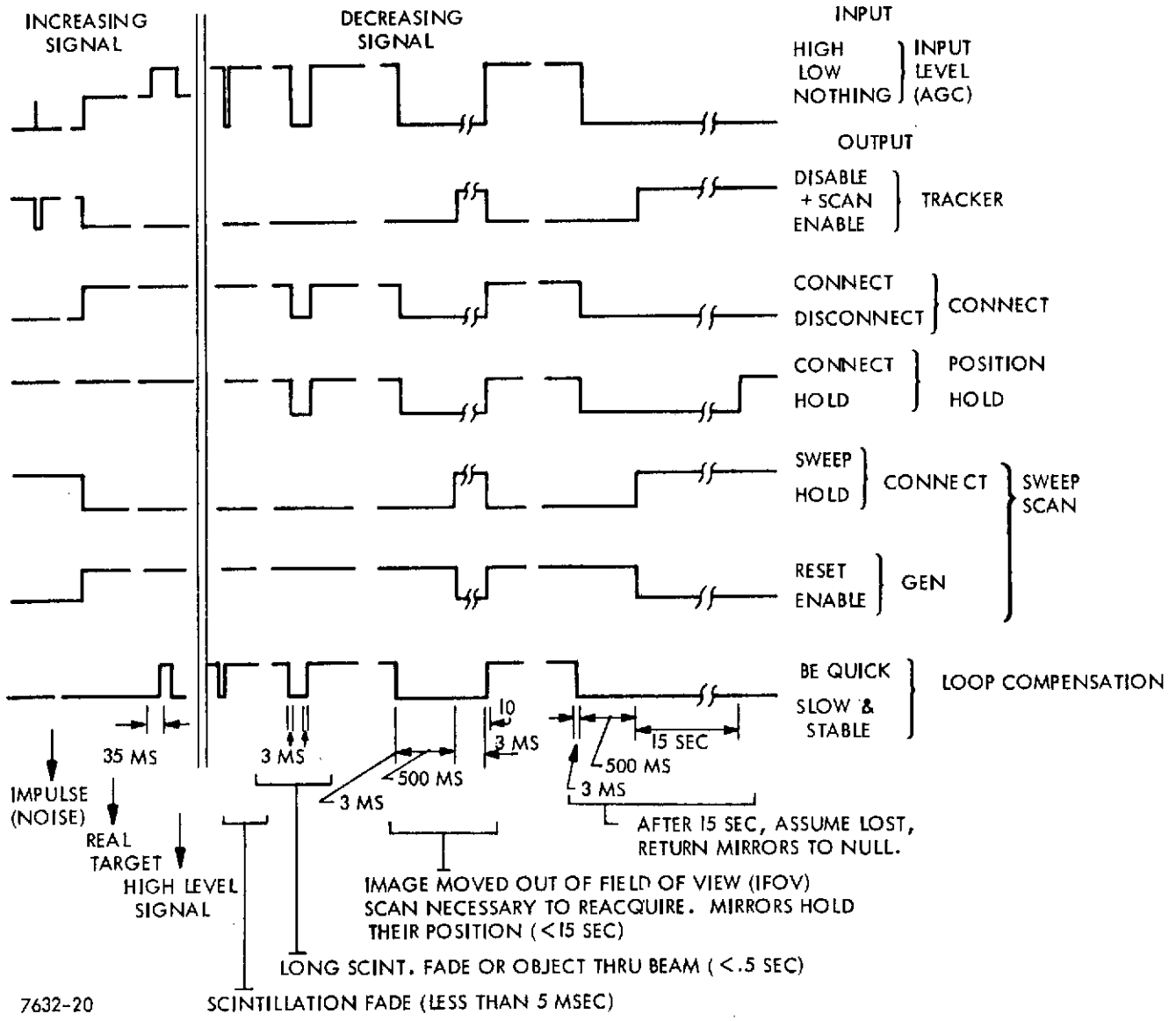

Figure 21. Mode Control Logic Sequence

continue to track and point during a fade, instead of being disconnected, as in the present design. The circuitry for this is incorporated in the beamsteering section. At this time, the circuitry has not been enabled and tested.

4.5 Circuit Design Discussion

The following is a description that will take the circuit concepts of the previous section and will point out the implementation in the circuit schematics. The schematics are grouped in Appendix D at the back of this report.

The tracker schematic is shown in Figure D1. Circuit Z6 of the X channel board is a crystal oscillator and is the source of the track scan signal. A 90^{o} shifted reference is created by Z7. Except for the preamp circuits, the remaining tracker circuitry is identical for the two boards. The reference track scan is amplified by Z2 and drives the coils that surround the image dissector. The current through the coil, which is 90^{o} lagging behind the input voltage is sensed by Z3, amplified and adjustable through Z4, and is then the reference signal for the error detecting analog multiplier, Z8. The error signals from the tube are amplified by Z6 and Z7 of the Y channel board. The errors are detected by the appropriate multiplier, Z8, and the error is integrated through Z5 and drive the deflection coils through the current driver Z9. The coils have an inductance of 30 millihenries and produce a deflection of 0.0105 inches per milliamp. The amount of deflection from the center of the tube face is detected by sensing the current through the coils with a 51 ohm resistor. This error from the center of the tube is amplified by Z1 and is used to control the beamsteerers. And slight error in the alignment of the outgoing beam with the center of the tube, boresight error, can be corrected through an adjustment at the error amp. Each board, also, has a voltage regulator to increase circuit isolation.

The receiver search scan generator is also shown on this schematic. It consists of a constant current device, CR1 and a 4-layer diode, CR2. The saw tooth pattern is dc adjusted and supplied to the coil driver through a switch and buffer amp. The capacitor at the switch, Z2, output serves as

slowly decaying memory, to prevent the tracker scan from being quickly pulled from the spot where a target was detected by the acquisition circuitry.

The automatic gain control is shown in Figure D2. In this circuit, the current is sensed in Z1A and compared with a threshold in Z1B. As the current increases, the current through Q1 is decreased, and thus the voltage from the VH15 high voltage power supply. The sensed output of the tube also amplified by Z2A and Z2B for use in the mode control and control box meter. A schematic representation of the image dissector and dynode amplifier is also shown.

The mode control thresholds and logic are shown in Figure D3. The output of the AGC goes through a switch to threshold circuit Q3, Q4A, and Q4B. An output of Q3 will enable the track for 20 milliseconds. However, if 4A is also activated, then the tracker and beamsteerers are activated. If the target disappears, a one-half second one shot will keep the system enabled for that long. If the target has not reappeared, a new search will be initiated. The logic circuits used in this section are low power MOS logic.

The beamsteerers, Figure D4, is enabled through switches Q5 and Q6. The error output of the tracker is first passed through the "zero" of Q3A. Q3B and Q8 form a pair of integrators that increase the accuracy of the loop. The motors are driven from PA-011 power amplifiers which is connected as a current driver. The input to this amp is a sum that includes tachometer feedback, offset bias, scan pattern voltage, as well as the tracker error output. A gain adjusting circuit Q1 and Q2A is also shown; however, it has not been connected into the loop. The scan generator is shown in Figure D5.

The outgoing beam divergence control loop is shown in Figure D6. The actual beam divergence is accomplished by moving a negative lense

in a Galilean telescope. The back and forth movement is caused by a spiral thread in a rotating barrel. The barrel is rotated by using a geared motor-pot combination. The circuit Z1A senses the difference between a command voltage and the voltage from the potentiometer. Either transistor Q1 or Q3 is turned on depending on the polarity of the error. Q2 and Q4 are switched so that the appropriate current path is enabled. The capacitor across R4 form a "lead" current path that help stabilize the control loop.

The communication transmitter, Figure D8, contains an audio pre-amp and high frequency VCO. The high frequency oscillator is controlled by the MV1405 varicap diode. The output is amplified and the output transformer, T1, is tuned with the capacitance of the optical modulator tied on. The DC offset voltage is generated by rectifying a sample of the high frequency output. The transmitter driver also contains a heater driver circuit. The electro-optical modulator contains a heater resistor and a thermistor to sense the temperature. With these, the temperature can be accurately controlled. It was noted, however, that better and more stable operation was obtained by operating the modulator at room temperature. The heater was therefore disconnected.

The receiver is shown in Figure D9. The output of the image dissector is distributed in this circuit. The low frequency components pass through the inductors, however, the high communication frequencies, 2.4 MHz are stopped and amplified. They are mixed with 13.1 MHz local reference oscillator to produce a 10.7 MHz product. This is filtered in a narrow band crystal filter. Following the filter is a commercial device which contains a limiting amplifier, a double-balanced mixer and an audio amplifier. The outputs are an amplified 10.7 product and also the detected audio voice. The audio is amplified in a high current circuit to drive a speaker. The

The 10.7 MHz is further amplified and more narrow band filter and detected. This signal acts as an indicator that a modulated signal is being received. It is low pass amplified and sent to the mode control.

5.0 RECOMMENDATIONS FOR SYSTEM IMPROVEMENTS

The following is a list of specific circuit recommendations that have emerged after the system troubleshooting has been accomplished. They are listed by system functional block, and the order does not indicate level of desirability.

5.1 Tracker

1. Offset the track scan frequency or the high voltage power supply oscillator frequency so that they are not harmonic related. At present, the third harmonic of the high voltage supply is being detected by the tracker processor.
2. Replace analog multiplier method of error detecting with a technique that has a better DC stability. Many such methods have been used and are available.
3. The output of the tube should be buffered immediately through short and low capacitance leads. The output would then be higher level and lower impedance and would, therefore, be more immune to pickup.
4. The track scan drive to the coil should be done through the coil driver, not in parallel to it.

5.2 Beamsteerers

1. When breaking loop during acquisition and loss-of-target, do this only at one place in the loop, instead of two places. In this way, offset and drift will be dealt with at one point instead of two.
2. Obtain greater stability of power amp. Use offset null feature in amp instead of technique used presently. Also, be more careful of input resistance to minimize effects of offset current.
3. Redesign mechanical structure so that flex pivots can be used at both ends of the outer gimbal axis. Also, find stiction-free method for electrically connecting to the inner axis motor and tachometer.
4. Find a drift-free method of implementing a long time constant, i.e., ten seconds, mode at "loss-of-lock." This will greatly decrease reacquisition time.

5.3 Mode Control

1. Change timing at loss-of-lock to enable tracker search scan 0.1 seconds after loss of lock. The sweep scan can still be initiated after 0.5 seconds.

5.4 Divergence Control

Replace switching-driver circuit with simple linear current amplifier.

5.5 Receiver

1. Rebuild circuit on solid ground plane board.

2. Use phase lock loop detector and tone decoder combination. This would eliminate need for second IF amplifiers and since it would be a coherent detection, narrow bandwidth operation would be possible. The device could be a signetics NESGIB phase lock loop.

5.6 Transmitter

1. Replace electro-optical modulator with a more reliable brand. The preset index of modulation and operating point are very unstable. Room temperature, contrary to manufacturer's contention, is the most stable operating condition.

APPENDIX A

SENSITIVITY COMPARISON OF SEVERAL IMAGE DISSECTOR SCAN PATTERNS USEFUL FOR OPTICAL COMMUNICATIONS

A. INTRODUCTION

In the great majority of its optical communications system applications ITT has chosen the image dissector (ID) photosensor for the tracking detector.[1] And in most of these systems this detector is expected to do double duty. The ID photosensor must not only track a beam's image and generate error signals, but also it must serve as a communications detector by passing a modulation spectrum impressed on the beacon. For this reason the high amplitude ID scan pattern commonly used in star tracker applications is not suitable. Use of such a pattern leads to undesirable periodic breaks in the communications link.

This report is concerned mainly with ID tracker scan patterns that continually pass a large fraction of the incident signal power. Due to this limitation caused by the dual use of the ID photosensor we expect a significant loss in tracker sensitivity. However this loss will vary greatly according to which ID scan pattern is chosen. This report has consequently been prepared to help the system designer in selecting the most suitable track scan pattern.

Actually, although five tracker scan configurations are considered here,[2] only three are suitable for an integrated (common communications and tracker photosensor) optcomm receiver. There are the conical scan and two versions of the cruciform scan. Performance of all these trackers is dependent on the energy distribution of the image to be tracked. Probably the most general image distribution to use is the Gaussian, but unfortunately it also is one of the most difficult to work with. Hence, in order to avoid mathematical

complexity we use for all the scan patterns considered here a uniform square target image. This hypothetical image distribution conveniently symplifies the analysis and we feel it does not distort the relative advantages of one track scan configuration over another.

The relativeness of this analysis should be kept in mind since the sensitivity calculated here can be much degraded by the choice of circuitry internal to the tracker. Furthermore, trackers are feedback systems, normally with a single dominate integrator, so that the noise bandwidth is about $\pi/2$ larger than the tracker bandwidth as usually described. In any case we expect the relative tracker performance calculated here to be in error significantly less than a factor of two.

Section B is concerned with ID trackers that use a conical track scan pattern. Sensitivity as described by B7 and B8 is valid for any rotationally symmetric target image. However we carry the analysis further by considering tracker sensitivity for a square image in B11.

In Section C we discuss a system that uses a low amplitude cruciform track scan and an integration type demodulator. In this configuration the demodulator integrates the photocurrent during the right hand track scan, and subtracts from this the integral of the photocurrent sensed during the left hand track scan. This sampled difference is used to generate the tracker error signal. We find in C15 that the optimum selection of parameters here leads to a track scan not useful for an integrated optcomm receiver. As a consequence, we must compromise the system and obtain the reduced sensitivity of C19.

Section D is also concerned with a cruciform track scan of reduced amplitude. However the demodulator here works by measuring the times when the photocurrent passes some threshold value. A variation of this technique is used in many ITT-developed star trackers.

★

Sections E and F describe tracker techniques that have been included here for comparison. One is a "standard" star tracker and the other an "ideal" tracker photosensor.

Section G brings together characteristics of the various trackers for comparison in terms of slew rate and sensitivity. One single quantity of interest is the relative track scan performance index, listed in Table 2G.

This work was funded in part by Contract NAS8-26245.

B. CONICAL SCAN PATTERN

In the conical scan tracker configuration an electron image of the beacon is swept around the periphery of the ID sampling aperture. As shown in Figure 1B, a tracking error e leads to a displacement in the center of the conical scan. The result is a periodic nutation of the beacon image relative to the sampling aperture periphery. Figure 2B illustrates the sinusoidal-like variations in the photocurrent caused by a small track error.

Considering a rotationally symmetrical beacon image of diameter d we note from Figure 3B that, for a scan amplitude of D/2, small track errors e result in a maximum area displacement relative to the sampling area periphery of ed (inches^2). The total photocurrent flux in the beacon image of area $(\pi/4)\, d^2$ is I (electrons/sec.). Consequently, the photocurrent change caused by the displacement e is proportional to the ratio of ed to the image area, i.e.,

$$\text{AC current semi-amplitude} = \frac{4Ie}{\pi d}. \quad \text{(electrons/sec)} \qquad \text{B1}$$

Since for this comparison we set the scan amplitude so that with zero track error half of the beacon photocurrent passes through the sampling aperture, the instantaneous photocurrent i in Figure 2B can generally be described by

$$i = (I/2)\,[1 + (8e/\pi d)\cos(\phi - \omega t)], \quad (e << d) \qquad \text{B2}$$

where the phase ϕ and frequency ω factors and their processing are discussed in another report.

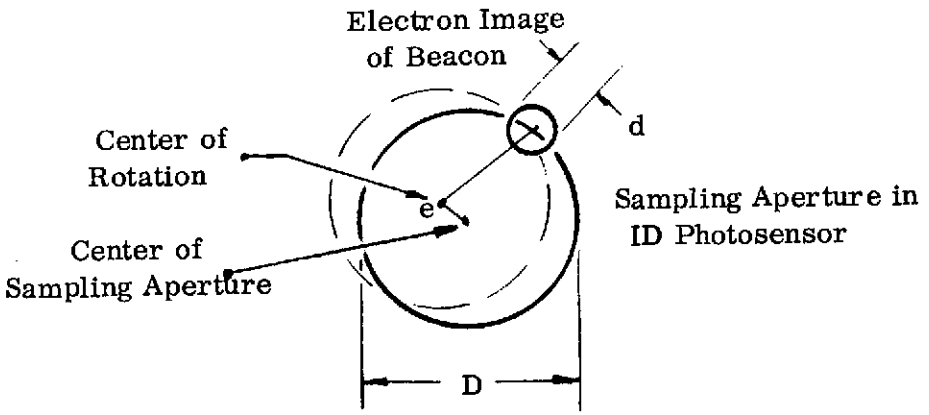

Figure 1B. Conical Scan Geometry

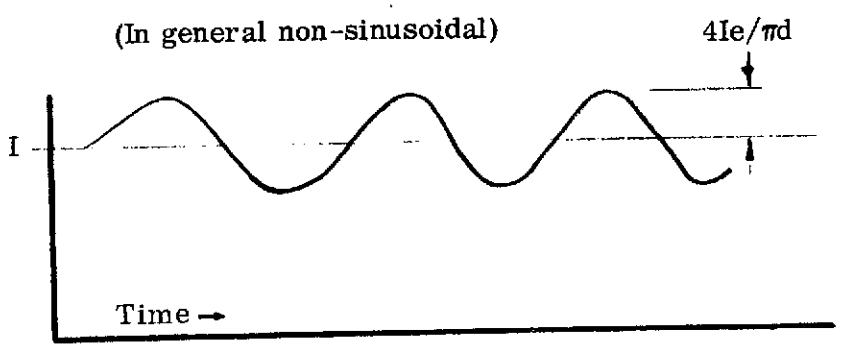

Figure 2B. Variation in Photocurrent with Time for Track Error e

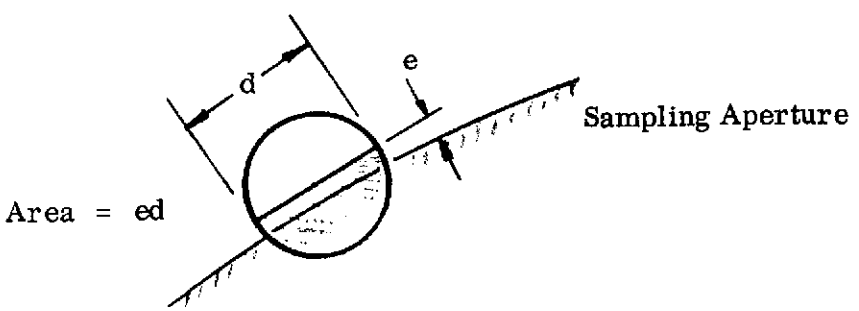

Figure 3B. Variation in Overlap Area

The mean square signal can be shown to be

$$\overline{\text{signal}}^2 = \left[T^{-1} \int_T (i - \bar{i})^2 \, dt \right] T^2 \quad . \qquad \text{(electrons)}^2 \qquad \text{B3}$$

If the integral of the cosine squared is taken over a whole number of cycles, its average value is 1/2, so that the combination of B2 and B3 is

$$\overline{\text{signal}}^2 = 8 \, (e \, I \, T/\pi d)^2 \, . \qquad \text{B4}$$

The rms photocurrent shot noise η^2 is caused by the average signal I and background I_{bg} currents during the interval T, i.e.:

$$\eta^2 = k^2 \, (T \, I_{bg} + T \, I/2) \qquad \text{(electrons)}^2 \qquad \text{B5}$$

where k is a factor ($k \geq 1$) used to describe dynode and amplifier noise. In order to calculate tracker sensitivity we set the mean square signal equal to the mean square noise and interprete the error e as the rms tracking error ϵ, leading to

$$\epsilon = \left[(I_{bg} + I/2) /8T \right]^{\frac{1}{2}} \pi d \, k/I. \qquad \text{(inches)} \qquad \text{B6}$$

The situation most often encountered is that in which the tracker is signal shot noise limited, i.e., ($I >> I_{bg}$). Then the last relationship can be solved directly for the required signal current Φ, thus[3]

$$\Phi \Big|_{\substack{\text{signal shot} \\ \text{noise limited}}} = (\pi \, d \, k / 4 \epsilon \,)^2 / T \, . \qquad \text{(electrons/sec)} \qquad \text{B7}$$

For the background-limited situation ($I_{bg} >> I$) equation B6 reduces to

$$\Phi \Big|_{\substack{\text{background} \\ \text{limited}}} = (I_{bg}/8T)^{\frac{1}{2}} \, \pi d k / \epsilon \, . \qquad \text{(electrons/sec)} \qquad \text{B8}$$

We are not restricted to considering rotationally symmetrical images. For instance, if the beacon electron image of Figure 1A is considered to be square of side length d, and if this square rotates about its own center in synchronism with the conical scan (a hypothetical but useful concept), we find that

$$i = (I/2)\left[\, 1 + (2\,e/d)\cos(\phi - \omega t)\,\right] \qquad \text{B9}$$

$$\overline{\text{signal}}^2 = (e\,IT/d)^2/2 \qquad \text{B10}$$

$$\Phi\Big|_{\substack{\text{signal shot}\\ \text{noise limited}}} = (dk/\epsilon)^2/T \qquad \text{(electrons/sec)} \qquad \text{B11}$$

The last three equations for the hypothetical square electron image vary by factors of $4/\pi$ from Equations B2, B4 and B7 and will prove more useful for comparison in later sections.[4]

C. PARTIAL CRUCIFORM SCAN WITH INTEGRATION

Figure 1C illustrates the cruciform scan. This class of track scan leads to sampled data with halves of the cycle period "T" being shared alternately by the horizontal and vertical error processing circuits. Considering here only the horizontal scan, we note from Figure 1C that the square beacon electron image with side length "d" is translated a distance "s" from its average position in the center of the square sampling aperture (side length D). The photocurrent variations resulting from scan translations to the right and left are depicted in Figure 2C. We note that if the scan is centered in the sampling aperture, and if the amplitude "s" is large enough so that the electron image is partially occluded by the aperture edge, there is a "V"-shaped attenuation of the photocurrent corresponding to the extremes of the right- and left-hand horizontal scans. These are represented by the solid lines in

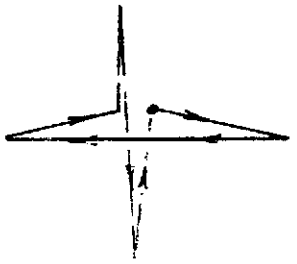

2 Axis Scan Pattern

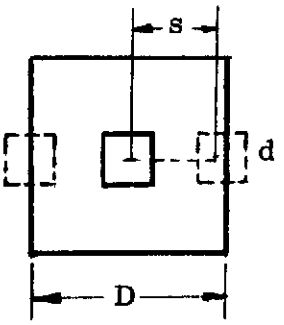

Scan Geometric Parameters

Figure 1C Cruciform Scan

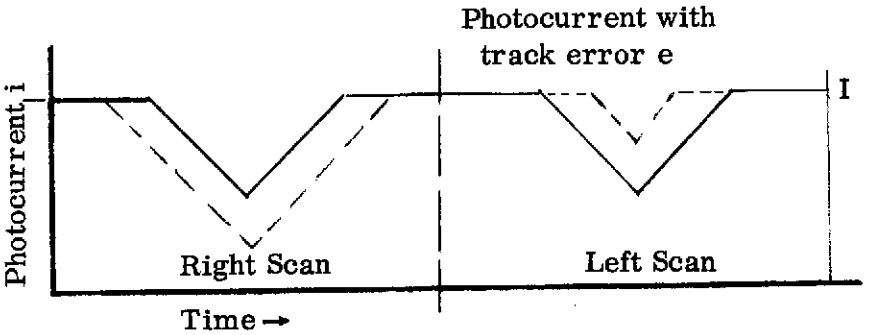

Figure 2C. Photocurrent Time Variations

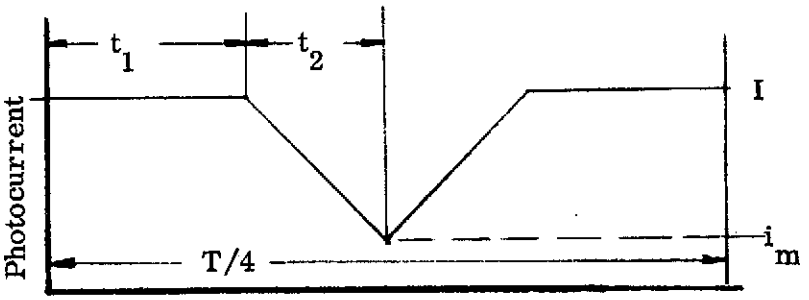

Right Scan Interval

Figure 3C. Scan Time Parameters

Figure C2. However, if there should be a displacement of the scan center position corresponding to a track error e, the "V" of the right and left scan intervals on the curve of Figure 2C will vary in opposite directions. We calculate below the difference in the integrated photocurrents during these two intervals, the measure of tracker error.

In T seconds the beacon image is deflected over both the vertical and horizontal axes, a total distance of 8s inches. The average velocity v of the image center is therefore $v = 8s/T$. The signal photocurrent between the start of the right-hand scan and the time the image begins to cross the sampling aperture perimeter is I, the full value of the electron image current. As noted in Figure 3C, this interval length is t_1 and the interval of decreasing photocurrent is t_2. The total charge (electrons) counted during the right-hand scan interval is seen by inspection to be Q_R where

$$Q_R = 2 I t_1 + (I + i_m) t_2 . \qquad \text{(electrons)} \qquad \text{C1}$$

The slope of the photocurrent change during t_2 is $I/(d/v)$ so that the minimum photocurrent value is

$$i_m = (1 - v t_2/d) I, \qquad d \geq v t_2 . \qquad \text{C2}$$

We can combine the last two relationships to obtain

$$Q_R = (2 t_1 + 2 t_2 - v t_2^2/d) I = (\frac{T}{4} - v t_2^2/d) I \qquad \text{C3}$$

Now we note that the electron image will move in the interval t_1 a distance $(D - d - 2e)/2 = v t_1$. Hence the relationships below follow directly.

$$(t_1 + t_2)\, v = s \quad , \tag{C4}$$

$$t_2 = s/v - t_1 = s/v - (D - d - 2e)/2v \quad ,$$

$$t_2 = \left[s - \frac{D}{2} + \frac{d}{2} + e \right] /v \quad , \tag{C5}$$

$$Q_R = (IT/4) - \left[e^2 + e(2s - D + d) + (2s - D + d)^2/4 \right] IT/8sd. \tag{C6}$$

The conditions for validity of the equations above are that[5]

$$\begin{aligned} &(1) \quad s + |e| \le (d + D)/2 \quad , \\ &(2) \quad (D - d)/2 \le s \quad , \\ &(3) \quad vt_2 \le d \le D \quad , \\ &(4) \quad |e| \le d \quad . \end{aligned} \tag{C7}$$

We can write the expression for the integrated photocurrent during the left-hand scan interval Q_L by noting that a positive error e for the right-hand scan is equivalent to a negative error for the left-hand scan. Thus,

$$Q_L = (IT/4) - \left[e^2 - e(2s - D + d) + (2s - D + d)^2/4 \right] IT/8sd. \tag{C8}$$

The track error signal is the difference between Q_L and Q_R. This imbalance is

$$\text{SIGNAL} = Q_L - Q_R = e\, IT\, (2s - D + d)/4\, sd. \tag{C9}$$

Further, we can determine what value of scan amplitude s leads to the highest sensitivity. Hence, through differentiation (∂ SIGNAL/ ∂ e) and by considering condition (1) above we find:

$$s\Big|_{\substack{\max \\ \text{sensitivity}}} = (D + d)/2. \tag{C10}$$

This leads to

$$\text{SIGNAL} = e\, IT/(D + d). \qquad \text{(electrons)} \tag{C11}$$

The signal noise of interest is made up of the total count of photoelectrons with zero track error. Let the mean square noise in signal = MSNS. Then

$$\text{MSNS} = k^2 \left[Q_R + Q_L \right] \Big|_{e = o} , \quad \text{(electrons)} \qquad \text{C12}$$

$$\text{MSNS} = k^2 \, ITD/2 \, (D + d) . \qquad \text{C13}$$

The total mean square noise is the sum of the signal and background shot noises, i.e.,

$$\sigma_n^2 = \text{MSNS} + T \, I_{bg} \, k^2/2 . \qquad \text{C14}$$

For the situation of negligible background and dark current, we may consider $\sigma_n = \sqrt{\text{MSNS}}$, and combine Equations C11 and C13 to determine the optimum tracker sensitivity.

$$\Phi \Big|_{\substack{\text{signal shot} \\ \text{noise limited}}} = k^2 \, D \, (D + d)/2 \, T\epsilon^2 . \quad \text{(electrons/sec)} \qquad \text{C15}$$

The condition of Equation C15 (i.e., $s = (D + d)/2$) precludes the use of this scan amplitude for continuous communications since for $e = 0$, there is no communications signal. We are more interested here in the condition $s = D/2$ which implies a 50% reduction in communications channel power at the scan extreme. This value of s leads to the following relationships:

$$\text{SIGNAL} = e \, IT/2D , \quad \text{(electrons)} \qquad \text{C16}$$

$$\text{MSNS} = k^2 \, (4 \, D - d) \, IT/8D , \qquad \text{C17}$$

$$\sigma_n^2 = \text{MSNS} + T \, I_{bg} \, k^2/2 , \qquad \text{C18}$$

$$\Phi \Big|_{\substack{\text{signal shot} \\ \text{noise limited}}} = k^2 \, D \, (4 \, D - d)/2 \, T^2 . \quad \text{(electrons/sec)} \qquad \text{C19}$$

D. PARTIAL CRUCIFORM SCAN WITH MEASUREMENT OF THRESHOLD CROSSING TIMES

This tracking technique is similar to that of Section C, except that instead of measuring charge difference as indicated in Equation C9, we measure threshold crossing time differences. Consider first the curve of Figure 2C, but with full modulation as shown in Figure 1D. Now consider the photocurrent after it traverses a low pass filter which smooths the points of slope changes (Figure 2D) so that we may approximate the non-zero slope portions of the curve with a sinusoidal form over the interval t_d where as before $t_d = d/v$. The maximum slope of the equivalent sine wave is

$$\text{max slope} = \pi f I, \qquad \text{D1}$$

where f is approximately equal to $(2\ t_d)^{-1}$. Thus we find the maximum slope (the best place for a threshold crossing measurement) to be $\pi I/2t_d$. The rms error Δ t in determining the time of a particular current level crossing is the ratio of the rms noise σ_n to the slope at the crossing. Hence

$$\Delta t = \sigma_n/\text{slope} = 2\sigma_n\ t_d/\pi I\ . \qquad \text{D2}$$

As indicated in Figure 1D, in order to obtain one track error sample, we can measure 4 threshold crossings. For Gaussian noise we will suffer one-half $(1/\sqrt{4})$ the error of one measurement. Hence the time error per sample is

$$\sigma_t = \Delta t/2 = \sigma_n\ t_d / \pi I\ . \qquad \text{(rms seconds)} \qquad \text{D3}$$

Consequently, the rms tracking error ϵ is determined from the velocity-time relationship and equation D3,

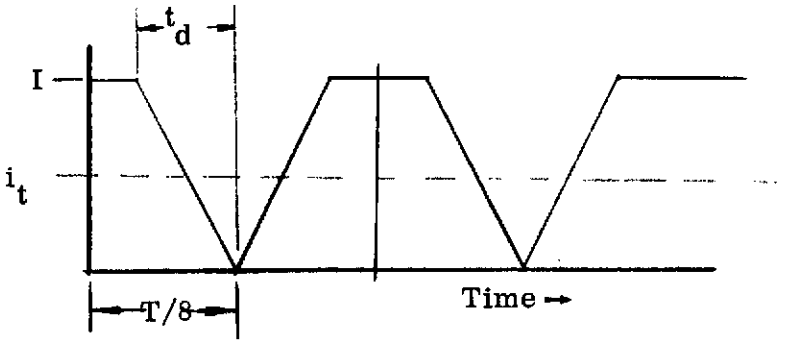

Figure 1D. Ideal Photocurrent Variations

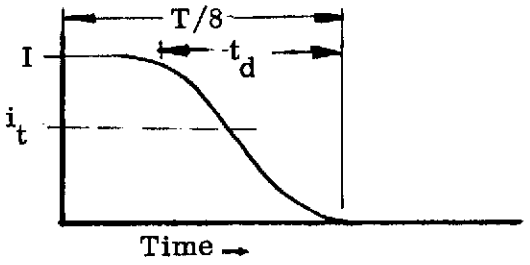

Figure 2D. Photocurrent Variation After Low Pass Filter

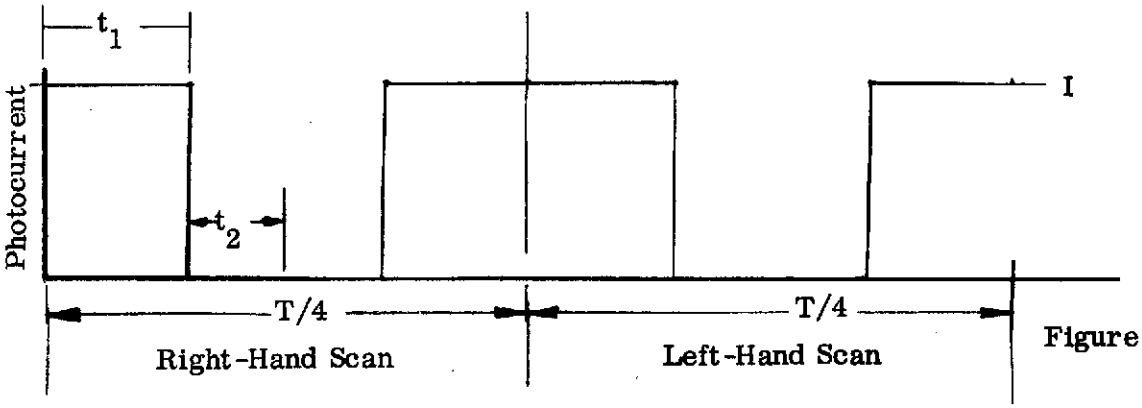

Figure 1E.

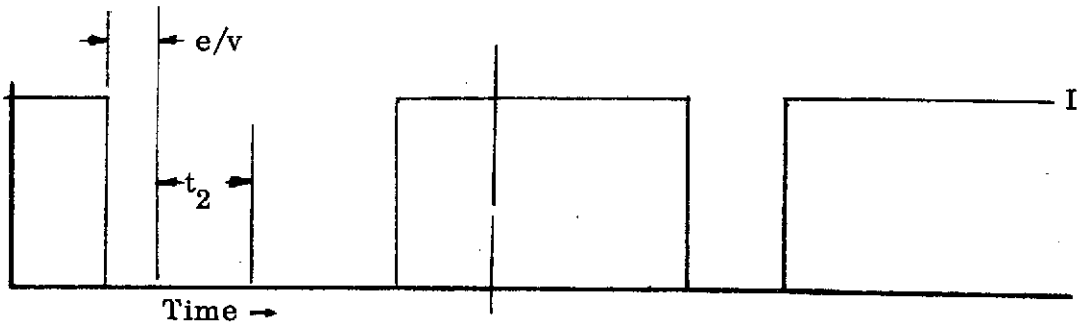

Figure 2E. Photocurrent Time Variation With Track Error e

$$\epsilon = v\,\sigma_t = d\,\sigma_t/t_d\,, \qquad \text{C4}$$

$$\epsilon = \sigma_n\, d/\pi I\,. \qquad \text{(inches)} \qquad \text{D5}$$

The rms noise σ_n (electrons/sec) is made up of contributions from many sources. As before, we are most interested in a signal shot noise limited tracker.

$$\sigma_n^2 = 2\,\Delta f\, k^2\,(I_{bg} + I/2) = k^2\,\Delta f\, I \Big|_{I_{bg} = 0}\,. \qquad \text{D6}$$

where Δf is the noise bandwidth. In order to use this scanning technique in the comparison we must express Δf in terms of the parameters already familiar. Referring to Figure 2D we note that a reasonably low value for Δf is $(\pi/2)/(2\,t_d)$. Hence it follows from the identities given above that

$$\Delta f \cong \pi v/4d. \qquad \text{D7}$$

Consequently, by combining Equations D5 and D6 we can determine the signal shot noise limited tracker sensitivity

$$\Phi \Big|_{\substack{\text{signal shot} \\ \text{noise limited}}} = \Delta f\,(k\,d/n\,\epsilon)^2\,. \qquad \text{(electrons/sec)} \qquad \text{D8}$$

If the bandwidth relationship given in D7 is accepted, then

$$\Phi \Big|_{\substack{\text{signal shot} \\ \text{noise limited}}} = 2\,sd\,(k/\epsilon)^2/\pi\,T. \qquad \text{D9}$$

E. "STANDARD" STAR TRACKER SCAN

What we consider a standard star tracker scan in this report is the limiting case in which the target electron image is much smaller than the sampling aperture size, i.e., $d/D \approx 0$. This situation, although not applicable to an integrated communications tracking receiver, is useful for comparison of relative sensitivities.

Figure 1E illustrates the time variations in photocurrent with zero track error. The transition in signal photocurrent as the infintessimal beacon electron image is swept across the edge of the sampling aperture is the full signal current I. Figure 2E shows that, if there exists a small track error e, the transition points will be moved in time (e/v) seconds, where v is the scan velocity. The charge Q_R measured during the right-hand scan is the product of photocurrent and time, i.e., $Q_R = 2\,I\,t_1$. From the definitions given previously and inspection of Figure 2E, we see that

$$t_1 = (D/2v) - ev, \qquad \text{E1}$$

$$vT = 8s, \qquad \text{E2}$$

$$Q_R = IT\,[\,D - 2\,e\,]/8s. \qquad \text{E3}$$

Likewise we note that $Q_L = IT\,[\,D + 2\,e\,]/8s.$ E4

Hence, the signal defined as the difference between the two measurements is

$$\text{SIGNAL} = Q_L - Q_R = IT\,e/2s,\ e \le D/2\,. \qquad \text{(electrons)} \qquad \text{E5}$$

The mean square signal shot noise MSSN is for $e = 0$,

$$\text{MSSN} = k^2\,[\,Q_R + Q_L\,], \qquad \text{E6}$$

$$= k^2\,IT\,D/4s.$$

For the more general situation we may include the noise effects of background photocurrent I_{bg} in the total mean square noise σ_n^2 ,

$$\sigma_n^2 = \text{MSSN} + k^2 I_{bg} T/2 . \qquad \text{E7}$$

Again, for the situation of negligible background and dark current, we can consider $\sigma_n = \sqrt{\text{MSSN}}$ and determine the tracker sensitivity

$$\Phi \Big|_{\substack{\text{signal shot} \\ \text{noise limited}}} = k^2 D\, s/T\, \epsilon^2 , \qquad \text{(electrons/sec).} \qquad \text{E8}$$

F. THE IDEAL OPTCOMM TRACKER

In the analyses above we have used particular assumptions so as to compare a number of scan techniques on a common basis. One question we might ask ourselves at this point is how these systems compare with an ideal optcom tracker sensor. This ideal sensor should use all the signal photoelectrons all the time for both tracking and communications. Such is not true of any of the systems described above, or of any tracker using an image dissector photosensor.

The concept of an ideal tracker photosensor is complicated by the variety of target image configurations to be dealt with. Hence, for each image distribution there is a corresponding sensor, described somewhat in the manner of a two-dimensional matched filter. However, for our present purposes we are considering square images. This simplification leads to a detector much like a four quadrant photosensor. The track error signal is

$$\text{SIGNAL} = 2\,I\,e/d\,, \qquad \text{F1}$$

and the mean square noise σ_n^2 is

$$\sigma_n^2 = 2\,k^2\,(I + I_{bg})\,\Delta f\,. \qquad \text{F2}$$

Of course, our ideal detector performs better with an ideal spectral filter in front of it, i.e., $I_{bg} = 0$.

Hence, by combining the last two relationships and employing the terminology used previously, we can determine the ideal tracker sensitivity.

$$\Phi \Big|_{\substack{\text{signal shot} \\ \text{noise limited}}} = (k\,d/\epsilon)^2\ \Delta f/2\,. \qquad \text{F3}$$

If we consider the sample period T to be equal to $(2\,\Delta f)^{-1}$, then

$$\Phi \Big|_{\substack{\text{signal shot} \\ \text{noise limited}}} = (k\,d/\epsilon)^2/4T. \qquad \text{(electrons/sec)} \qquad \text{F4}$$

G. SCAN PATTERN COMPARISON

Table 1G reviews results of the previous analyses. In the third column of the table is listed the track scan shot noise limited sensitivity.[6] We have divided each by the common factor $(k/\epsilon)^2/T$ since our purpose here is comparative analysis. Note that the conical scan is a factor of 4 away from the ideal. Also, the partial cruciform time measurement scan is next best and can be quite good for small track scan amplitudes (and sampling apertures).

TABLE 1G. TRACK SCAN LIMITED SENSITIVITIES

SCAN TYPE	EQUATION NO.	SIGNAL SHOT NOISE LIMITED SENSITIVITY $[\Phi \div (k/\epsilon)^2/T]$	COMMENTS
Conical	B11	d^2	50% average power for communications
Partial Cruciform Integration, Optimum	C15	$D(D+d)/2$	No Communications
Partial Cruciform Integration Optcomm	C19	$D(4D-d)/2$	50% power for communications
Partial Cruciform Time Measurement	D9	$2sd/\pi$	Up to 50% power for communications
"Standard" Star Tracker	E8	sD	Infinitesimal Image, No Continuous Communications
"Ideal" Optcomm Tracker	F4	$d^2/4$	100% Image Power Available for Communications

TABLE 2G. COMPARISON OF TRACK SCAN PERFORMANCE LIMITS

SCAN TYPE	SLEW RATE LIMIT (SRL)	RELATIVE POTENTIAL SLEW RATE RPSR α SRL/T	RELATIVE TRACKER PERFORMANCE (RPSR/Φ)
Conical	d	1/d	d^{-3}
Partial Cruciform Integration, Optimum	.707D	$1.41/(D + d)$	$2.82/(D + d)^2 D$
Partial Cruciform Integration Optcomm	.707D	$1.41/(4D - d)$	$2.82/(4D - d)^2 D$
Partial Cruciform Time Measurement	.707D	1.11 D/sd	$1.74 D/s^2 d^2$
"Standard" Star Tracker	.707D	1/s	$1/s^2 D$

However, sensitivity is seldom the only criterion for selecting a track scan configuration. Another important tracker parameter is slew rate, the speed (inches/second) that the tracker can follow a moving target image. In the second column of Table 2G we find the geometric factor which limits a tracker's slew rate. We use the factor ($\sqrt{2}/2$) D for the cruciform track scan limits since a target moving diagonally to the tracker axes will be lost if it moves faster than this in one scan period. However the slew rates along the axes may be greater.

If we consider the slew rate limit in a sample period and divide by the period length (as calculated by the equations listed in Table 1G) we have the relative potential slew rates of the various tracker schemes. Note here that again the partial cruciform time measurement track scan performs well, with a potential speed 11% greater than that of the conical scan.

The last column of Chart 2G lists a factor indicative of tracker performance, i.e., the quotient of potential slew rate and sensitivity. Since normally we wish to work with the condition that $d << D \leq s$, the conical track scan seems to be worthy of first consideration. However the partial cruciform time measurement scan does best in the range where $D \approx d$. Hence with the target size only slightly smaller than the sampling aperture, the two track scan configurations are competitive, but the conical scan allows the designer to have that performance while choosing a larger sampling aperture size based on some other criterion.

Actually we are being rather conservative in rating the conical scan slew rate limit in 2G. This type of scan, if properly demodulated, offers an error signal for slew track errors as large as D/2, although the signal is nonlinearly related to the target-sampling aperture separation. Hence tradeoff studies of the conical versus various forms of the cruciform scan for the usual parameter values can indicate much more advantage to the conical scan than shown in Table 2G.

APPENDIX B
THE CONICAL SCAN TRACKER

A. SCOPE AND INTRODUCTION

In this report we discuss an image dissector (ID) tracker system that uses a conical or circular track scan. This conical scan (CS) tracker functions much like other ID trackers. However, interest has grown recently[1] in the CS tracker since a comparative analysis[2] of ID tracker schemes indicated that it had a number of unique advantages (and drawbacks). This comparative analysis was directed towards trackers useful for optical communications systems, but the results are also valid for other applications.

We present a tutorial approach here, deriving during the analysis what we hope are all the fundamental equations required to build a system model. Because of similarities we pass over subjects such as the raster search, acquisition threshold, mode control, and other subsystems common to all ID trackers.

Section B is concerned with the dependency of sensor photocurrent on the target intensity distribution, sampling aperture, and time parameters. We use the term target or beacon image here interchangeably as the distribution of photoelectrons at the photocathode, the center of which is to be tracked. The final relationship B12 is valid for any rotationally symmetric image.

Section C discusses the treatment of track error information on the anode photocurrent by the track preamplifer and demodulator. C13 describes the track error signal as a function of circuit parameters.

Section D treats the same circuit elements from the standpoint of system noise. All noise sources are included with the restriction that they be white.

We discuss the tracker as a feedback system in Section E. E4 describes the tracker transfer function. This equation relates tracker output error to target image location on the ID photocathode. We then continue the transfer function approach to determine the fluctuations E20 at the tracker output resulting from noises considered previously.

In Section F we derive the CS tracker sensitivity F5. In its simplest form F9B we describe the potential performance of a shot noise limited conical scan tracker.

At first we intended that Section G be a design study for both a demonstrative exercise of the previous analysis and a specification for a tracker application. However, this proved to be rather more lengthly and less desired than expected, and we have substituted some comments on consistent and optimum CS tracker system design.

Section H is a list of references and explanatory notes.

Since we derived most of these equations about two months prior to writing the report, this author had a little difficulty in recalling the meanings of specific symbols (there are about 45). For this reason we have included as Section I a listing and explanation of symbols.

B. CALCULATION OF THE TRACKER PHOTOCURRENT

Referring to Figure 1B, we note a plane view of the image dissector (ID) photocathode. The large circle of diameter D represents the image of the sampling aperture, displaced a distance s from the ID electrical center. The focused image of the beacon has an equivalent diameter d, and is swept (or scanned) on a circle of radius A, the center of which is displaced ϵ from the sampling aperture center. This is of course just a convenient fallacy, since in reality the beacon image is not moved on the photocathode and the image of the sampling aperture is. We call the vector $\vec{\epsilon}$ the track error. Noting that the detected current from the ID photosensor is proportional to the beacon image photocurrent passing through the sampling aperture we now calculate that dependence on the track error $\vec{\epsilon}$.

Consider the vector diagram of Figure 2B. The track error[3] in polar coordinates consists of a length ϵ and an angle ϕ. The conical scan is described by the rotating vector $\vec{A}$ of length A and rotating angle ωt. Thus:

$$\vec{\epsilon} = \epsilon\, e^{i\phi}, \qquad \text{B1}$$

$$\vec{A} = A\, e^{i\omega t}. \qquad \text{B2}$$

The location of the center of the beacon image relative to the center of the sampling aperture is the vector sum of $\vec{\epsilon}$ and $\vec{A}$. We are interested in the length of a vector $\vec{\delta}$ shown in Figure 2B. This length is the instantaneous displacement of the center of the beacon image from the periphery of the

Figure 1B. Photocathode Geometry

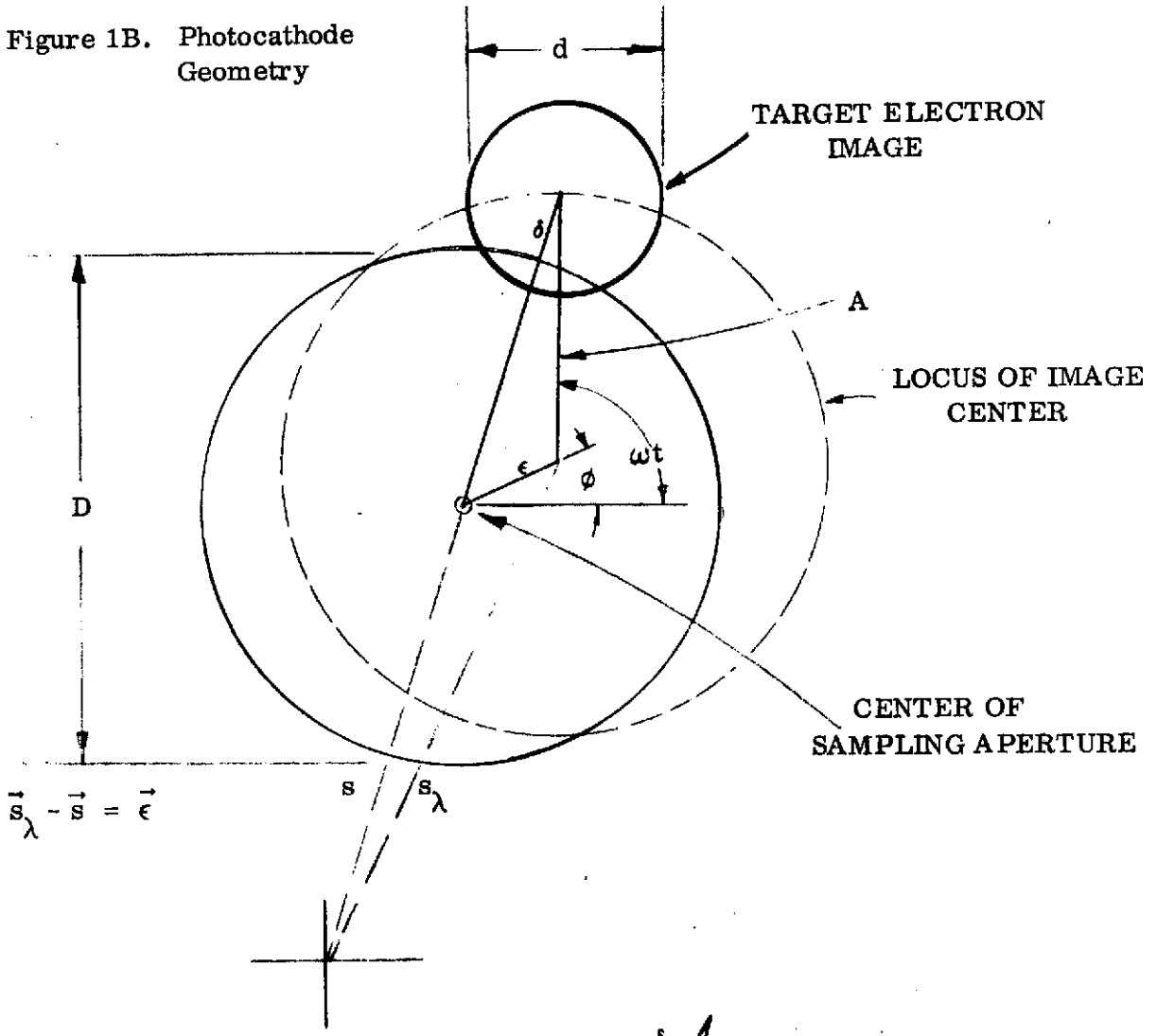

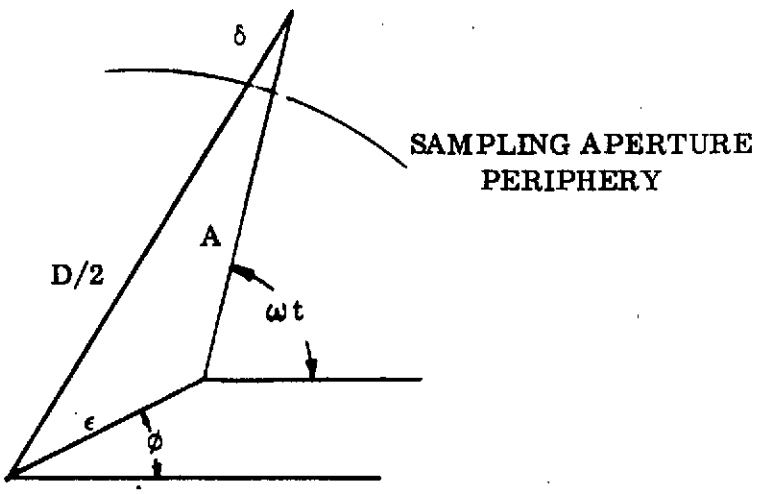

Figure 2B. Photocathode Vector Diagram

sampling aperture. We note that $\vec{\delta}$ and a parallel vector of length D/2 make up a triangle with $\vec{\epsilon}$ and $\vec{A}$. Hence:

$$\overrightarrow{\delta + D/2} = \epsilon\, e^{i\phi} + A\, e^{i\omega t} \quad . \tag{B3}$$

Also, since $\vec{\delta}$ and $\vec{D/2}$ are parallel

$$\left| \overrightarrow{\delta + D/2} \right| = \left| \vec{\delta} + \overrightarrow{D/2} \right| = \delta + D/2 \, . \tag{B4}$$

Consequently, we can find by simplifying B3 that

$$(\delta + D/2)^2 = \epsilon^2 + A^2 + 2A\epsilon \cos(\omega t - \phi) \, . \tag{B5}$$

At this point we must make an approximation in order to preserve the simplicity of modeling a linear system. This approximation is that the scan semiamplitude A is much larger than the track error ϵ, i.e.,

$$A^2 >> \epsilon^2 \quad . \tag{B6}$$

The relationship B6 permits us to write B5 as

$$\delta = -D/2 + A + \epsilon \cos(\omega t - \phi) \quad . \tag{B7}$$

It is not difficult to show that for the typical circularly symmetrical beacon image, the tracker sensitivity is maximized when the conical scan amplitude is half the sampling aperture diameter.[4] With this special case B7 becomes

$$\delta = \epsilon \cos(\omega t - \phi) \, ; \qquad (A = D/2). \tag{B8}$$

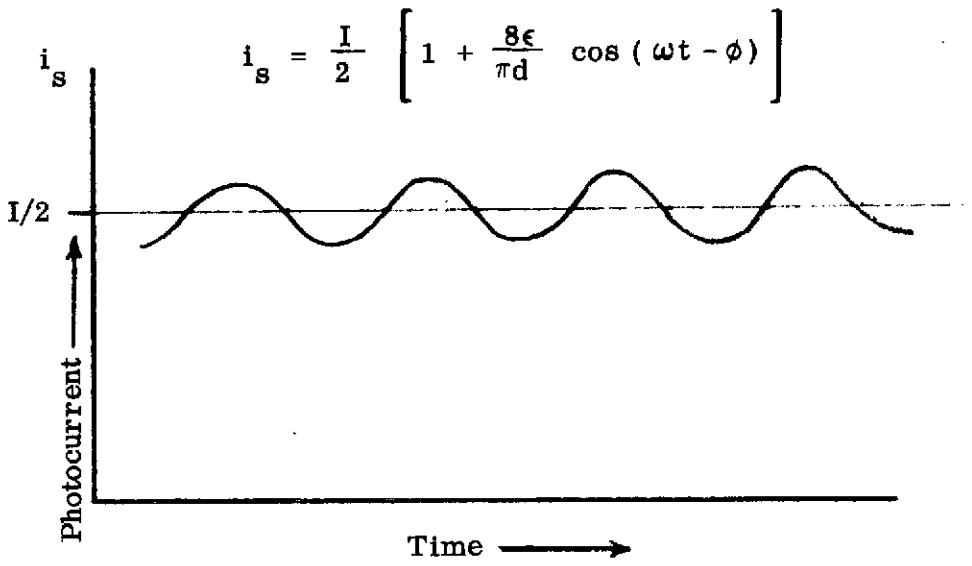

Figure 4B. Photocurrent Time Variation With Track Error ϵ

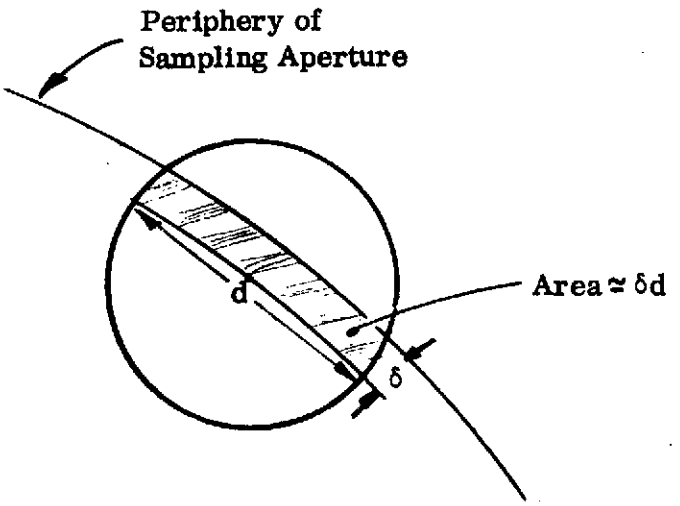

Figure 3B. Swept Image Area with Image Translation δ

At this point the definition of image diameter d should be reviewed. This subject is discussed in the notes at the back of this report.[5]

Now the equivalent circular (pill box distributed) beacon has an area $\pi\, d^2/4$. For a small track error ϵ, δ is also small, and the resultant variations in the area swept by the periphery of the scanning aperture is approximated by the product $\delta\, d$ as shown in Figure 3B. If the total photocurrent generated by the beacon image is I (electrons/second), the signal photocurrent i_s is that fraction of the image passing through the sampling aperture. The beacon image area of overlap is

$$\text{Area} = 1/2\,(\pi\, d^2/4) + \delta\, d\,, \qquad \text{B9}$$

and the fractional area is

$$\text{Fractional Area} = 1/2 + 4\,\delta / \pi d\,. \qquad \text{B10}$$

The instantaneous photocurrent i_s is equal to the product of the image photocurrent I and the fractional image area, thus:

$$i_s = \frac{I}{2}\,(1 + 8\,\delta / \pi d)\,, \quad \text{(amps or electrons/sec).} \qquad \text{B11}$$

By employing the relationship B8 we find that

$$i_s = \frac{I}{2}\left[1 + \frac{8\,\epsilon}{\pi\, d}\cos(\omega t - \phi)\right]\,. \qquad \text{B12}$$

Figure 4B depicts the photocurrent-time relationship of B12 for a small track error ϵ.

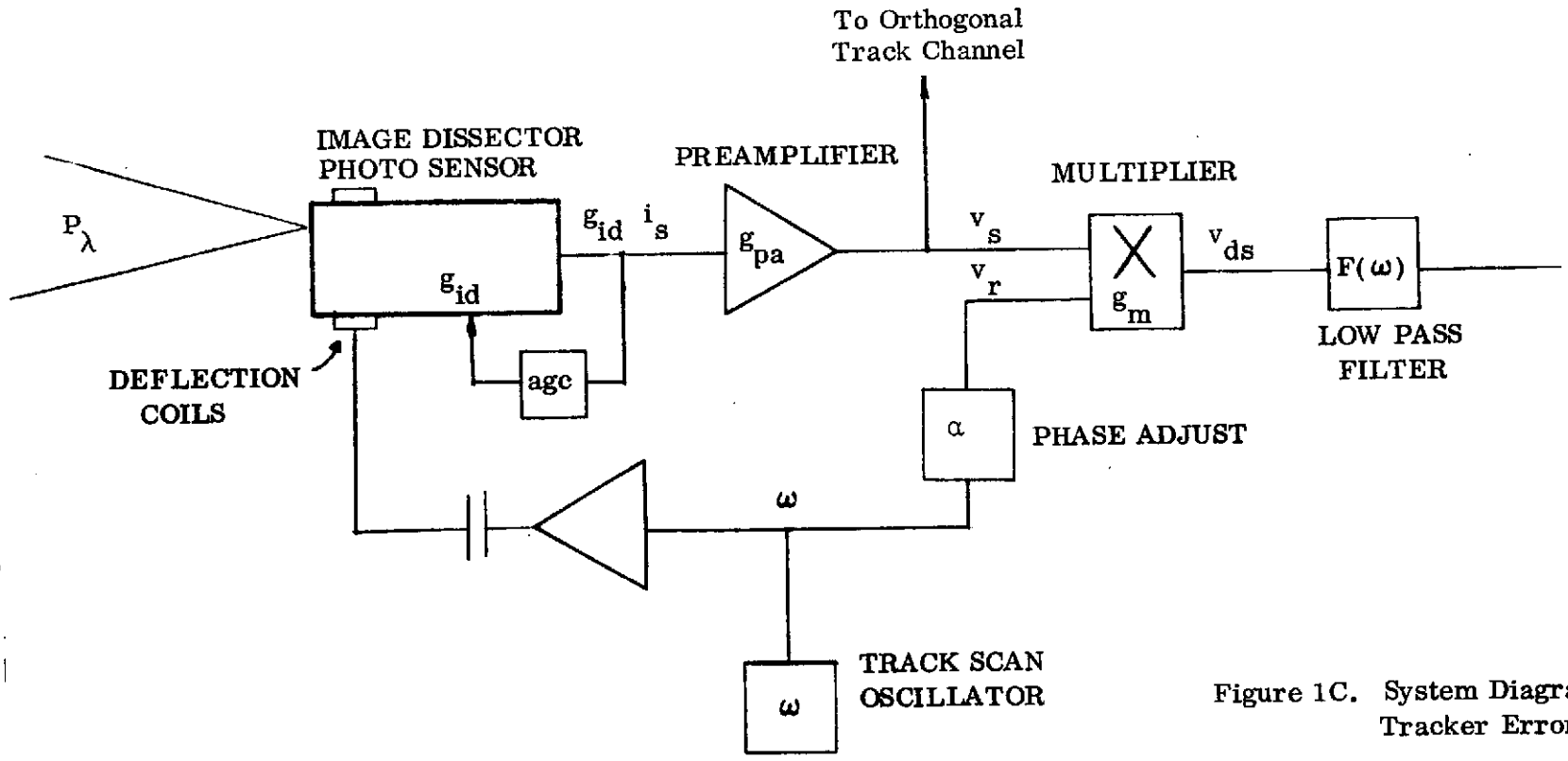

Figure 1C. System Diagram for Tracker Error

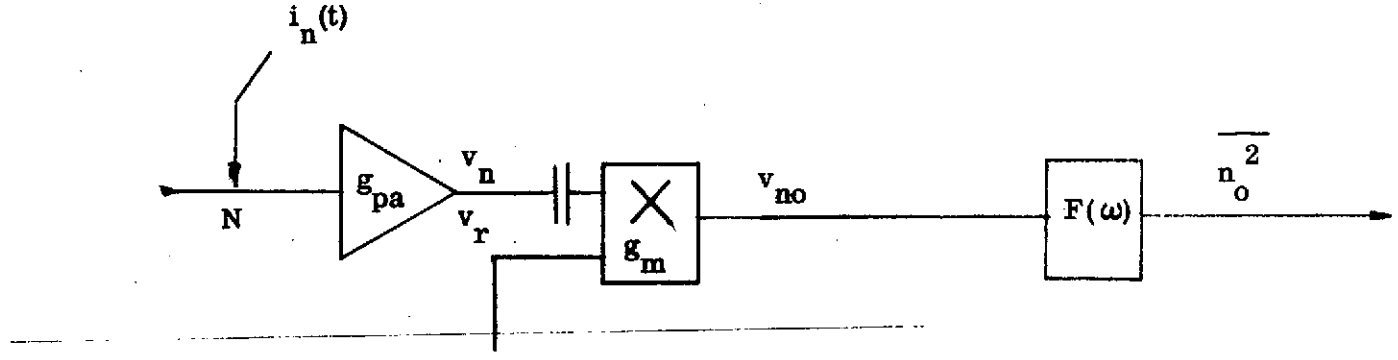

Figure 1D. Noise Through The Demodulator

C. TRACK ERROR DETECTION

Equation B12 describes the instantaneous photocurrent for an arbitrary track error vector (ϵ , ϕ) as depicted in Figure 1B. In this section we discuss demodulation of the beacon photocurrent i_s in order to extract a signal proportional to the track error.

Referring now to Figure 1C, we see that the photocurrent is first increased by the electron multiplier in the ID photosensor (gain = g_{id}) and then changed to the signal voltage v_s by the preamp (gain = g_{pa} , volts/electron/sec or v/amp),

$$v_s = g_{pa}\ g_{id}\ i_s \quad . \qquad \text{(volts)} \qquad \text{C1}$$

At this point the signal is passed to two similar demodulator channels in order to obtain output errors in Cartesian coordinates.

As Figure 1C indicates, a multiplier (gain = g_m) synchronously demodulates[6] the signal v_s with a reference v_r. The multiplier output is the demodulated signal v_{ds}. The oscillator (angular frequency = ω) generates both the reference v_r and the track scan waveforms. From the multipler we find

$$v_{ds} = g_m\ v_r\ v_s \quad . \qquad \text{(volts)} \qquad \text{C2}$$

If the preamp is AC coupled, we find from B12 that

$$v_s = 4\, g_{pa}\ g_{id}\ I\ \epsilon\ \cos\ (\omega t - \phi)\ /\ \pi d \, . \qquad \text{C3}$$

Let the reference be described by

$$v_r = a_r \cos(\omega t + \alpha), \quad \text{volts} \qquad \text{C4}$$

where α is some small phase error in the reference. Then we see that

$$v_{ds} = 2 a I e \cos(\omega t - \phi) \cos(\omega t + \alpha), \quad \text{volts} \qquad \text{C5}$$

where

$$a = 2 g_{pa} g_{id} g_m a_r / \pi d . \quad \text{(volts/amp inch).} \qquad \text{C6}$$

With the aid of the identity

$$2 \cos(\omega t - \phi) \cos(\omega t + \alpha) = \cos(\phi + \alpha) + \cos(\phi + \alpha - 2\omega t), \qquad \text{C7}$$

we find v_{ds} to be composed of two spectral components:

Baseband: $a I \epsilon \cos(\phi - \alpha)$, (volts) C8

At 2ω : $a I \epsilon \cos(\phi + \alpha - 2\omega t)$. C9

Also, because of the imperfections of the multiplier there will be some residue amplification at the frequency ω. However, a low-pass filter can effectively remove all but the baseband signal of C8.

The displacement error we are interested in measuring in this channel is the component of $\vec{\epsilon}$ along the "x" axis. The size of this error (refer to Figure 1B) is $\epsilon \cos \phi$.

Thus we see that a phase error α in the reference signal v_r is equivalent to a rotation error in the tracker. Let e be the tracker error along the "x" axis. Then we can write the baseband error signal v_e:

$$e = \epsilon \cos \phi , \qquad \text{(inches)} \qquad \text{C10}$$

$$v_e = a\, I\, e \left[\cos \alpha + \sin \alpha \tan \phi \right] . \qquad \text{(volts)} \qquad \text{C11}$$

Equations C8 and C11 are used for analyzing the effects of phase errors in the reference v_r. We may note that for the condition $\alpha = 90^{\circ}$, we have the track error signal for the "y" axis.

The detected image power can vary because of changes in range or signal scintillations. Consequently, the resultant beacon anode current is not a reliable constant unless we incorporate an automatic gain control into the system. The ratio of the variations in the output I_{out} to the variations in the input I_{in} of an AGC'd amplifier is the AGC transfer function[7]

$$\Delta I_{out} / \Delta I_{in} = \frac{K_1}{1 + K_2\ G(\omega)} . \qquad \text{C12}$$

where K_1 and K_2 are constants, and $G(\omega)$ is the response of a simple low-pass filter. At low frequencies $G(\omega)$ is very large and there is little variation in I_{out}. The action of the AGC is to keep the product $g_{id}\, g_{pa}\, I$ constant. We shall discuss later in Section G4 the significance to system performance in controlling the values of g_{id} and g_{pa}.

Referring again to Figure 1C we note that the signal output from the low pass filter is the product of v_e from C11 and the filter function $F(\omega)$. For the condition of zero reference error this signal is v_{tr}:

$$v_{tr} = a\,I\,e\;F(\omega). \qquad \text{(volts)} \qquad \text{C13}$$

This voltage v_{tr} is used in a feedback loop to drive the track error e to zero.

D. NOISE

Referring to Figure D1 we let $i_n(t)$ be the sum of all the system additive noise currents referenced to the preamp input. We assume that all these current fluctuations are white (Gaussian) caused by background radiation, current shot noise, Johnson noise, etc.

Let the spectral density ($amps^2$/hertz) of the mean square noise be N.

Then:

$$N = \overline{i_n^2} = \overline{v_n^2} / g_{pa}^2 , \qquad (amps^2/hertz) \qquad \text{D1}$$

where $\overline{v_n^2}$ is the mean square spectrum ($volts^2$/hertz) of the noise into the multiplier, and the bar signifies a time average. The term v_n can be considered to be made up of two independent statistical components, n_c and n_s, out of phase but with the same characteristics:

$$v_n = n_c \cos \omega_n t - n_s \sin \omega_n t, \qquad volts/\sqrt{hertz} \qquad \text{D2}$$

where

$$g_{pa}^2 N = \overline{v_n^2} = \overline{n_c^2} = \overline{n_s^2} \; ; \; \overline{n_c n_s} = 0 . \qquad \text{D3}$$

The multiplier output is v_{no}, where

$$v_{no} = g_m v_r v_n$$

$$= g_m a_r \cos \omega t \, [n_c \cos \omega_n t - n_r \sin \omega_n t]. \qquad \text{D4}$$

The mean square output voltage spectrum is

$$\overline{v_{no}^2} = \overline{(g_m a_r n_s \cos \omega t)^2} +$$

$$\overline{g_m^2 a_r^2 (n_c^2 - n_s^2) \cos^2 \omega t \cos^2 \omega_n t} \quad , \qquad \text{D5}$$

which is equivalent to

$$\overline{v_{no}^2} = g_{pa}^2 g_m^2 a_r^2 N \overline{\cos^2 \omega t} \, . \qquad \text{D6}$$

We are interested in the noise power spectrum about baseband which is simply

$$\overline{v_{no}^2} = g_{pa}^2 g_m^2 a_r^2 N/2 \, . \quad (\text{volts}^2/\text{hertz}) \qquad \text{D7}$$

We can integrate D7 over the frequencies of interest to determine the total noise power. If the low-pass filter of figure 1D is described by the function $F(\omega)$ then the output total mean square noise $\overline{n_o^2}$ is

$$\overline{n_o^2} = \int_o^\infty df \; \overline{v_{no}^2} \; |F(\omega)|^2 \, . \quad (\text{volts}^2) \qquad \text{D8}$$

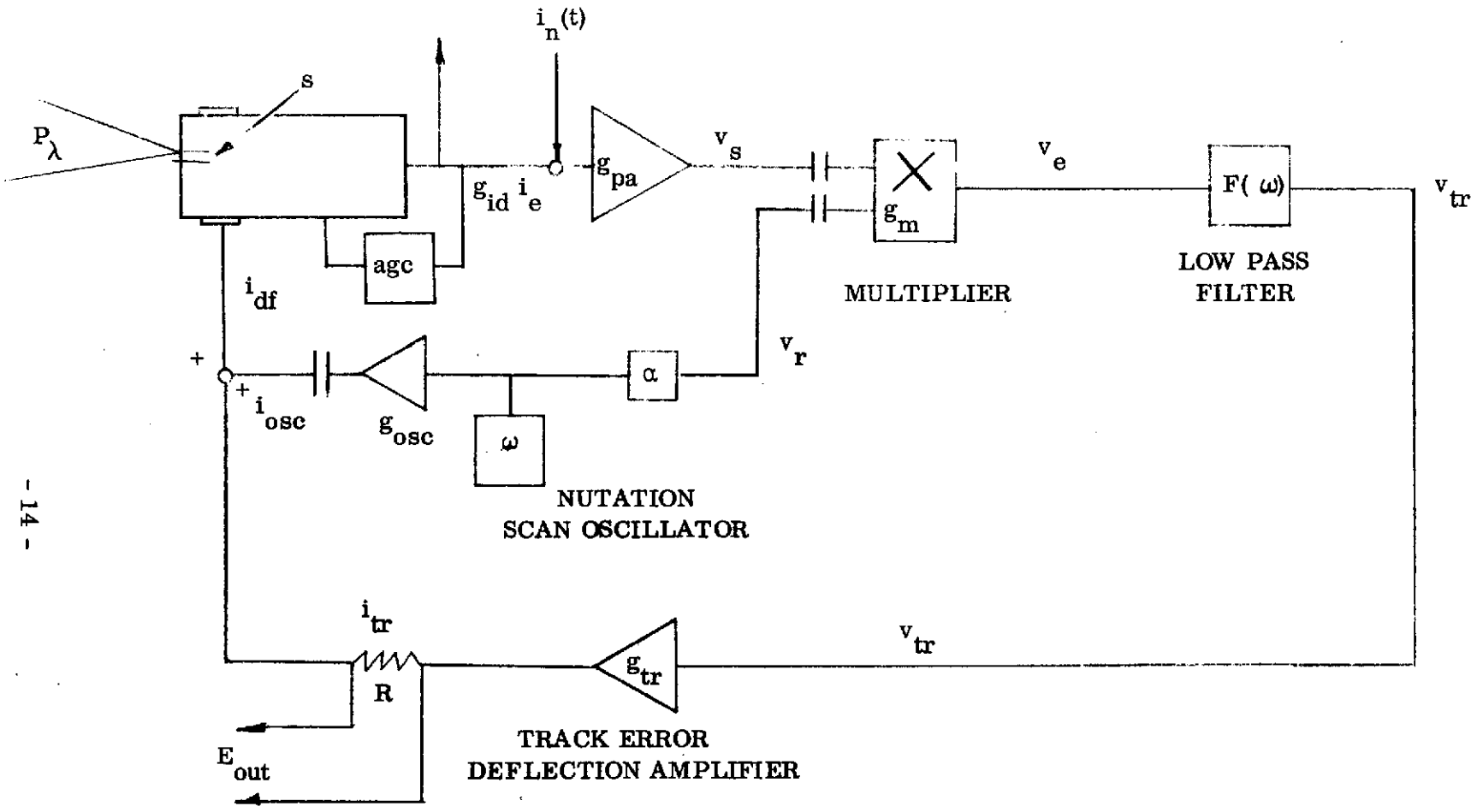

Figure 1E. Conical Scan Tracker Diagram

Since $\overline{v_{no}^2}$ is assumed "white" and not a function of frequency we can write

$$\overline{n_o^2} = g_{pa}^2 \; g_m^2 \; a_r^2 \; (N/2) \int_o^\infty df \; |F(\omega)|^2 . \quad (volts^2) \qquad D9$$

It is sometimes convenient to define a total mean square noise relative to the preamp input as

$$\overline{n^2} = \int_o^\infty df \, N \, | \, F(\omega) \, |^2 \quad , \qquad (amps^2) \qquad D10$$

so that the filter noise output is given by

$$\overline{n_o^2} = g_{pa}^2 \; g_m^2 \; a_r^2 \; \overline{n^2} \; / \, 2 \quad . \qquad (volts^2) \qquad D11$$

E. TRACKER SYSTEM TRANSFER FUNCTIONS

Figure 1E is a diagram which includes all the functions discussed previously. The beacon's radiant power P_λ (watts) is converted to photo-current I. An oscillator at frequency ω (radians/sec) generates the conical scan through a current amplifier (gain = g_{osc}). The resulting variations in the signal current are converted into a voltage v_s. Capacitor symbols in the figure represent AC coupling.

The error voltage v_s is synchronously demodulated with a reference v_r to obtain v_e. By passing v_e through the low-pass filter $F(\omega)$ we obtain the track correction voltage v_{tr}. Deflection coil track current i_{tr} is generated from v_{tr}. This current is summed with the conical scan deflection current i_{osc}

to form the total deflection current i_{df}. Tracker error output E_{out} is derived from a current sampling resistor.

Referring again back to Figure 1B we note that for a track error e along the "x" axis only

$$e = s_\lambda - s , \qquad \text{(inches)} \qquad \text{E1}$$

where s_λ is the distance of the beacon image center (averaged over a scan cycle) from the ID tube electrical center. From C13 and Figure 1E we see that

$$i_{tr} = a g_{tr} \; I \; F(\omega) \; e . \qquad \text{(amps)} \qquad \text{E2}$$

Displacement s of the scanning aperture is proportional to the deflection coil current i_{tr}

$$s = g_{df} \; i_{tr} . \qquad \text{(inches)} \qquad \text{E3}$$

By combining the last three equations we can determine the tracker transfer function

$$E_{out}/s_\lambda = Ri_{tr}/s_\lambda = Ra \, g_{tr} \, I \, F(\omega) \left[1 + g_{oL} \right]^{-1} \qquad \text{E4}$$

where $g_{oL} = a \, I \, g_{df} \, g_{tr} \, F(\omega)$ = open loop gain. E5

In order to analyze the tracker performance considering noise we assume that the noise effects are independent of the beacon image position. Then we may set s_λ equal to zero so that E1 becomes

$$\tilde{e} = - \tilde{s} . \qquad \text{(inches)} \qquad \text{E6}$$

Spectral noise at the input to the preamp is the sum of the spectral contributions from the photosensor $\tilde{e}$ and the additive noise in $i_n(t)$ in D1. Referenced to the output of the multiplier these two fluctuations are v_{no} from D7 and a $I\tilde{e}$ from C11, where $\tilde{e}$ is interpreted here as noise-caused. Hence, prior to the low-pass filter the total instantaneous spectral noise v_{nt} is

$$\tilde{v}_{nt} = v_{no} + a I \tilde{e} \quad . \qquad \text{(volts)} \qquad \text{E7}$$

Now we know that

$$\tilde{v}_{tr} = v_{nt} F(\omega) \quad , \text{ and} \qquad \text{E8}$$

$$\tilde{s} = g_{df} g_{tr} \tilde{v}_{tr} \qquad \text{(inches)} \qquad \text{E9}$$

By combining E6 through E9 we find

$$\tilde{s} = g_{df} g_{tr} F(\omega) v_{no} (1 + g_{oL})^{-1} \qquad \text{E10}$$

where the open loop gain g_{oL} was defined in E4. In E10 both $\tilde{s}$ and v_{no} are random variables representing spectral noise. The total noise power in track position σ_s^2 is the integral of $\overline{s^2}$ taken over the frequency spectrum:

$$\sigma_s^2 = \int_0^\infty \overline{s^2} \, df \quad , \qquad \text{(inches}^2\text{)} \qquad \text{E11}$$

so that

$$\sigma_s^2 = g_{df}^2 \, g_{tr}^2 \int_0^\infty df \; \overline{v_{no}^2} \; \left| \frac{F(\omega)}{1 + g_{oL}} \right|^2 \quad . \qquad \text{E12}$$

We can write E12 in terms of the mean square noise spectral density N discussed in Section D. By combining E12 with D7,

$$\sigma_s = g_{pa}\, g_m\, a_r\, g_{df}\, g_{tr}\, F_n \sqrt{N/2}\,, \qquad \text{(inches)} \qquad \text{E13}$$

where

$$F_n^2 = \int_o^\infty df \left| \frac{F(\omega)}{1 + g_{oL}} \right|^2 . \qquad \text{(hertz)} \qquad \text{E14}$$

If we wish to determine the rms noise output σ_n from the sampling resistor of Figure 1E we use

$$\sigma_s = g_{df}\, \sigma_n / R \qquad \text{E15}$$

to write

$$\sigma_n = C\, F_n \sqrt{N/2}\,, \qquad \text{(volts)} \qquad \text{E16}$$

where the constant C is equal to $R\ g_{pa}\ g_m\ a_r\ g_{tr}$ (ohms).

Equations E4 and E15 are most useful in tracker design.

The integral in E14 can be evaluated for most applications by considering $F(\omega)$ to be an ideal[8] integrator.

Then

$$F(\omega) = g_i\, (j\omega)^{-1} \qquad \text{E17}$$

$$\left| \frac{F(\omega)}{1 + g_{oL}} \right|^2 = \left| \frac{g_i}{\omega_o + j\omega} \right|^2 = \frac{g_i^2}{\omega_o^2 + \omega^2} .$$

where $\omega_o = a\, I\, g_i\, g_{df}\, g_{tr} = 2\pi f_o$ = break frequency. $= \omega_{g_{OL}}$. E18

Then E14 becomes

$$F_n^2 = g_i^2 \int_o^\infty df\, (\omega_o^2 + \omega^2)^{-1} ,$$

$$F_n^2 = g_i^2 / 4\omega_o . \qquad \text{(radians/sec)} \qquad \text{E19}$$

Hence, for the loop filter described by E17, Equation E16 leads to the mean square output noise

$$\sigma_n^2 = c^2\, g_i^2\, N / 8\, \omega_o \qquad (\text{volts}^2) . \qquad \text{E20}$$

F. Reduced Tracker Analysis

Equations E4 and E20 described signal and noise across the sampling resistor of Figure 1E. By properly combining these two we can determine the noise equivalent input (or accuracy) of the conical scan tracker. The loop filter function of E4 can be written with E17 as

$$F(\omega)\, (1 + g_{ol})^{-1} = g_i / (\omega_o + j\, \omega) , \qquad \text{F1}$$

where ω_o is defined as in E18.

Within the frequency response, i.e., the break frequency, F1 has the approximate value g_i / ω_o and hence in this region we can approximate E4 with

$$E_{out} = s_\lambda\, R\, a\, I\, g_{tr}\, g_i / \omega_o . \qquad \text{(volts)} \qquad \text{F2}$$

Now let us take the mean square of both sides of F2, and interpret $\overline{E_{out}^2}$ as the mean square signal MSS related to a mean square beacon image position $\overline{s_\lambda^2}$. Hence

$$MSS = \overline{s_\lambda^2} \left[a\ g_{tr}\ g_i\ RI / \omega_o \right]^2 . \qquad F3$$

By setting the mean square signal in F3 equal to the mean square noise of E20 we may interpret $\overline{s_\lambda^2}$ as the mean square noise equivalent distance (or accuracy) σ_e^2 along one coordinate axis on the photocathode.

We might mention here that the magnitude of the total mean square track error σ_ϵ^2 is the vector sum of the mean square track errors of both the "x" and the "y" axis channels. Assuming these two are equal we have

$$\sigma_\epsilon^2 = 2\ \sigma_e^2 \qquad (\text{Inches})^2 , \qquad F4.$$

Now, by combining E20 with F3 we find that

$$i^2 = C^2\ N \omega_o / 8\ \sigma_e^2\ R^2\ a^2\ g_{tr}^2 ,$$

$$i = (\pi\ d / 4 \sigma_e\ g_{id})\ (N \omega_o / 2)^{\frac{1}{2}} \qquad (\text{amps}) \qquad F5$$

Equation F5 relates[9] the target photocurrent i, break frequency ω_o , noise spectral density N, and single axis track error σ_e .

The noise power spectral density N is made up of the noise in the photocurrent (shot type) and the system additive internal noise σ_{int}^2 . Thus

$$N = 3.2 \times 10^{-19}\ k^2\ [\, i_{dc} + i_{bg} + I/2\,]\ g_{id}^2 + \sigma_{int}^2 \qquad \text{F 6}$$

$$(\text{amps}^2/\text{hertz}),$$

or as written in natural units often preferred in analysis,

$$N = 2\,k^2\ [\, i_{dc} + i_{bg} + I/2\,]\ g_{id}^2 + \sigma_{int}^2 \qquad \text{F7}$$

$$(\text{electrons}^2/\text{sec}^2/\text{hertz}).$$

In the equations above

I = beacon image photocurrent in amps or electrons/sec,

i_{dc} = photosensor dark current in the same units,

i_{bg} = system background caused photocurrent,

k = dynode and amplifier noise factor ($k > 1$), (unitless).[10]

The units of σ_{int} are, of course, the same as those of I. Two cases are of greatest interest: the shot noise limited case and the background limited case. For the signal shot noise limited situation F7 is

$$N = k^2\ g_{id}^2\ I \qquad \text{F8}$$

and so F5 reduces to

$$I = \pi\ f_o\ (\pi\ k\ d/\ 4\ \sigma_e)^2, \qquad \text{F9A}$$

$$I = \omega_o\ (\pi\ k\ d/\ 4\ \sigma_\epsilon)^2. \qquad \text{(photoelectrons/sec)} \qquad \text{F9B}$$

The last equations are perhaps the most useful in this report since they allow us to make quick estimates of tracker capability.

The second case of interest occurs when the tracker performance is limited by its own internally generated noise. For this situation we see that $N = \sigma_{int}^2$ and that F5 reduces to

$$i = (\pi d \sigma_{int} / 4 g_{id} \sigma_{\epsilon}) \sqrt{\omega_o} \quad . \qquad \text{F10}$$

The units of F10 may be either amps or electrons/sec.

G. COMMENTS

In Section F we essentially completed our analysis of the conical track scan image dissector tracker. We turn now to a number of peripheral subjects that should be considered in the preliminary design of such a tracker.

G1. All image dissector trackers are similar so why develop one using a conical track scan? The answer to this (discussed in a report comparing different ID trackers) is that the CS tracker offers the system designer a number of valuable tradeoffs differing from those available with the conventional cruciform track scan. Most important of these is greater sensitivity.

We define tracker sensitivity as the minimum target photocurrent i required to track with a given accuracy and bandwidth (or tracker time constant). Equations F9 indicate that the CS tracker is about a factor of four away from the ideal tracker, and by far the most sensitive ID tracker. Other ID trackers require more optical target power and, consequently, a larger lens aperture, etc.

G2. The CS tracker is the natural choice for use in an integrated (same photosensor used for both tracking and information detection) optical communications receiver. The reason for this is that the conical scan pattern inherently allows a continuous photocurrent (I/2 or more in the previous analysis)

to be processed. If the beacon or target radiation is modulated at a rate many times the conical scan frequency there should be no interference between the track and information channels. If there is modulation on the detected radiation, the photocurrent i must be interpreted as an average value within the track spectrum.

Of course, trackers using a cruciform track scan are used in an integrated optcomm receiver by limiting the scan amplitude so that target photocurrent is never completely extinguished during the scan cycle. However, this design greatly degrades tracker sensitivity so that it can be an order of magnitude or more poorer than the CS tracker.

G3. Other factors involved in CS tracker design are not always advantageous. Tracker slew rate is proportional to target image diameter d (instead of sampling aperture diameter D).[11] Hence, proportionately shorter tracker time constants ω_o^{-1} are required for a given slew rate. Target image diameter can determine many tracker system parameters more directly than in a system using the full extinguishing cruciform track scan and a very large D/d ratio.

Tracking accuracy is proportional to target image diameter so that the sampling aperture size is free to be determined by other factors (such as search raster configuration, etc.).

G4. What about gain control? There are two approaches to this and, unfortunately, only one is often considered. As we mentioned in duscussing equation C12, gain control is used to keep constant the product $g_{id}\, g_{pa}\, I$. If the photosensor dynode gain g_{id} is fixed, then, when AGC is active the preamp gain g_{pa} is varied inversely with target photocurrent. Under this condition loop gain g_{oL} is constant. As a consequence, the break frequency ω_o is also constant. The AGC circuit is set so that ω_o always has its maximum desired value. The inference of this can be seen by inspection of F5, but for

simplicity in an example let us look at F9B. Suppose that we are tracking a target whose detected radiant power varies. Suppose also that tracking becomes unstable for track errors σ_ϵ larger than

$$\sigma_\epsilon > (3.2)^{-1} d , \qquad \text{G1}$$

Then, since the break frequency ω_o is held constant, relationship G1 will be violated for all target photocurrent values less than some level, say I_o. This value I_o is the minimum that the tracker can work with. As I increases above I_o, σ_ϵ decreases, but as the gain g_{pa} decreases σ_ϵ reaches its asymtotic value determined by noise internal to the system.

The purpose of automatic gain control is to increase system adaptability to a changing target condition such as intensity fluctuations. The AGC technique just described partially fails in this. In fact, it operates contrary to one of the most important reasons for selecting a CS tracker which (consistant with that discussed in G1) is to obtain as low a value of I_o as is practicable. Indeed, for most applications the design engineer, if questioned, would have difficulty justifying constant ω_o (bandwidth) as the goal for AGC in a CS tracker.

For a moment let us look at a CS tracker that has no gain control whatsoever. For this comparison F9B still holds, but the important difference is what happens as the signal photocurrent I varies. We can refer to E18 to recall what circuit factors determine ω_o and find that ω_o varies directly with I.

Hence we see from F9B that, with all the tracker system elements at constant gain, the target photocurrent I can vary without restriction with no great effect on the error σ_ϵ. At low intensity levels, ω_o (or the tracker slew rate) decreases, of secondary importance in most applications (Under these conditions the tracker with constant ω_o described previously would not

operate). As I increases, the break frequency ω_o increases and again, performance exceeds that of the AGC'd system.

In practice, an increasing I eventually leads to saturation of some circuit element, so feedback gain control is desirable. Also, as I decreases, Equation F9B becomes less and less valid and the other noise terms in F7 must be considered. Logic (left to the reader) indicates that availability of the minimum I_o required to track, together with the greatest dynamic range, occurs if feedback gain control is implemented on the ID photosensor electron multiplier.[12] This automatic dynode gain control (ADC) allows tracker operation from the signal shot noise limiting condition up to target intensity levels nearly damaging to the photocathode, i.e., the greatest possible range. Normally no other gain control is required.

G5. A coherent detector such as the multiplier suggested here compares two sine waves and is subject to the phase error effects described by C11. Actually, this phase comparison is encountered in the demodulator of most ID trackers. But with the CS tracker only simple sine waves are involved so there is less of a design problem. Higher track scan rates are more easily accomplished since there are no harmonics to consider in the deflection coil driver design. On the other hand, higher track rates are needed for the same tracker slew rate.

G6. This work was partially funded by Contract NAS8-26245.

J. R. Riehl

H. NOTES AND REFERENCES

1. To our knowledge the only previous recorded reference of a conical scan applied to an image dissector was this author's as described in Technical Proposal to NASA/MSFC, Aircraft Optical Communications Package and Optical Acquisition Equipment, ITTA 301530, 27 October 1969. Although the proposal was successful, the CS tracker was considered to be too risky to develop on that particular program. We have searched the technical literature and found nothing, but certainly conical scan ID trackers must have been developed (though perhaps not successfully).

2. Sensitivity Comparison of Various Image Dissector Scan Patterns Useful for Optical Communications, J. R. Priebe, January 1972. This report presents a relative performance comparison of ID trackers limited by the track scan configuration. Its content was prepared for a NASA presentation in October 1971.

3. The conical scan discussed here is analogus to that used in tracking radars. For example, see Introduction to Radar Systems, M. I. Skolnick, (McGraw Hill 1962) page 167.

4. It is not too difficult to work with the condition $A \neq D/2$, since only the rate of change of photocurrent with δ is of importance. However, we treat here only the condition described in B8.

5. We wish to discuss here the definition of spot diameter since image irradiance distributions vary widely. Let the rotationally symmetrical distribution of the image of the focal plane be $H(\rho, \theta)$ watts/cm^2 in polar coordinates.

Then the image radiant power is P_λ watts, where

$$P_\lambda = \int_0^{2\pi} d\theta \int_0^{\infty} \rho \, d\rho \; H(\rho, \theta) = 2\pi \int_0^{\infty} \rho \, d\rho \; H(\rho).$$

In X-Y coordinates we can write

$$P_\lambda = \left| \lim_{X \to \infty} P_\lambda^* (x) \right. ,$$

where $$P_\lambda^* = \int_{-\infty}^{X} dx \int_{-\infty}^{+\infty} dy\, H(x, y) .$$

The trackers discussed in this report have a sensitivity dependent on the rate of change of the photocurrent passing through the sampling aperture as the target image moves across the aperture periphery. This sensitivity is consequently proportional to $\partial P^* / \partial X = s^*$ at the spot center where $X = 0$. For the pill box distribution where the irradiance is uniform within a circular area,

$$H(\rho, \theta) = H/(\pi d^2/4) \text{ watts/cm}^2, \quad \rho \leq d/2$$
$$= 0 \qquad\qquad\qquad\qquad \rho > d/2$$

and $$s^* = \frac{4H}{\pi d} .$$

For an image with a Gaussian intensity distribution

$$H(x, y) = H(2 \pi \sigma^2)^{-1} \exp [- (x^2 + y^2) /2 \sigma] \text{ watts/cm}^2,$$

$$s^* = H/ \sqrt{2 \pi \sigma} .$$

Thus, compared to a uniform spot, the Gaussian spot has for this report an equivalent diameter

$$d = 4\sigma \sqrt{2/\pi} = 3.19\ \sigma .$$

6. A number of phase detecting devices can be used such as an electronic switch, mixer, ring demodulator, etc. Of these, the product detector implemented with an analog multiplier is the most straightforward and efficient (i.e., the output signal-to-noise ratio is greatest). If the principal reason for choosing a CS tracker is its sensitivity, it is inconsistent to compromise system performance with a lower efficienty demodulator.

7. For some depth with regards to AGC see Automatic Volume Control as a Feedback Problem, B. M. Oliver, Proceedings of the IRE, April 1948, page 466.

8. In practice we have to compromise with an integrating operational amplifier having the transfer function

$$F(\omega) = -(R_f/R_i) / (1 + j\omega R_f C),$$

There is little real difference between this and E17. However, care must be taken to assure that $F(\omega)$ does the only effective filtering in the system loop for all anticipated values of the signal current I.

9. Actually, during the derivation of F5 the meaning of I has changed to $\hat{\imath}$, what we call the tracker sensitivity. This is the minimum photocurrent required to obtain simultaneously the other performance parameter values.

10. We use here the factor k for multiplicative white noise. For example, in an ideal electron multiplier with gain g for each stage, k can be no smaller than g/ (g-1) . For system considerations k is usually much larger and includes the noise figures of preamplifiers, etc. See Threshold Sensitivity and Noise Ratings of Multiplier Phototubes, E. H. Eberhardt, Applied Optics, February 1967, page 252.

11. However, as discussed in the report identified in Note 2 above, the CS tracker has a higher inherent slew rate (inches per second) than many other ID trackers.

12. Implementation of photosensor dynode gain control is discussed in the technical note: AGC for the Space Shuttle Transceiver Tracker, J. R. Priebe, 12 January 1972.

I. LIST OF SYMBOLS

D	Sampling aperture diameter (inches).
A	Conical scan semiamplitude (inches).
d	Equivalent target image diameter (inches).
ϵ	Track error absolute magnitude (inches), see B1.
ϕ	Track error vector direction (radians), see B1.
ω	Conical track scan frequency (radians/sec.), see B2.
δ	Displacement of target image center from periphery of sampling aperture (inches), see 2B and B3.
I	Total target image photocurrent (electrons/sec. or amperes).
i_s	Photocurrent from target image that passes through the sampling aperture (electrons/sec. or amperes), see 4B.
P_λ	Total radiant power in the target image (watts), see 1C.
g_{id}	Current gain of the electron multiplier in the image dissector photosensor (amps/amp), see C1.
g_{pa}	Gain of the tracker circuit preamplifier (volts/amp.) see C1.
v_s	Track signal from preamplifier (volts), see C1 and C3.
g_m	Multiplier gain (volts/volt^2).
v_r	Reference sine wave into multiplier (volts), see C4.
α	Phase error (radians), see C4.
v_{ds}	Demodulated signal from the modulator (volts), see C2.
a_r	Amplitude of the reference into the multiplier (volts), see C4.

e	Tracker error along the system "x" axis (inches), see C10.
$F(\omega)$	The tracker loop filter function, (volts/volt), see 1C and C13.
$i_n(t)$	Sum of all system noises referenced to the preamp input (amps), see 1D.
N	Noise spectral density referenced to preamp input (amps^2/hertz), see D1.
$\overline{v_n^2}$	Noise spectral density referenced to multiplier input (volts^2/hertz), see D1 through D3.
$\overline{v_{no}^2}$	Mean square noise spectrum from the multiplier (volts^2/hertz), see D4 through D7.
$\overline{n^2}$	Total effective system noise relative to the preamp input (amps^2), see D10.
s_λ	In reality the distance of the center of the target image from the EO center of the ID photosensor (inches), see 1B, E1 and E4.
s	In reality the average (over a scan cycle) distance of the sampling aperture center from the EO center of the ID photosensor (inches), see 1B.
i_{tr}	Current generated in the tracker circuitry which is applied to the deflection coils to move the sampling aperture (amps), see 1E and E3.
g_{df}	The deflection sensitivity of the deflection coils on the ID photosensor (inches/amp), see E3.
E_{out}	The tracker output error signal (volts).
g_{oL}	The instantaneous open loop gain of the tracker (unitless), see E4.
a	The product of a number of terms as defined in C6, (volts/amp inch).

g_{tr}	Gain of the track error deflection amplifier (amps/volt), see E2.
$\sim$	The tilde is used in this report to identify a statistically random variable.
v_{nt}	Total instantaneous spectral noise out of the multiplier (volts), see E7.
σ_s	The rms noise in track position relative to the photocathode (inches), see E11.
σ_n	The rms noise in the tracker output, comparable with E_{out}, (volts), see E15.
F_n^2	The tracker noise equivalent bandwidth (hertz or radians/sec), see E14.
C	A convenient simplifying constant (ohms), see E16.
g_i	Gain of the ideal loop filter or integrator (radians/sec), see E17.
ω_o	The tracker response break frequency = $2\pi f_o$ (radians/second), equivalent to the inverse of the tracker time constant τ_o, see E18.
σ_e	The rms tracker error along one axis, relative to the photocathode (inches) see F4.
σ_ϵ	The total rms tracker error relative to the photocathode, the vector sum of the "x" and "y" axis errors (inches), see F4.
σ_{int}^2	The power spectral density of noise generated internal to the tracker circuitry referenced to the preamp input ($amps^2$/hertz). These fluctuations are independent of the noise sources in the photosensor, see F6.
k	A multiplicative noise factor which increases the rms value of a noise current (unitless), see F6.

APPENDIX C

NOISE ANALYSIS OF CONICAL SCAN TRACKER

The purpose of this section is to calculate the tracking error as a function of all variables. From these relationships the trade-offs among the variables can be seen and evaluated. The analysis is in four sections: Inherent errors in the overall specific system, errors due to tracking in a dynamic environment, and acquisition considerations.

TRACKER PERFORMANCE

We first calculate the value for the noise equivalent angle that results from shot noise and its being processed through the tracker loop. The calculations will determine the noise as inches on the photocathode which can be easily converted into angle error by dividing by the focal length. The task is divided into three sections: tracking error detector sensitivity, noise at the output of the tracker, and response of the loop to these signals. A functional block diagram is shown in Figure C-1.

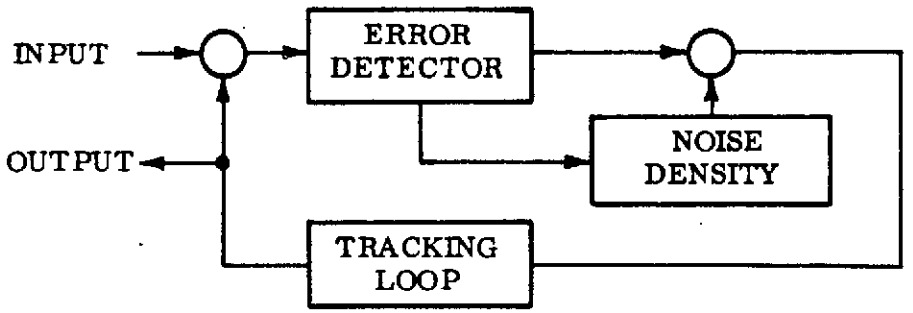

Figure C-1. Block Diagram for Tracker Performance Evaluation

The error detector has an image dissector, load resistor and preamps, and a coherent demodulator. During tracking operation inside the tube, a small aperture, through which the tube can detect optical power, is in effect moved in a circular pattern on the face of the tube. The task of the tracking loop is to keep this circular pattern centered on the position of the optical image of the beacon. If the image is centered, the optical power detected by the tube will be constant in every part of the circular scan. If, however, the image moves from the scan center, the intensity detected will vary as the image is scanned. The phase and relative amplitude of the detector output will be demodulated to get information as to the angle and radial position of the moved image.

This information is applied to the servo loop, which will move the scan so that it will again center itself on the image. The scan's position, then, monitors the position of the optical image on the face of the tube to within the error limitations of the loop.

a. Error Detector

With the above functional description, one derives a mathematical description of the process. The image dissector is a scannable detector. Its sensitivity to optical power on the photocathode is given in units of amperes per watt. For the spectral region in which we are operating, 0.63 μm, the sensitivity is 0.032 A/W, corresponding to an effective quantum efficiency of 6.3 percent. This sensitivity includes the attenuation due to an accelerating wire mesh electrode behind the photocathode. The photoelectrons which are focused through the scanning aperture are amplified in a dynode chain amplifier. The output of the tube at the anode is a current. By accumulating these factors, one can describe the current output of the anode that results from image power (electrons) that goes through the scanning aperature.

The next question is, how many get through? The image with W watts can cause Y amperes at the anode, using an effective sensitivity APW and a dynode gain GD

$$(W)\ (APW)\ (GD) = Y \tag{1}$$

if all electrons go through the aperture. The image diameter is about 25 μm (0.001 in.) in diameter and is labeled DS. The exact description to be used in this analysis assumes a diffraction limited optical system. The optical image diameter, DO, is

$$DO = \frac{\lambda f}{D} \tag{2}$$

where

D = aperture size of the optical telescope

λ = wavelength of the light

f = focal length of the telescope system

This is about the half-power diameter of the Bessel function that describes the Airy disk.

The electron image this will produce at the aperture will be slightly defocused by the electron optics, resulting in an electron image diameter of

$$DS = DO \text{ (defocus factor)} \tag{3}$$

For a first approximation a circular aperture much larger than the electron image will be considered.

One can speak in terms of the electron image scanning around a stationary aperture or of the aperture scanning a stationary image. Both are essentially true. The image is stationary at the photo cathode, and the aperture is stationary at the back of the magnetic focusing section. It is appropriate in this description to choose the point of view of the electrons from the stationary optical image being scanned magnetically (electrostatically) around the physical aperture at the back of the focusing section. The scan of these electrons is designed to have a scan radius equal to the aperture radius. When there is no error, the center of the electron image will be on the edge of the aperture during the complete scan, which allows 50% of the energy to remain in the detection aperture for communications.

If, however, there is a positioning error between the center of the aperture and the center of the scan, more photoelectrons will enter the aperture during one part of the scan, and less during the opposite part of the scan as shown in Figure C-2. When the error exists, the current out of the anode will vary sinusoidally at the scan frequency.

To derive the amplitude of this sine wave, let us assume that the aperture is much larger than the image size. A following section will derive a correction for the case in which this assumption is not true. A gaussian model will be used for the spot. The half-power width will be made equal to the half power width of the Bessel function. The amplitude of the current can be calculated by mathematically describing a gaussian function sampled by a moving edge. The amplitude for a given position error is, within a few percent, equal to that calculated by modeling the image as a uniform intensity circular spot with a diameter equal to DS, and with a photoelectron flow that is multiplied by an amplitude factor ($\pi/4$). The a-c amplitude of the output current is the difference between the electron flow through the aperture when the image is centered on the aperture edge and when it is not.

The amount of increase in the current is the electron flow intensity (A/unit area) multiplied by the difference in the area, error x DS, as diagrammed in Figure C-3. Therefore the amplitude ΔI is

$$\Delta I = \text{(intensity)} \times \text{(error} \times DS\text{)}$$

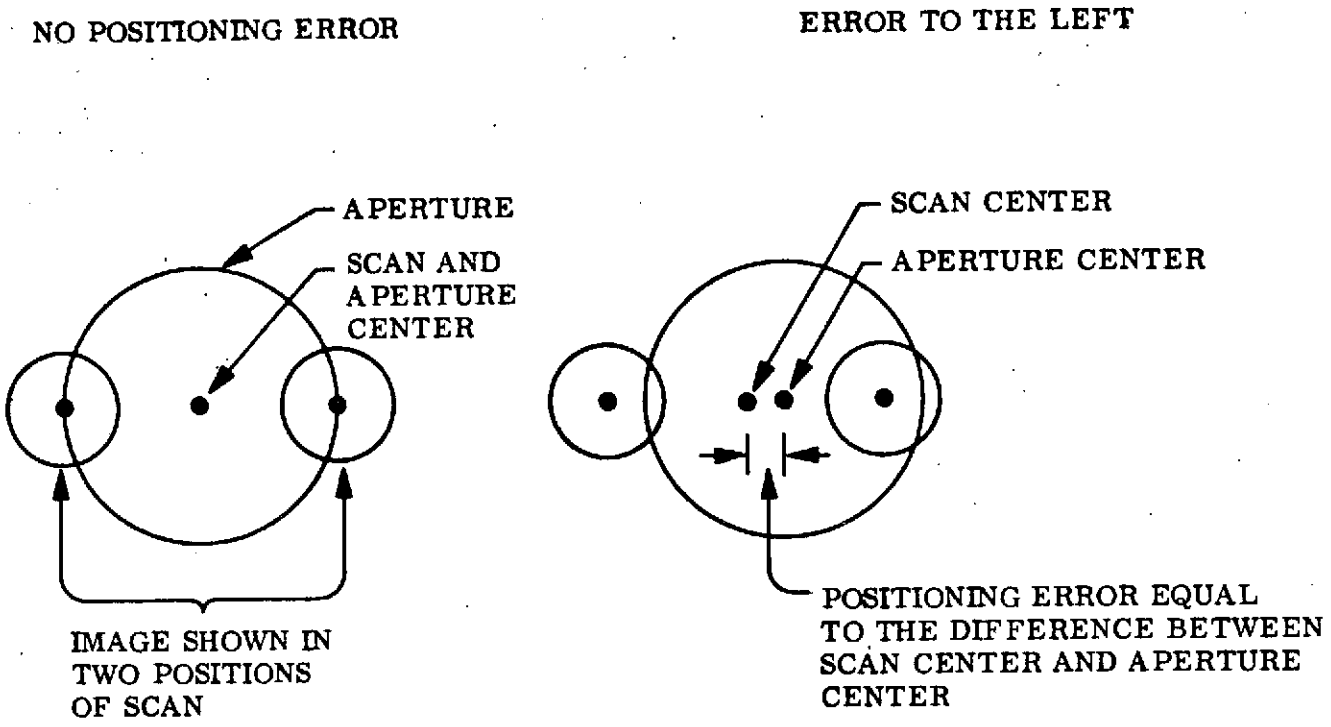

Figure C-2 Tracking Error Generation

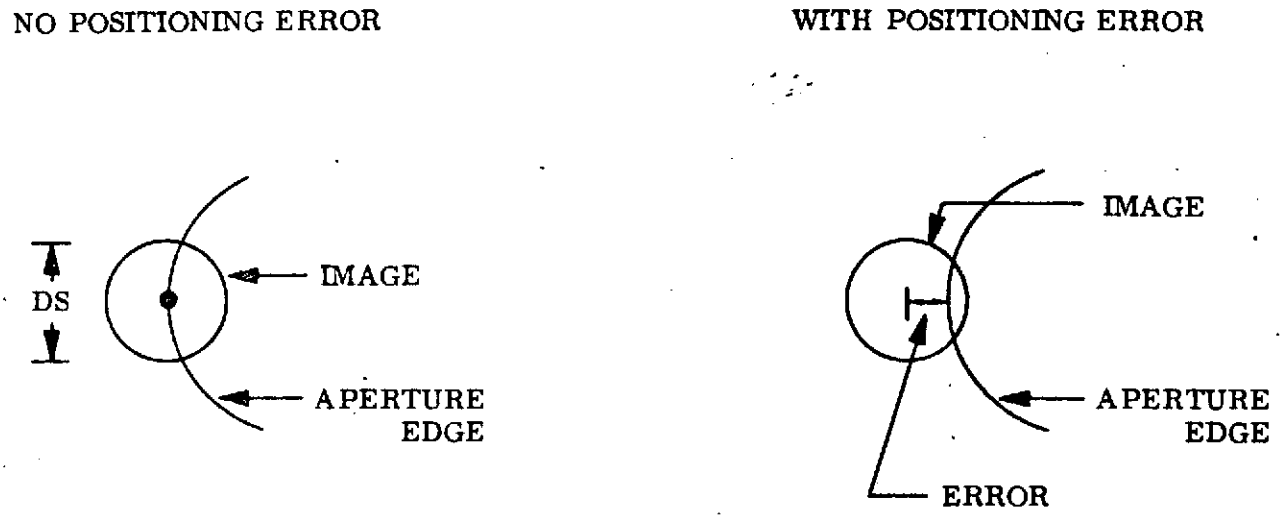

Figure C-3. Model for Error Signal Generator

Since the model has uniform intensity, the following output current variation is obtained using Eq. (1),

$$\frac{(\pi)\ (W)\ (APW)\ (GD)}{(4)\ \frac{\pi\ (DS)^2}{4}}\ (X_e)\ (DS) = \Delta I \tag{4}$$

where

ΔI = amplitude output current

X_e = position error in inches

DS = electron image size

GD = gain of dynode chain

APW = effective photocathode sensitivity

W_i = total optical power on photocathode due to the image.

The more exact description for the current out of the anode is a sum of the sine wave due to positioning errors, an average d-c current level, d-c current due to background illumination of the photocathode and dark currents in the tube.

Putting this together, the total output current is obtained:

$$\begin{aligned} I\ \text{total} = &\left[\left(W_{BKGD} + \frac{W_i}{2}\right) APW + i\ \text{dark}\right] GD \\ &+ \left[\frac{W_i (APW)\ (X_e)\ (DS)}{(DS)^2}\right] \times \sin \omega_{es} t + \phi_\theta)\ GD \end{aligned} \tag{5}$$

where

i dark = 2.6×10^{-14} A for the tube and is variable from tube to tube. It will be ignored in most calculations as it is much smaller than the other currents

W_{BKGD} = Light power from background sources of illumination

ω_{es} = Scanning frequency in radians

The power in the background is given by

$$W_{BKGD} = (IFOV)^2 \text{ (spectral radiance) (optical bandwidth) (lens area)} \qquad (6)$$

where IFOV is the instantaneous field of view.

The expression for the sine wave current out of the tube is proportional to the tracking error signal. The error signal must be amplified and coherently detected to produce correction voltages to quadrature magnetic coils that correct the scan position. The tube output current passes through a shunt resistor R_L to produce an output voltage. It is amplified first in a low noise preamplifier, then by other a-c coupled amplifiers, and is presented to two coherent detectors operating in quadurature. The detectors are a chopper type of doubly balanced mixer. The phase of the input is alternately inverted at double the scan frequency. The output d-c signal level esulting from detecting a sine wave of amplitude A is

$$\frac{2}{\pi} A \cos(\theta - \phi) = \text{d-c output}$$

where $\theta - \phi$ is the phase difference between the error signal phase and the phase of the chopping signal. The $(2/\pi)$ factor is necessary to convert the sine wave amplitude to a d-c average voltage level, using this demodulation technique. In one detector, θ is 90 deg out of phase with the other. Thus in one detector an up-down error signal is generated and in the other, a left-right command. For the rest of the analysis only one axis will be considered since the analysis for the other axis is identical. Summarizing the total error detected by combining Eq. (4), the $2/\pi$ factor, load resistance, and d-c preamplifier gain gives:

$$\text{error voltage} = \frac{2W\ (APW)\ (GD)\ (R_L)\ (GTPA)\ (X_e)}{\pi\ (DS)} \qquad (7)$$

where

GTPA = the gain of the amplifiers and

R_L = the load resistor.

b. Noise Density

The sources of noise considered in this section will be the shot noise and the preamplifier input noise level. It will be shown that, if the dynode gain is high, the preamplifier noise can be dropped from the equation for this system. Shot noise at the photocathode is due to the noticeable variation in a d-c current because it is a flow of discrete particles rather than a continuous flow. The equation is well known and there is no need to derive it for this report.

It is thus

$$I_{rms} = \sqrt{e\ 2\Delta f\ (i\ \text{total average})\ (K)} \tag{8}$$

where

$e = 1.6 \times 10^{-19}\ \frac{\text{coulomb}}{\text{electron}}$

Δf = noise bandwidth in Hertz before detection

K = noise factor = 1.5

by adding into this expression the current as derived in Eq. (5), one obtains

$$I_{rms} = \sqrt{\left[\left(W_{BKGD} + \frac{W_i}{2}\right) APW\right] e\ 2\Delta f\ K} \tag{9}$$

At the output of the tube, the noise is multiplied by the gain of the dynodes, hence

$$I_{rms}\ (\text{output}) = \left[\left(W_{BKGD} + \frac{W_i}{2}\right)\ (APW)\ e\ 2\Delta f\ K\right]^{1/2}\ GD$$

Like the position error signal at the output of the tube, this noise is amplified by the preamplifier. At this point the shot noise can be compared with the preamplifier noise.

The preamplifier noise is more than a factor of ten below the shot noise. It can, therefore, safely be said that the system is shot-noise-limited on signal, and the preamplifier noise can be dropped from consideration. The shot noise is amplified and presented to the coherent detectors, with an rms value as follows:

$$V_{rms} = \sqrt{\left(W_{BKGD} + \frac{W_{image}}{2}\right) APW\ (e)\ (2\Delta f)\ K\ \ [(GD)\ (R_L)\ (GTPA)]} \tag{10}$$

The coherent detector will do two things to the broadband of noise presented to it. It will double the noise power in the frequency range near d-c and it will detect noise in the frequency regions around the odd harmonics of the chopping frequency which is 20 kHz. The amplitude of the detection is inversely proportional to the harmonic number. The rms amplitude, including the harmonics, must be corrected by the following factor:

$$\text{Correction to rms noise} = \sqrt{1 + \left(\frac{1}{3}\right)^2 + \left(\frac{1}{5}\right)^2 + \left(\frac{1}{7}\right)^2} + \text{etc.}$$

Considering that the preamplifier bandwidth may be as high as 100 kHz, the harmonics beyond 5 are additionally attenuated. Working the result of these factors to the 15th harmonic yields

$$\text{Correction to rms noise} = \sqrt{1.178}$$

Add this factor to the power doubling and the total increase in noise due to the coherent detector is by a factor $\sqrt{1.178 \times 2}$.

The total rms noise voltage after detection becomes,

$$V_{rms} = 2(GD)(R_L)(GTPA)\sqrt{\left(W_{BKGD} + \frac{W_i}{2}\right) APW\,(e)\,(\Delta f)\,K\,(1.178)} \qquad (11)$$

c. Tracking Control Loop Response

The error voltage and noise voltage in the tracking loop have been described. This section will consider the tracking accuracy and also the loops response to the noise input. The tracking loop block diagram is shown in Figure C-4.

The sum of error voltages and noise is fed to an rc low-pass filter. It has a 1-Hz corner frequency, and can therefore, act as an integrator in the frequency range being considered. Following this integrator are an amplifier, a current driver, and a deflection coil. The cathode of the image dissector is the summing point in the loop. As the optical image moves on the face of the tube, the scan will no longer be centered on the image. The amplified and detected error voltage will drive a current in the coil to deflect the scan so that it will decrease the error, again becoming centered on the image.

The most useful output of the loop is an indication of the position of the optical image. Since the scan is deflected to follow the image, the image position can be measured by monitoring the coil deflection current. A resistor R_S placed in series with the coil, will generate the desired position measurement. The accuracy of the tracking loop, will first be calculated with the image position as input I and the center of the scan position as the output O.

$$\frac{GD}{1+GH} = \frac{O}{I} = \frac{(\text{Error det})\,(GC)\,(GT)\,(C)/(1+ST)}{1+(\text{Error det})\,(GT)\,(GC)\,(C)/(1+ST)}$$

where

G defines characteristics of the forward loop

H defines characteristics of the feedback loop

GT = tracking amplifier gain

GC = current driver gain

C = coil deflection sensitivity

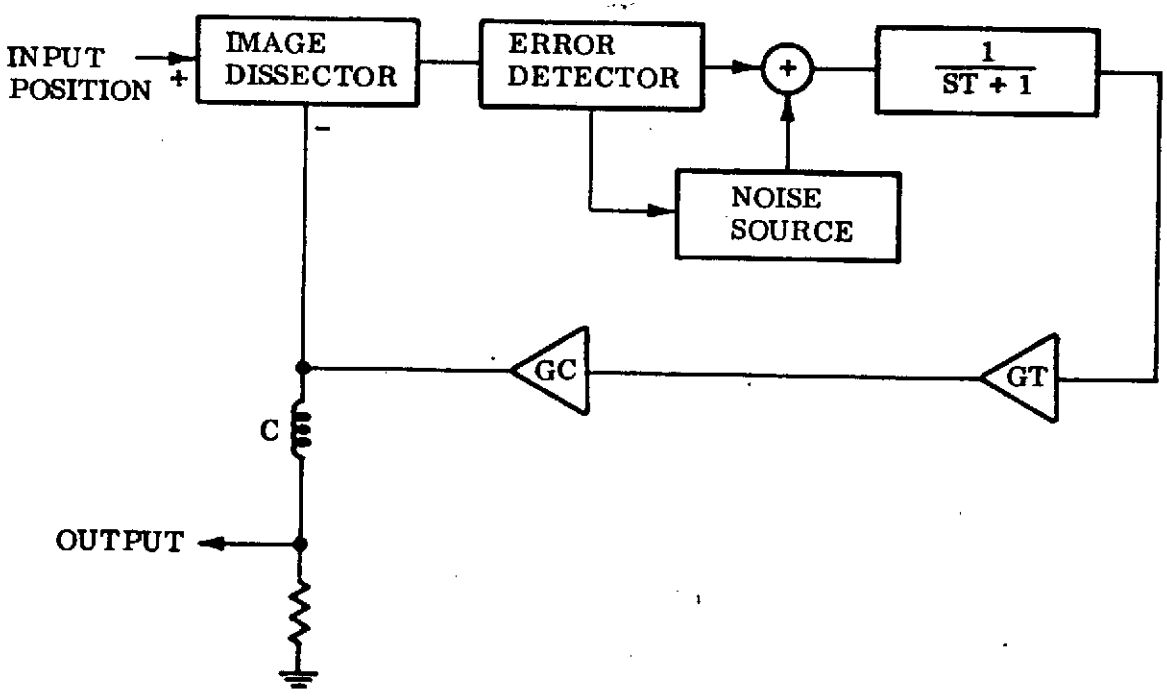

Figure C-4. Tracking Loop Block Diagram

ST = RC time constant of the simple lowpass filter

S = radian frequency

GDC = (Errordet) (GT) (GC) (C)

Errordet = result of Eq. 7

Continuing,

$$\frac{O}{I} = \frac{(GDC)}{ST + 1 + GDC}$$

$$\frac{O}{I} = \left(\frac{GDC}{GDC+1}\right)\left(\frac{(GDC+1)/T}{S + (GDC+1)/T}\right) \tag{12}$$

The form of Eq. (12) is a standard form of a low pass filter. At frequencies below (GDC + 1)/T, the output of the loop is

$$\frac{O}{I} = \frac{GDC}{(GDC+1)} \frac{(GDC+1)/T}{(GDC+1)/T} = \frac{GDC}{GDC+1} \simeq 1$$

The corner frequency of the loop is the frequency at which

$$S = \frac{(GDC+1)}{T} = (TTR)^{-1}$$

where TTR is the dynamic time constant of the tracker. Due to overall system requirements, the GDC has been adjusted to result in a bandwidth of 1 kHz.

Using standard servo loop concepts, the position accuracy is equal to the position of the image, divided by the gain in the loop, at direct current. Likewise, the tracking error of an image that is moving at a velocity V_S is equal to the velocity divided by the bandwidth. Therefore, the position error PE due to the image being positioned away from the center by a distance Pi is as follows:

$$\frac{O}{I} = \frac{O}{Pi} = \left(\frac{GDC}{GDC+1}\right)\left(\frac{(GDC+1)}{(GDC+1)}\right)$$

or

$$PE = Pi - O$$

$$PE = Pi - Pi\left(\frac{GDC}{(GDC+1)}\right) = \frac{Pi}{GDC+1} \tag{13}$$

In this application, the image will be very close to the central position. Therefore, the position error will be small. The velocity of the image O, Vi, will cause an error in the tracking of

$$VE = Vi\,(TTR) \tag{14}$$

where

TTR = tracker time constant = 1/bandwidth in radians

The response of the tracking loop to movement of the optical image has now been calibrated. It remains to calculate the effects of noise in the system, and the apparent movement of the image due to noise. Using servo loop analysis, the output O is due to a noise input I.

Thus:

$$\left(\frac{O}{I}\right)_{noise} = \frac{G}{1+GH} = \frac{(1/ST+1)\ (GT)\ (GC)\ (C)}{1 + (1/ST + 1)\ (GDC)}$$

or

$$\frac{O}{I} = \frac{(GT)\ (GC)\ (C)}{ST + 1 + (GDC)}$$

multiplying by T/T gives

$$\frac{O}{I} = \frac{(GT)\ (GC)\ (C)/T}{\frac{S + 1 + GDC}{T}}$$

But, since $\frac{GDC}{\text{error det}}$ = (GT) (GC) C, substitution gives

$$\frac{O}{I} = \frac{\left((GDC)/\text{error det}\ /T\right)}{S + \frac{1+GDC}{T}}$$

This can then be rearranged to produce

$$\frac{O}{I} = \frac{GDC/\text{error det}}{GDC+1} \times \frac{(GDC+1)/T}{S + (1+GDC)/T} \qquad (15)$$

This transfer function is characterized by an amplifier followed by a lowpass filter with a corner at the chosen bandwidth [(GDC + 1)/T] of the tracking system. The output, due to a noise voltage input is

$$O_{noise} = \left[1/(\text{error det})\right] \times \left[\text{Noise voltage}\right] \times \frac{(GDC+1)/T}{S + (GDC+1)/T} \qquad (16)$$

In Eq. (11), the noise rms voltage could not be calculated because the system bandwidth was not known. At this time, however, it is known that the bandwidth is (GDC + 1)/T. The bandwidth needed, however, is the noise bandwidth; that is, it

implies a transfer function of unity gain up to the bandwidth frequency and infinite attenuation beyond that frequency. The circuit has unity gain to the bandwidth frequency (3-dB point) and drops at 6 dB/octave beyond that frequency. The correction for the system is to multiply the 3-dB-bandwidth by 1.571. Combining these factors, the rms apparent movement of the image is as follows:

$$P_{rms} = \frac{1 \text{ (Noise density)} \sqrt{BW(1.571)}}{\text{(error det)}} \tag{17}$$

where

P_{rms} = apparent rms movement of the electron image

BW = 3-dB base bandwidth $- \frac{GDC+1}{2\pi T}$ hertz

Combining equations (11), (12), and (17)

$$P_{rms} = \frac{\pi (DS)\ (2)\ (GD)\ (R_L)\ (GTPA)}{(Wi)\ (APW)\ (GD)\ (R_L)\ (GTPA)\ (2)} \times \tag{18}$$

$$\sqrt{W_{BKGD} + \frac{Wi}{2}(APW)(e)(K)(1.178)(BW)(1.571)}$$

Simplifying this equation gives

$$P_{rms} = \pi (DS) \sqrt{\frac{W_{BKGD} + W_i/2}{W_i^2 (APW)}} \left(\sqrt{BW}\ (6.66 \times 10^{-10}) \right) \tag{19}$$

The noise equivalent angle in space is simply

$$NEA = \frac{P_{rms}}{f}$$

Where f is the focal length of the optical system.

d. AGC and Aperture Size Corrections

This first cut at analyzing the tracking loop is now completed. For a final result, it is necessary to include two more factors:

- The effects of the AGC circuit incorporated within the tracker preamp.
- The effect of the aperture size on tracking performance.

In Eq. (19), the bandwidth term can be expanded to include the effect of the AGC circuit. The BW is given by

$$BW = \frac{GDC+1}{2\pi T} \simeq \frac{GDC}{2\pi T}$$

Substituting for GDC from Eq. (7) and its definition results in

$$BW = \frac{1}{2\pi T} \frac{(GT)\ (GC)\ (C)\ (W_i)\ (APW)\ (GD)\ (R_L)\ (2)\ (GTPA)}{(\pi DS)} \qquad (20)$$

The term in this equation that will be constantly changing is the optical image power, Wi. Because of this, the circuit bandwidth could be constantly changing. To eliminate the problem, a feedback gain control is built into the gain of the total preamplifier GTPA, that the product (Wi) (GTPA) is constant. This is called an AGC loop.

The AGC threshold is the maximum voltage due to the image at the GTPA output if the amplifiers were d-c coupled. Depending on the particular AGC process, the physical voltages may be quite different. Equation (20) however, is affected only by the maximum voltage due to the image, the need for it being held at this effective threshold, and the requirement that it be unaffected by the physical implementation.

The AGC voltage is developed in a manner such that it is proportional to Wi. This voltage may be caused by the d-c current from the tube, or by a distinguishable modulation of the current from the image. This voltage is then monitored at the output of the GTPA amplifier, as shown in Figure C-5, and the AGC loop holds the voltage con ant at that point. This voltage is the threshold voltage.

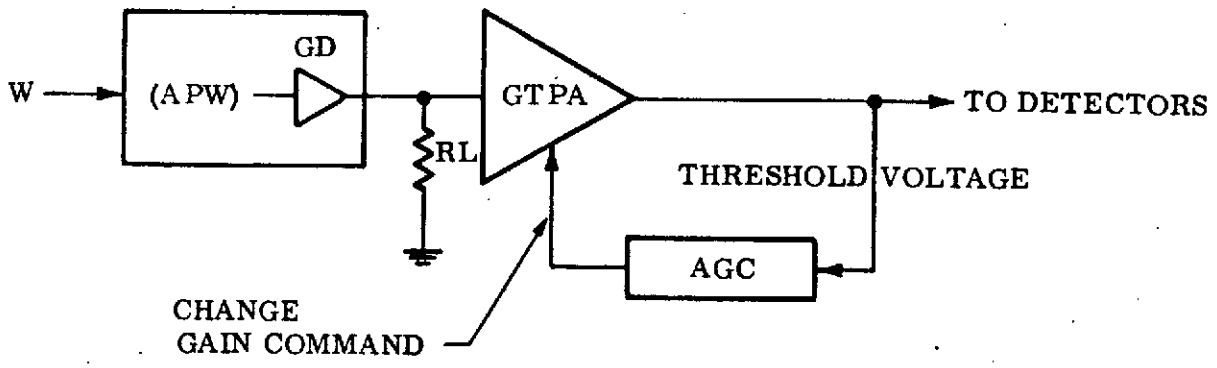

Figure C-5. AGC Block Diagram

The equation is:

$$\text{Threshold Voltage} = (W_i)(\text{APW})\ (\text{GD})\ (R_L)\ (\text{GTPA})$$

or

$$\text{GTPA} = \frac{(\text{AGC Threshold})}{(W_i)(\text{APW})\ (\text{GD})\ (R_L)}$$

Substituting the new expression for GTPA into the bandwidth equation gives

$$BW = \frac{(\text{AGC Threshold})\ (\text{GT})\ (\text{GC})\ (\text{C})}{(\text{T})\ (\pi^2)\ (\text{DS})} \tag{21}$$

Having chosen the gains and thresholds such that the bandwidth is the desired value, the system will keep that bandwidth as long as the input power changes are within the dynamic range of the AGC loop. If the power becomes less than that which the loop can correct, the bandwidth will decrease proportionally with the power level – Eq. (20) – with GTPA at its maximum value. Likewise, the bandwidth will increase proportionally if the upper limit of the AGC dynamic range is exceeded – Eq. (20) – with GTPA at its minimum value. Within the range of the loop however, P_{rms} is

$$P_{rms} = (6.66 \times 10^{-10})\left[\left(\frac{W_{BKGD} + W_i/2}{W_i^2\ (\text{APW})}\right)\left(\frac{(\text{VAGC})\ (\text{GT})\ (\text{GC})\ (\text{C})\ (\text{DS})}{(\text{T})}\right)\right]^{1/2} \tag{22}$$

where VAGC is the AGC threshold voltage.

Outside the range of the loop, the apparent movement of the image is

$$P_{rms} = 6.66 \times 10^{-10}\left[\left(\frac{W_{BKGD} + W_i/2)}{Wi}\right)\left(\frac{(\text{DS})\ (\text{GD})\ (R_L)\ (\text{GTPA})\ (\text{GT})\ (\text{GC})\ (\text{C})}{\text{T}}\right)\right]^{1/2} \tag{23}$$

with

GTPA = maximum, below dynamic range

GTPA = minimum, above dynamic range

and where

P_{rms} Rms apparent movement of image on the photocathode

W_{BKGD} = Background light power passing through the color filter and through the scanning aperture

W_i = Light power in image of object being tracked

DS = Linear dimension of electron image of object

Before leaving the subject of the AGC, there are two aspects that deserve consideration. First, consider allowing the background current to also activate the AGC. In the present system, the P_{rms} is proportional to the square root of the background power level. By allowing background power to reduce the GTPA, in addition to the image power, the P_{rms} can be made partially or completely independent of the background power. Going through the equations quickly,

$$\left((K)\ (W_{BKGD}) + W_i\right)\ (GTPA) = \text{const.}$$

The bandwidth becomes

$$BW \propto \frac{W_i}{W_i + K\ (W_{BKGD})}$$

and

$$P_{rms} \propto \left[\frac{2\ (W_{BKGD}) + W_i)}{K\ (W_{BKGD}) + W_i}\right]^{1/2} \left[\frac{1}{W_i\ (APW}\right]^{1/2}$$

where K is the factor that can be varied.

If K = 2, P_{rms} is independent of W_{BKGD}. The price one pays is that the bandwidth is decreased, by the factor $K\ (W_{BKGD})$.

$$BW \propto \frac{W_i}{W_i + K\ (W_{BKGD})}$$

If the tracker is tracking an image through a scintillating path, the velocity error VE of an image moving with velocity Vi from angular scintillation will increase by

$$VE = Vi/2\pi\ BW$$

Therefore, the total error of the tracking depends on the amount of angular scintillation, the image power, the background power, and the K factor chosen. The interrelationships depend on a thorough analysis of the complete environment of the tracker and are beyond the scope of this analysis.

Figure C-6 and C-7 show the typical relationship among these factors. Figure C-6 shows the relationship between noise rms movement and background power level, at a fixed value of image power.

Similarly, the velocity error for a moving, or scintillating, target will be higher as the bandwidth is decreased. At a certain value of scintillation and W_i, we get the curves shown in Figure C-7.

The total error is the square-root of the sum of the squares of these (random) velocity and noise errors. When there is a good model for the frequency versus amplitude response, and where assumptions can be made about the W_i and W_{BKGP} levels, the value of K can be chosen to minimize the pointing error at those operating points.

The second question to be considered, before leaving the AGC section, has to do with the particular level of the AGC threshold. Disregarding background for the moment, one can see from looking at Eq. (23), which is P_{rms} outside the AGC range,

$$P_{rms} = 6.66 \times 10^{-10} \left[\left(1/2\right) \frac{(DS)\ (GD)\ (R_L)\ (GTPA)\ (GT)\ (GC)\ (C)}{T} \right]^{1/2}$$

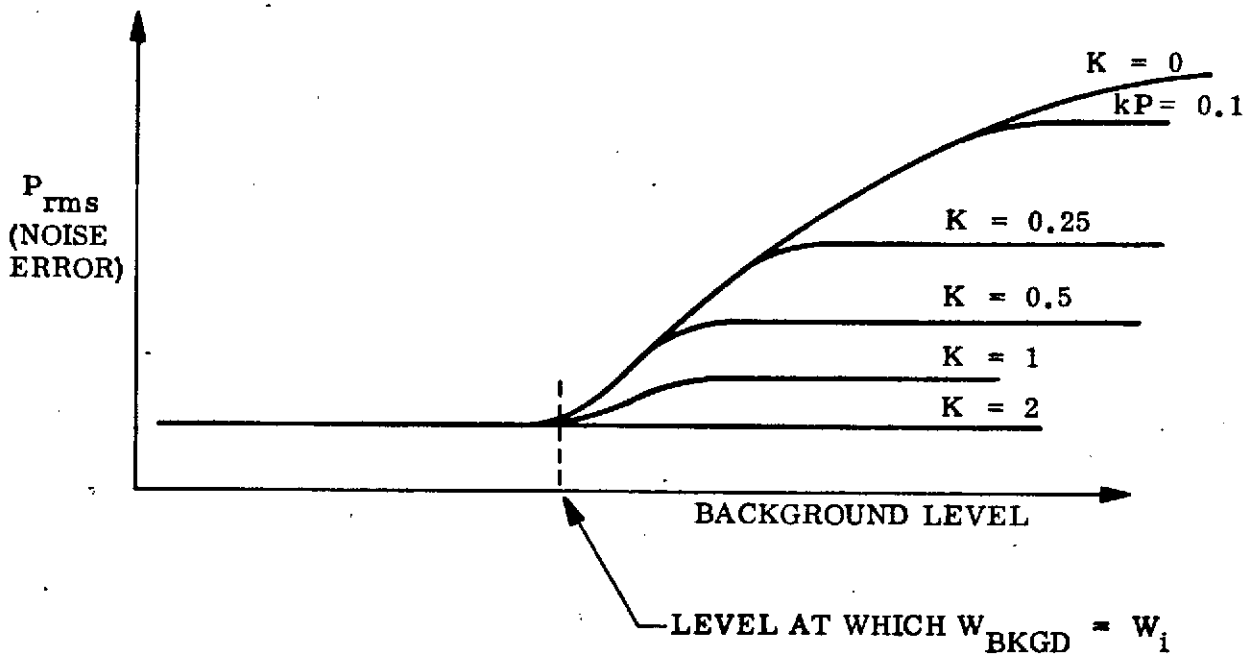

Figure C-6. Noise Error as a Function of Background Power

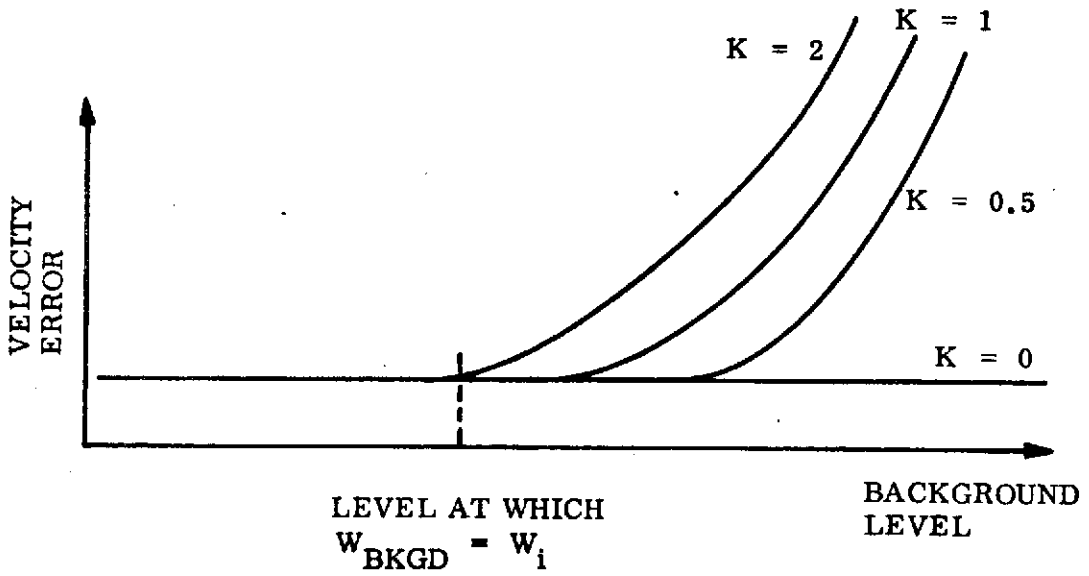

Figure C-7. Velocity Error as a Function of Background Power

Thus the noise angle is independent of input power, and depends only on the gain of GTPA maximum. Since $(W_i) \times (GTPA)$ is directly related to the threshold level, it can be said that the P_{rms} depends on the W_i power level at which the AGC begins to control the gain of (GTPA), and the system bandwidth is held constant, i.e., 1 kHz. A graph of P_{rms} versus W_i illustrates the point in Figure C-8. Velocity error as a function of W_i is shown in Figure C-9.

Depending on the design of the system, the W_i that exceeds the AGC threshold can have various values. The P_{rms} for signals below any particular Wi threshold is constant.

The price one pays for having a high level of W_i threshold is that the system is operating at a reduced bandwidth for optical powers less than that level.

The total error is the square-root of the sum of the squares of these (random) errors. As before, the tradeoff cannot be completed for our system until a reliable frequency versus amplitude model for scintillation can give numbers to be calculated and compared. The W_i threshold for the system was set at 2.0×10^{-13} W.

e. Tracking Efficiency

In the analysis, up to Eq. (19), it was assumed that the scanning aperture is much bigger than the image size. There is good reason, however, for not designing a tracker with such parameters. It is true that the received background power is proportional to the area of the aperture, and that, by reducing the size of the aperture, this noise level can be reduced. However, as the aperture size is reduced, the tracking ability can be impaired. For example, the percentage of the image power is reduced by an excessively small aperture, and P_{rms} is increased. There is also a possibility that the tracking mechanism is less efficient with very small apertures. To evaluate the nature of the tradeoffs in this question, a gaussian-shaped spot and an aperture were modeled on a computer, and the effects on P_{rms} were calculated. The gaussian spot had the same half-power width, DS, as the Bessel function that describes the diffraction image, which was converted to an electron image at the aperture.

The calculation first described the image as two-dimensional with an intensity that varied in a gaussian manner as the distance from the center increased. An aperture was described, and through the Law of Cosines, it could be positioned at any radial distance from the center. To integrate the total intensity within the aperture, the computer calculated the intensity at each small segment of the aperture and then summed these values.

The increments that made up the aperture were one-tenth of the deviation of the gaussian distribution. These values of intensity through an aperture were subtracted from the

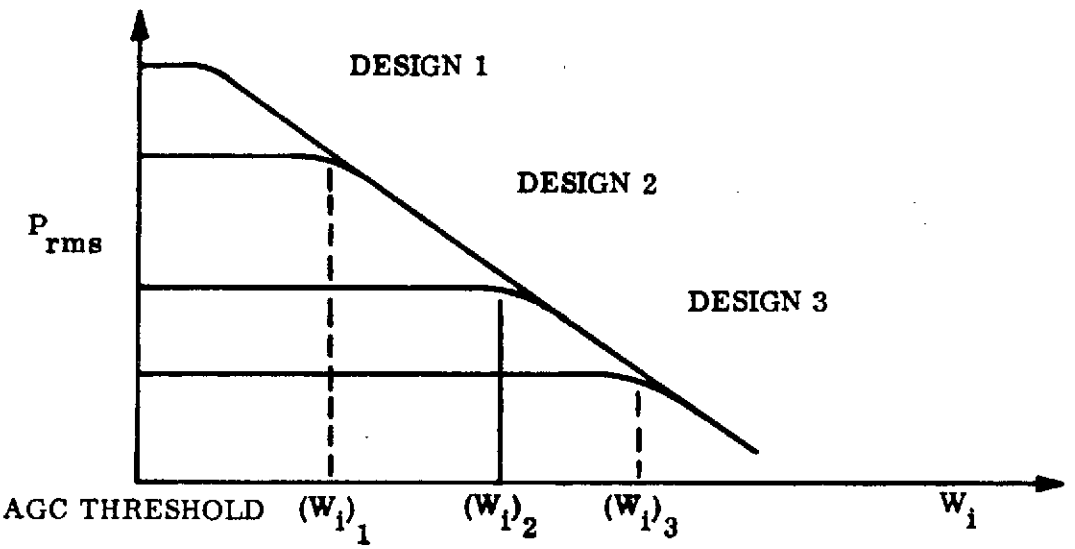

Figure C-8. Noise Error as a Function of AGC Threshold

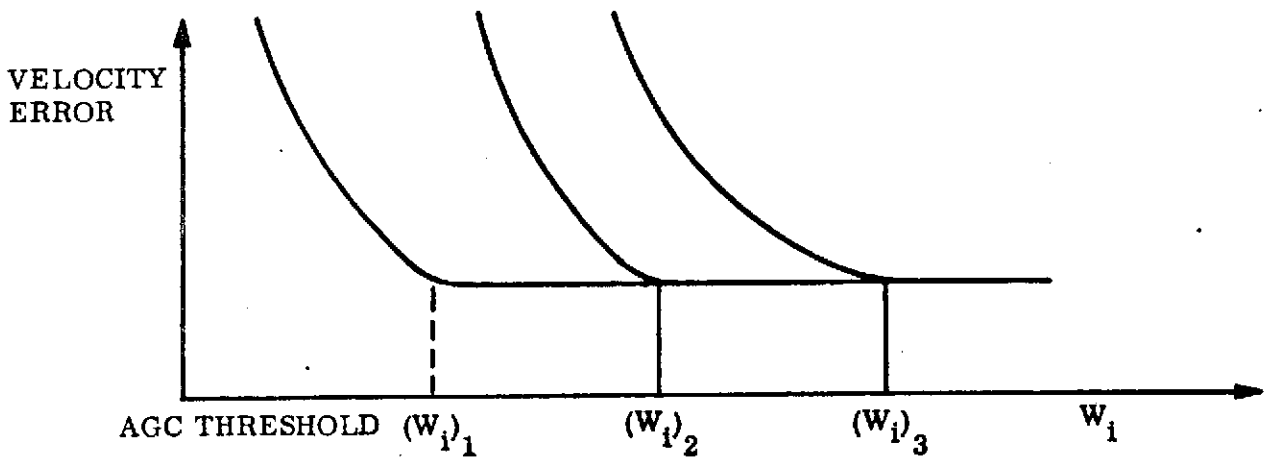

Figure C-9. Velocity Error as a Function of AGC Threshold

intensity for an aperture that was displaced radially, by an amount of exactly one aperture diameter. This subtraction of aperture pairs was continued for all positions of the pair with respect to the image center.

A plot of these values versus position is the plot of the error detector output as a function of position. The family of curves is shown in Figure C-10. The slope of the error detector curve acts like a correction of the d-c error volt/error as shown in Eq. (7). A plot of the computed function (the correction factor) is shown in Figure C-11.

On receiving the curves from the computer, the question arises as to what is happening physically to the system to cause these curves. Therefore, a simple model was sought that would produce curves that match those generated by the computer. The closest match came from a calculation of the maximum intensity of an image that can pass through an aperture of the various sizes.

This match means that the major effect on tracking a Gaussian image is the reduction of the optical power as the aperture size is reduced. This physical model makes it much easier to modify the equations of the system. Every place where the optical power Wi appears, it should be replaced by

$$(\text{Correction factor}) \times W_i$$

(1) Background. The particular value of the ratio that one should use, depends on the effect of the aperture size on the background light level. This analysis assumes that other overall system considerations determine the optical system design, i.e., f-number and objective lens size. The background light will illuminate the photocathode surface of the tube. The amount of electron current that passes through the aperture then depends only on the area of the aperture. On the basis of these considerations the effects on P_{rms} can be calculated. Rewriting Eq. (22),

$$P_{rms} = (\text{const.}) \left(\frac{W_{BKGD} + W_i/2}{W_i^2} \right)^{1/2}$$

shows the relationship between W_{BKGD} and W_i. Figure C-12 presents a family of curves showing the following:

- Vertical Axis – Log of the power terms in P_{rms} equation, with log = 0 for the situation of larger aperture with no background.
- Horizontal Log of Aperture-Size/DS Ratio.
- Family of Curves for Background Power Level Indication – Ratio of curves for $W_{BKGD}/(W_i/2)$, when DS = Aperture, i.e., if ratio = 10 and with an aperture size equal to DS, there is 10 times as much current due to background as due to the half-image power.

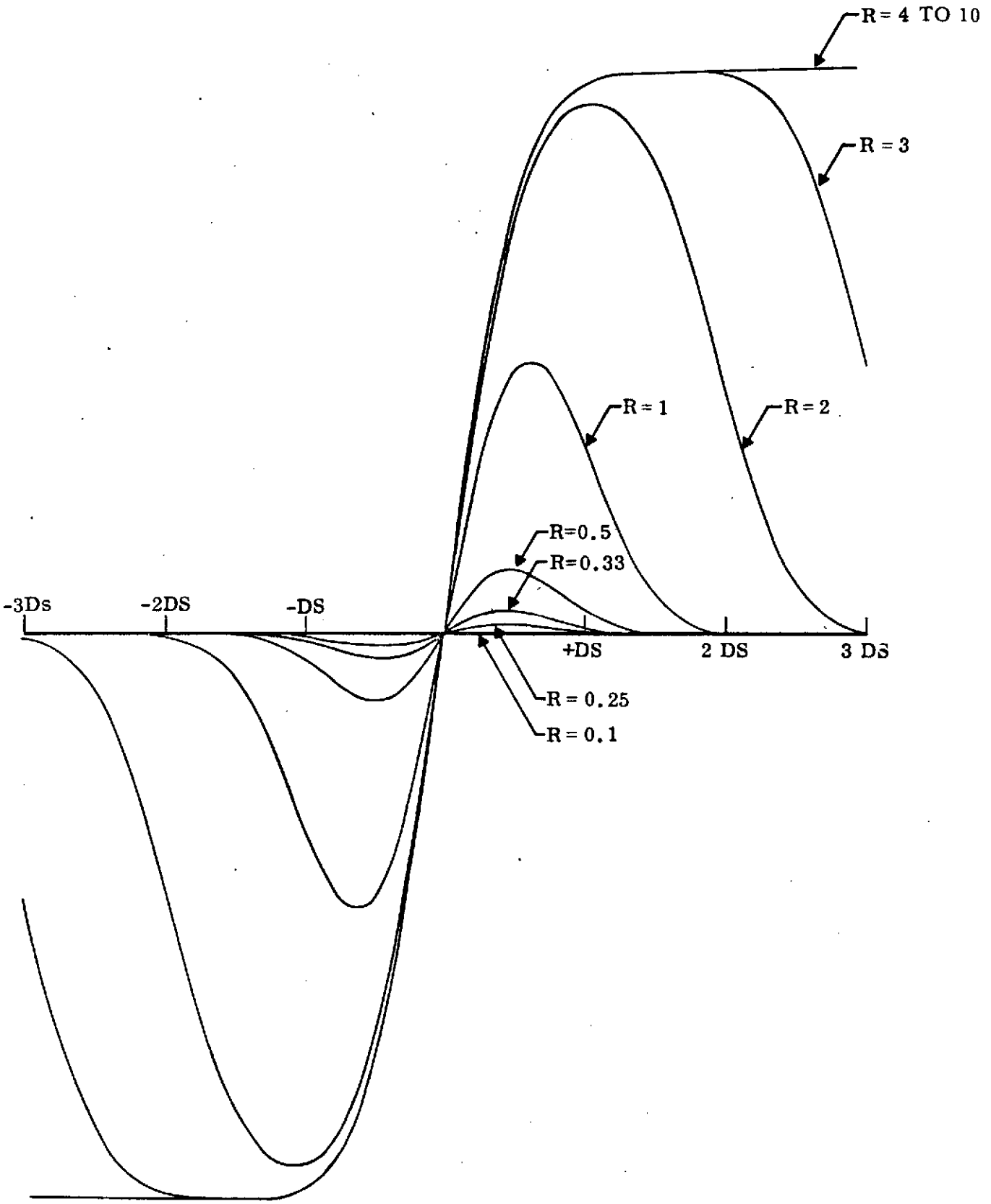

Figure C-10. Error Signal as a Function of Position Error

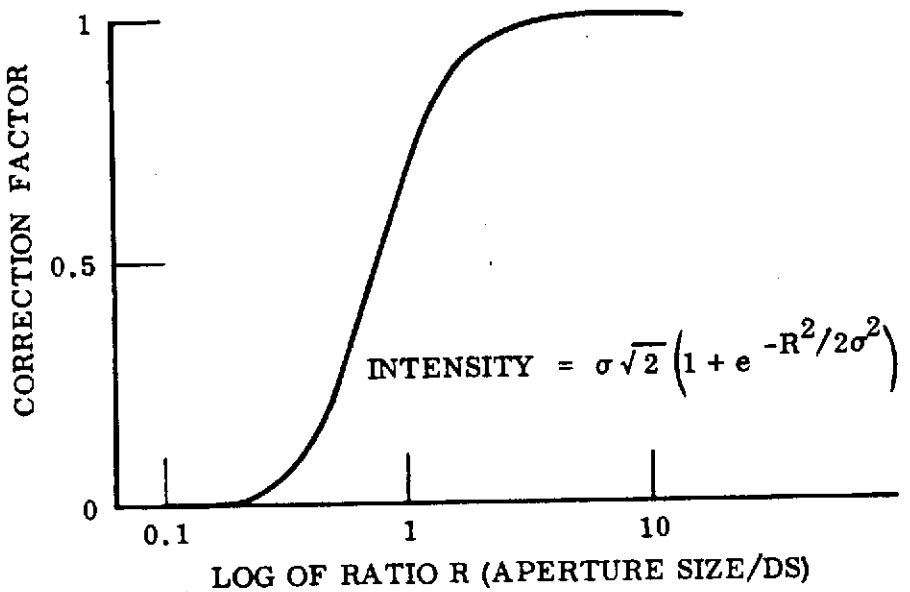

Figure C-11. Correction Factor for Received Optical Power

The curves are the solution to the equation

$$P_{rms} = \frac{\sqrt{(\text{BKGD density})\ (\pi R^2) + K W_i/2}}{\text{computed error detector slope}}$$

where

R = aperture radius

$KW_i/2$ = image power as a function of aperture size

Computed error detector slope is as shown in Figure C-10 and almost equals $K W_i$.

The curves in Figure C-12 show that if the aperture is very small, the noise, P_{rms}, is high. This is because the tracker has trouble even detecting the image. If the aperture is too large, the background light can swamp the image current causing noise. However, one can see from these curves that, if one chooses an aperture equal to DS (the electronic spot size) under high background conditions the increase in noise is at a minimum and at low background levels P_{rms} is increased only by a factor of $\sqrt{2}$.

Summarizing this section, at an image-diameter-to-aperture-diameter-ratio of 1, the effects of background light can be greatly reduced with little effect on the system performance. If the background levels are still too high for proper tracking, one can resort to the techniques discussed in the AGC section.

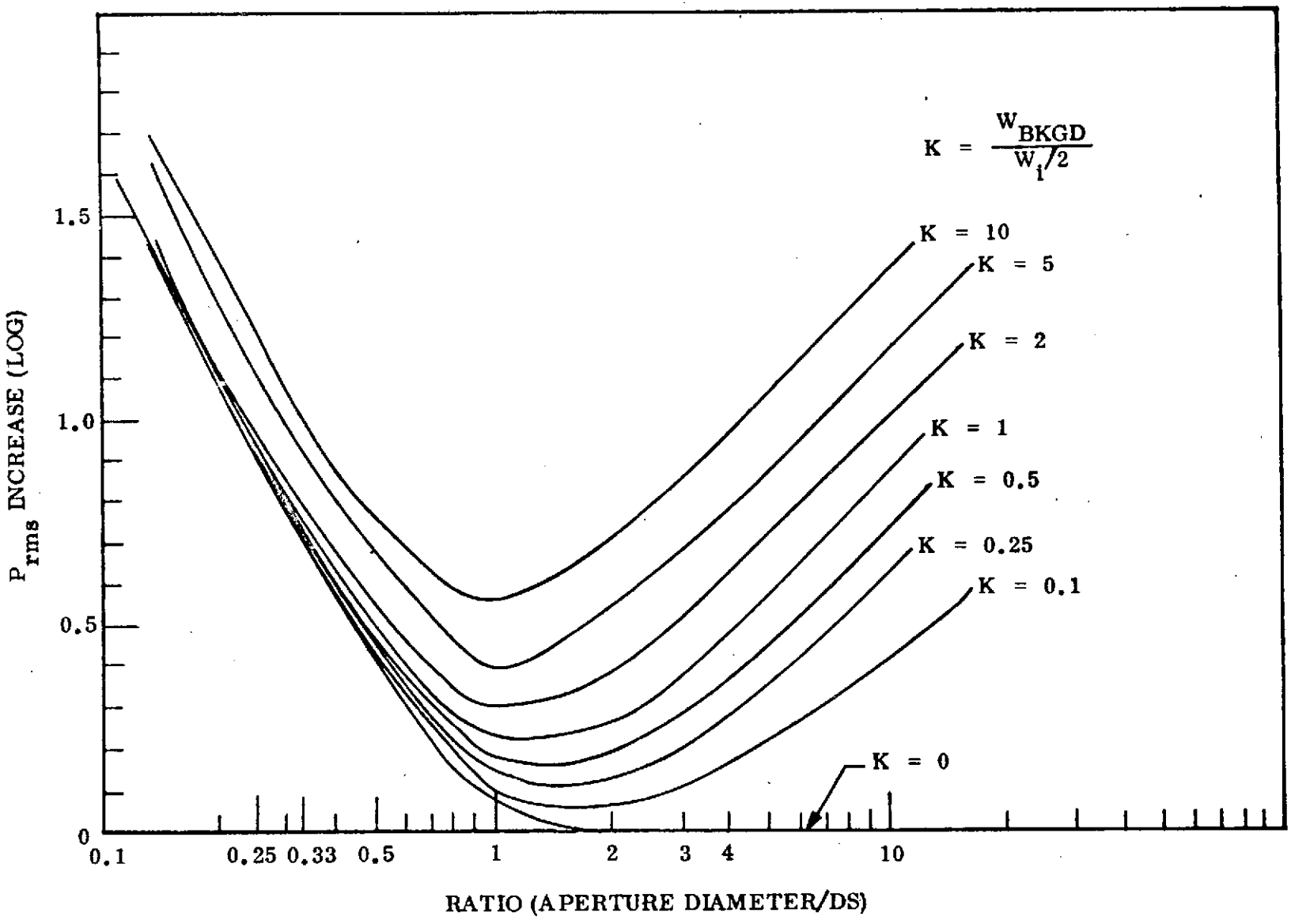

Figure C-12. Relative P_{rms} Versus Ratio at Various Background Light Illumination Levels

FOLDOUT FRAME

FOLDOUT FRAME

1

2

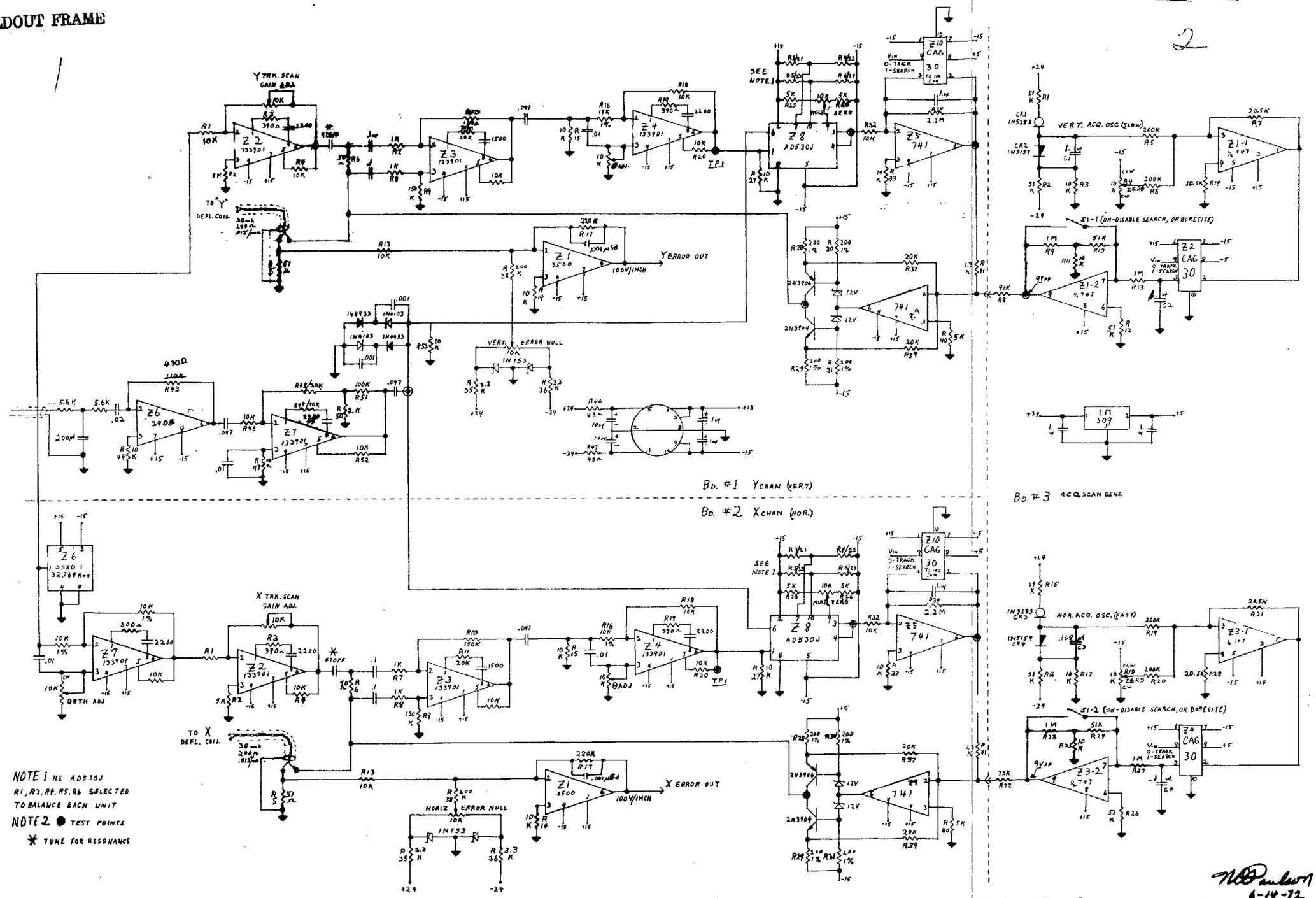

Figure D1. Conical Scan Tracker

Revised 6-14-72
Revised 9-8-72
Revised 5-28-73 HOSTETTER

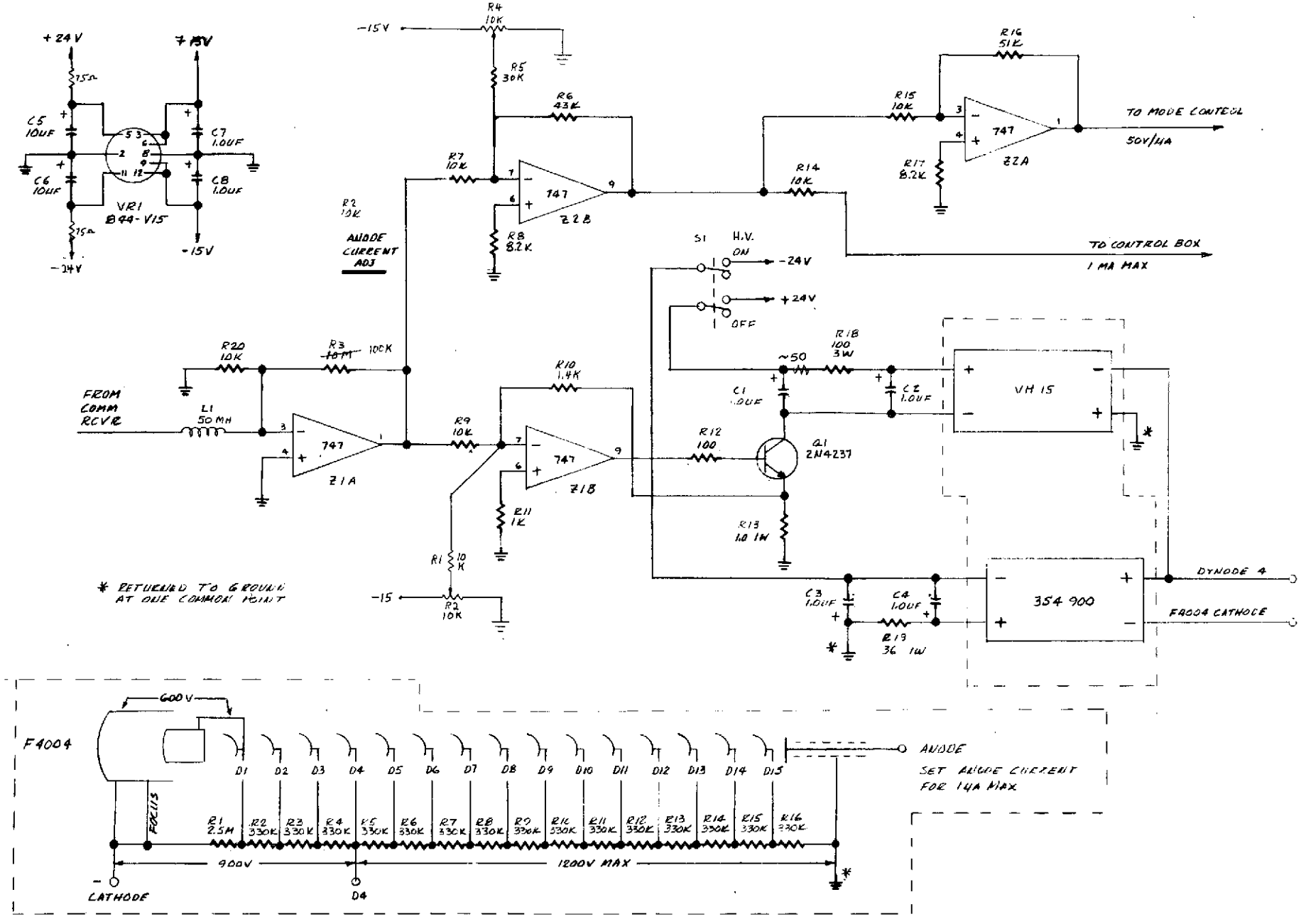

Figure D2. Dynode Control

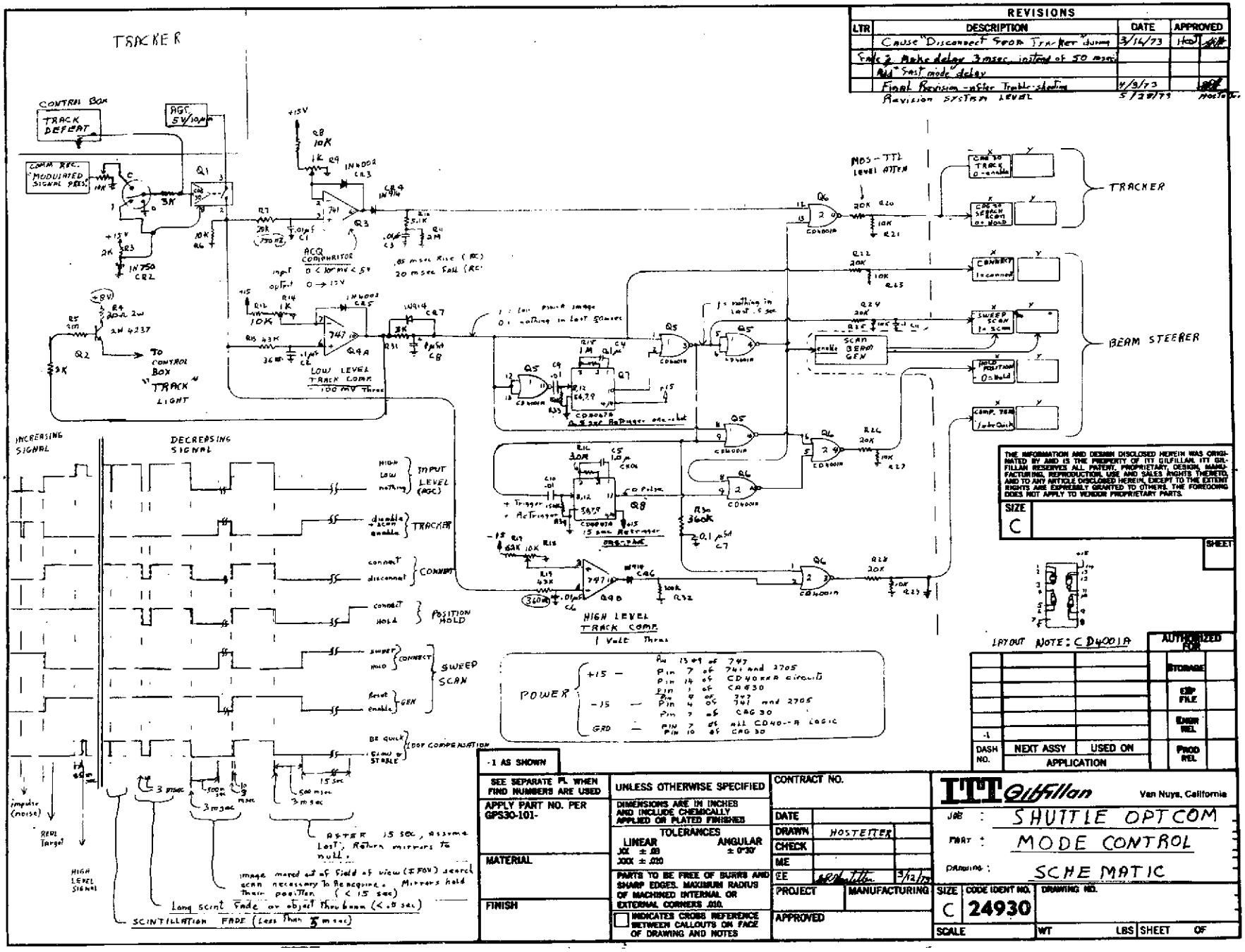

Figure D3. Schematic, Shuttle OPTCOM Mode Control

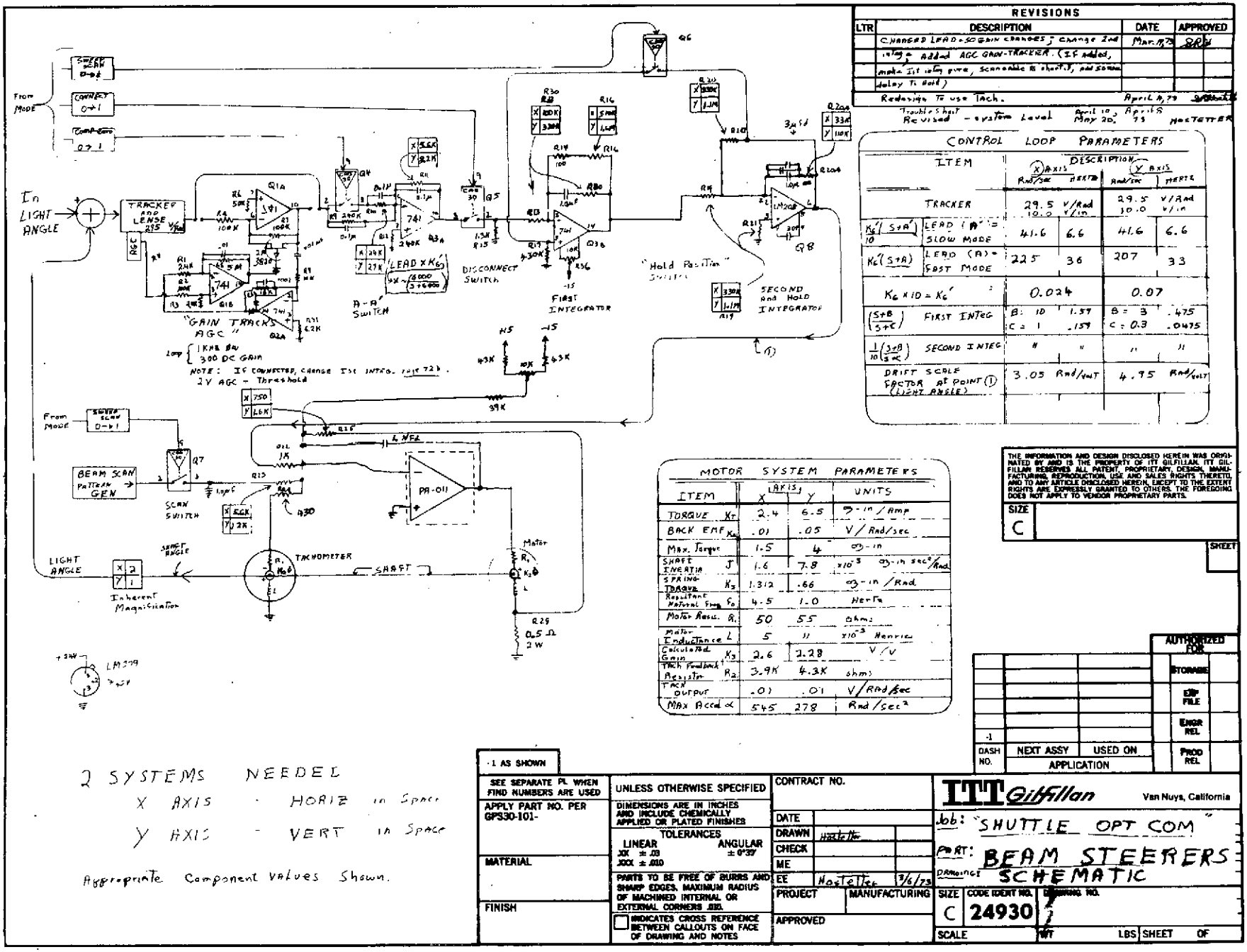

Figure D4. Schematic, Shuttle OPTCOM Beam Steerers

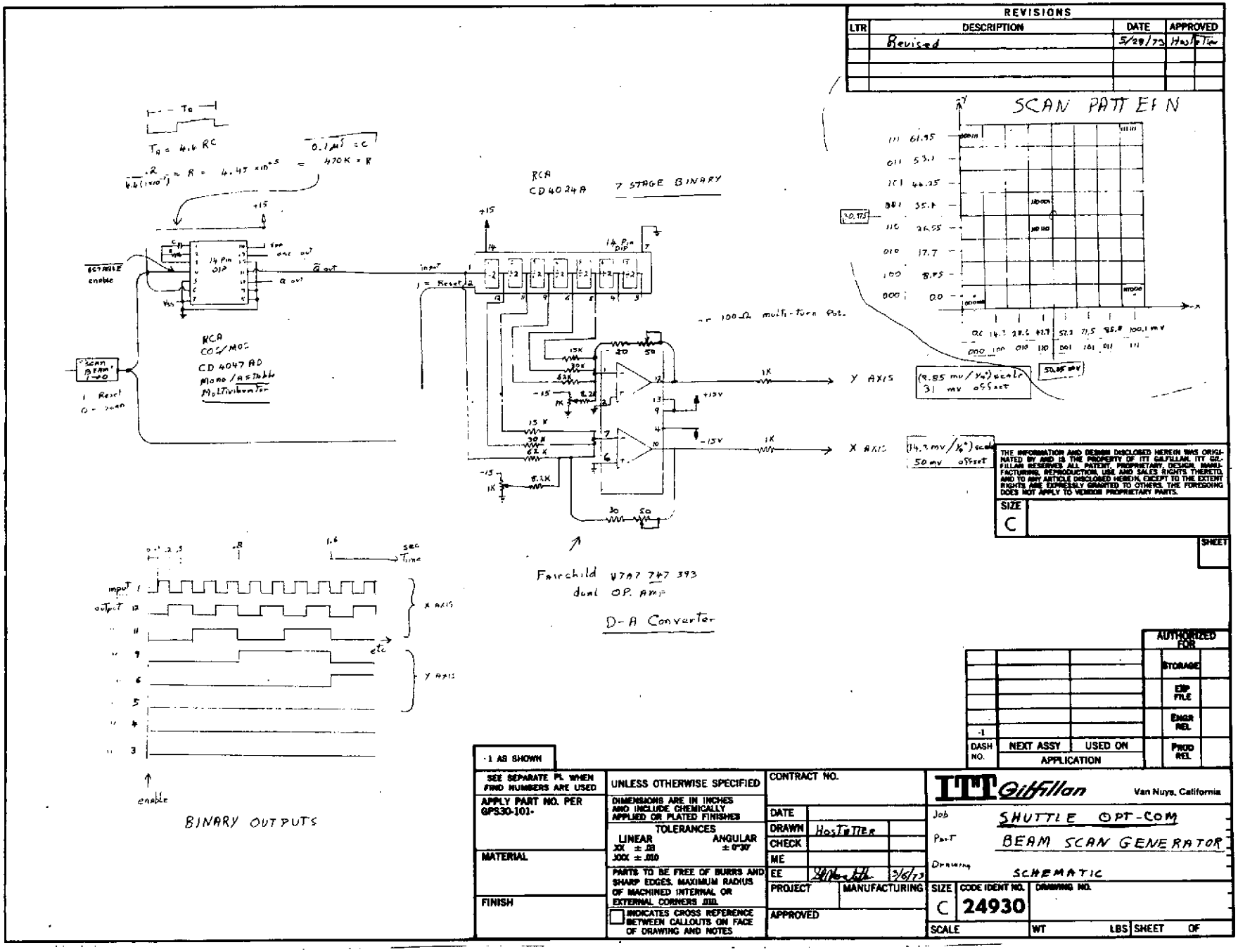

Figure D5. Schematic, Shuttle OPTCOM Beam Scan Generators

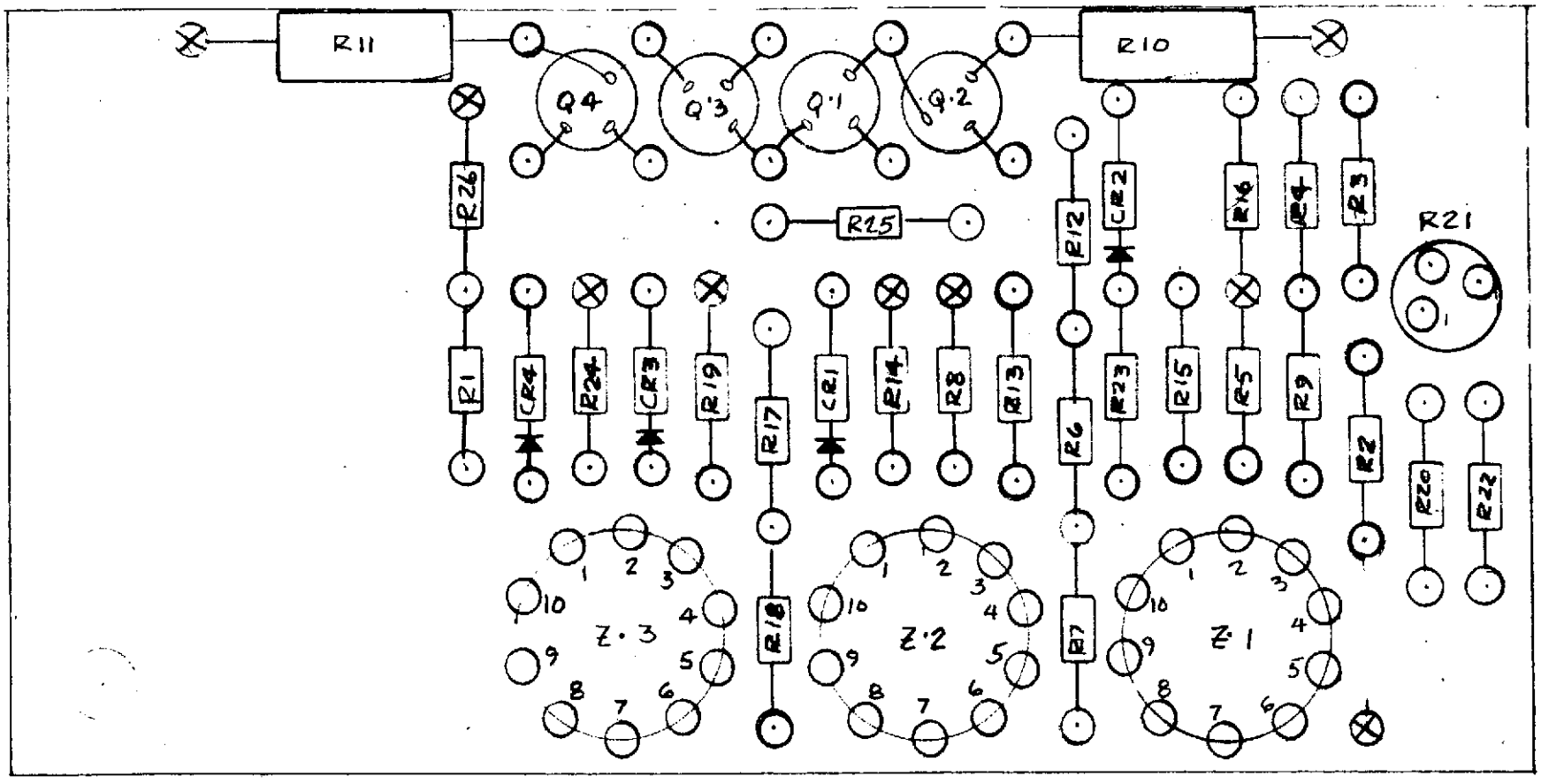

Figure D6. Beam Divergence

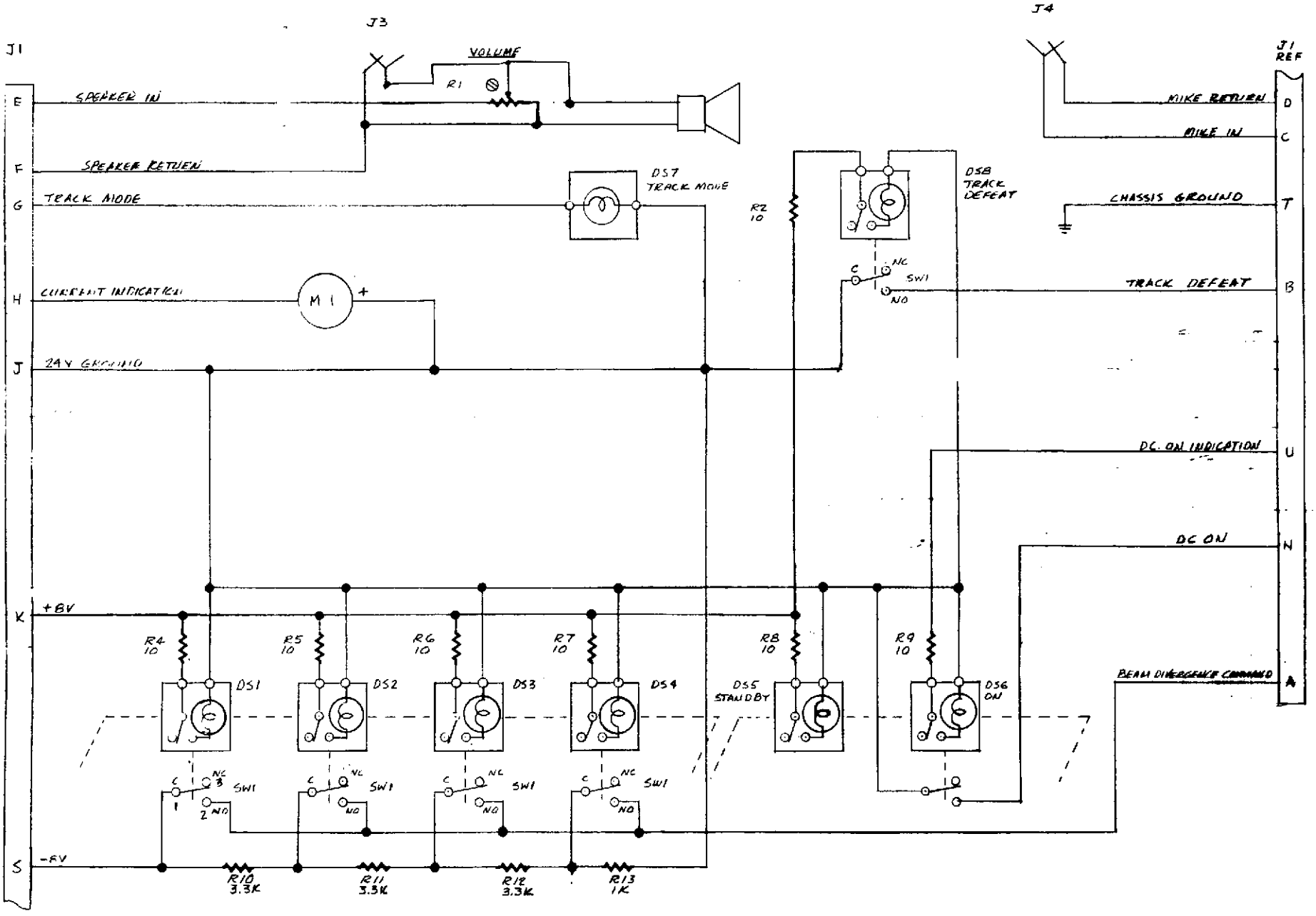

Figure D7. Control Box

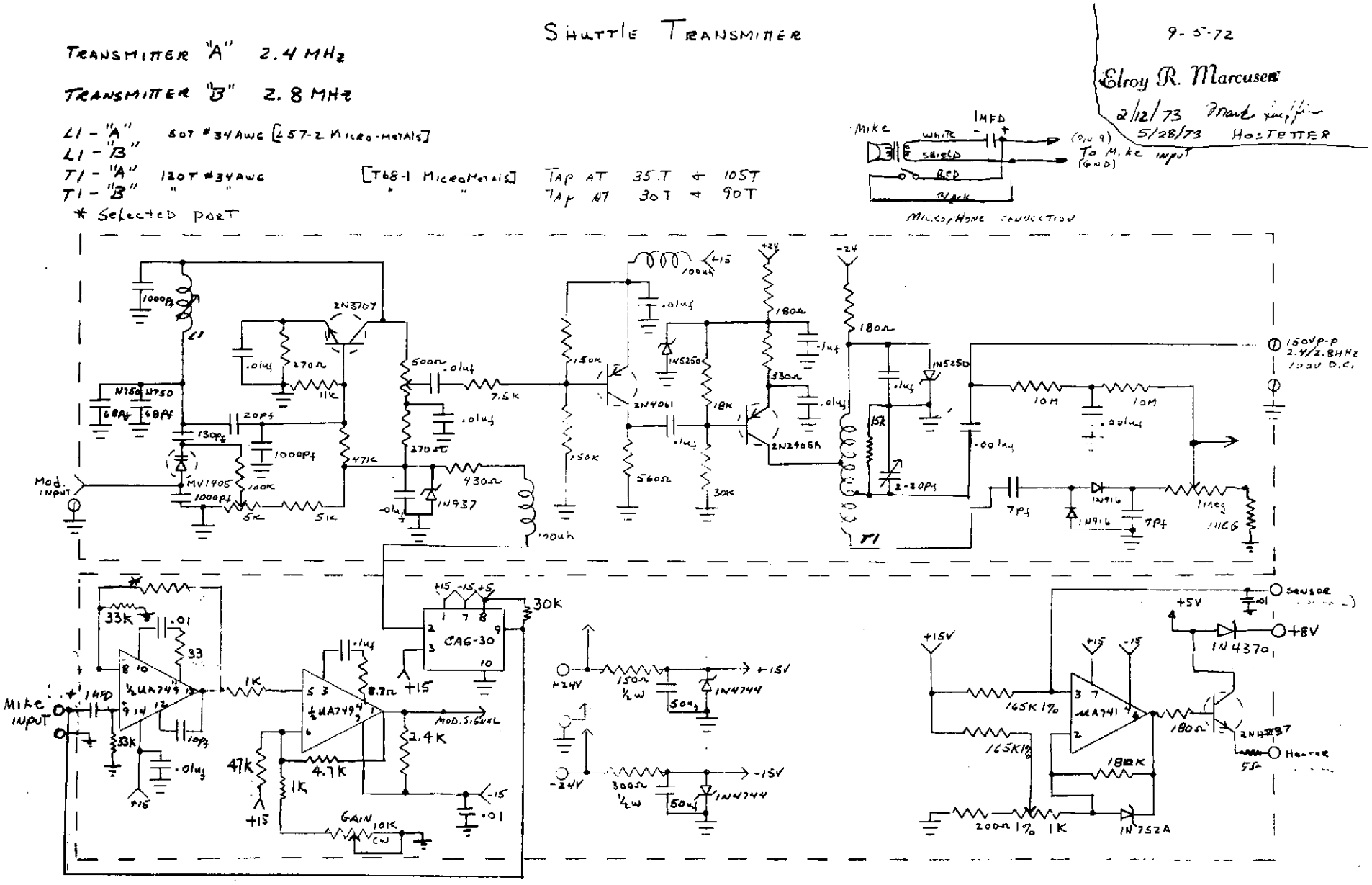

Figure D8. Shuttle Transmitter

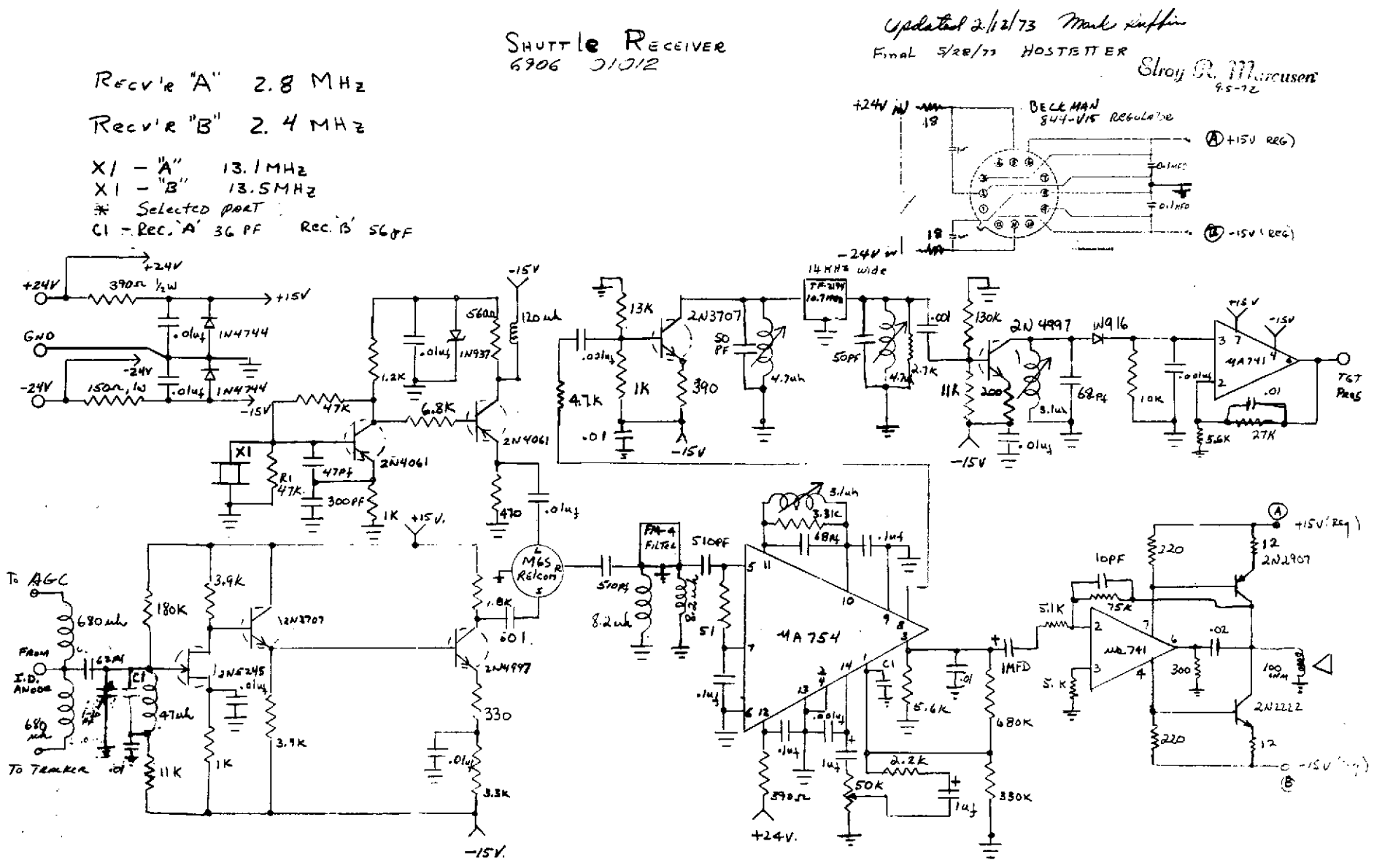

Figure D9. Shuttle Receiver

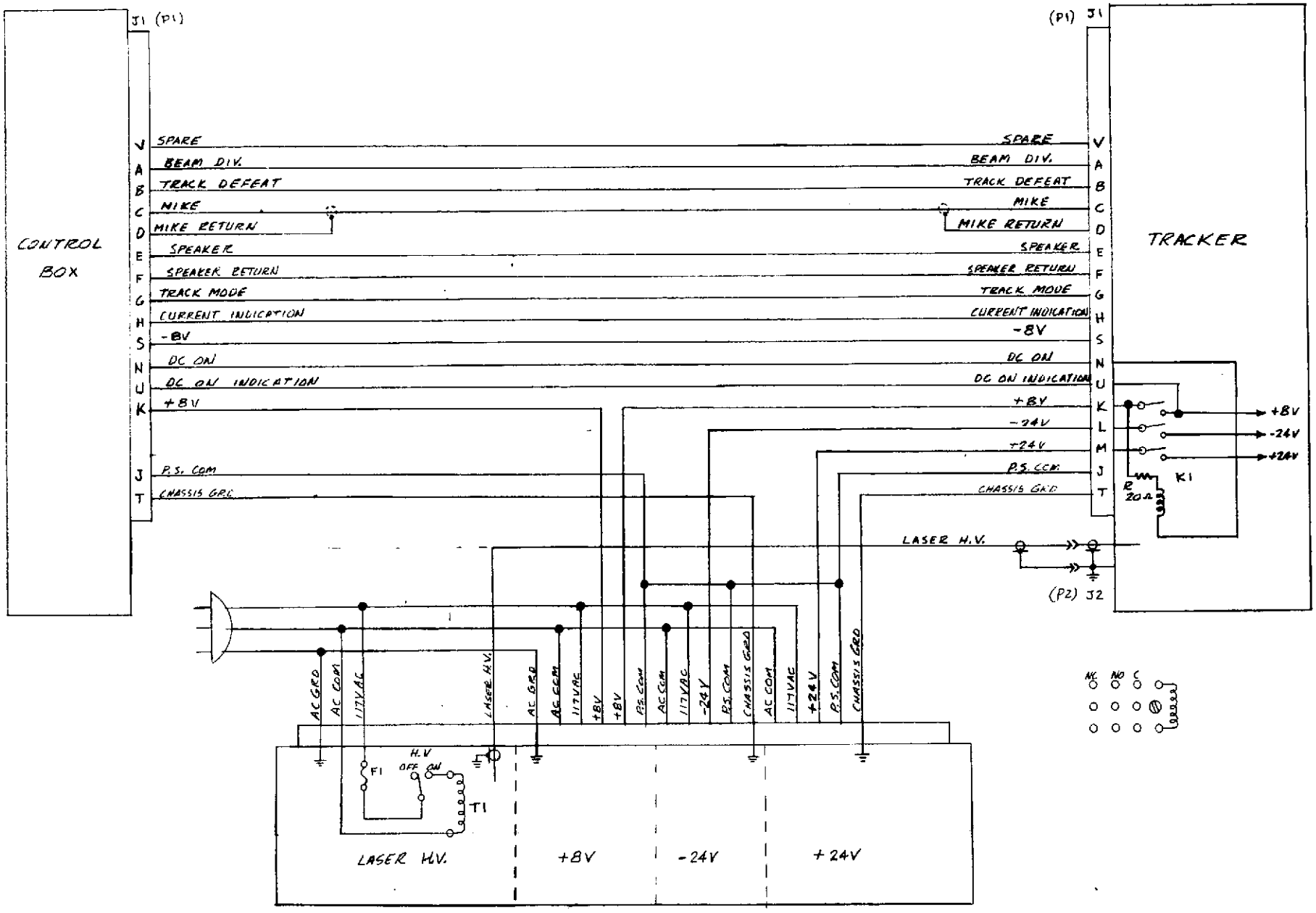

Figure D10. Wiring Harness

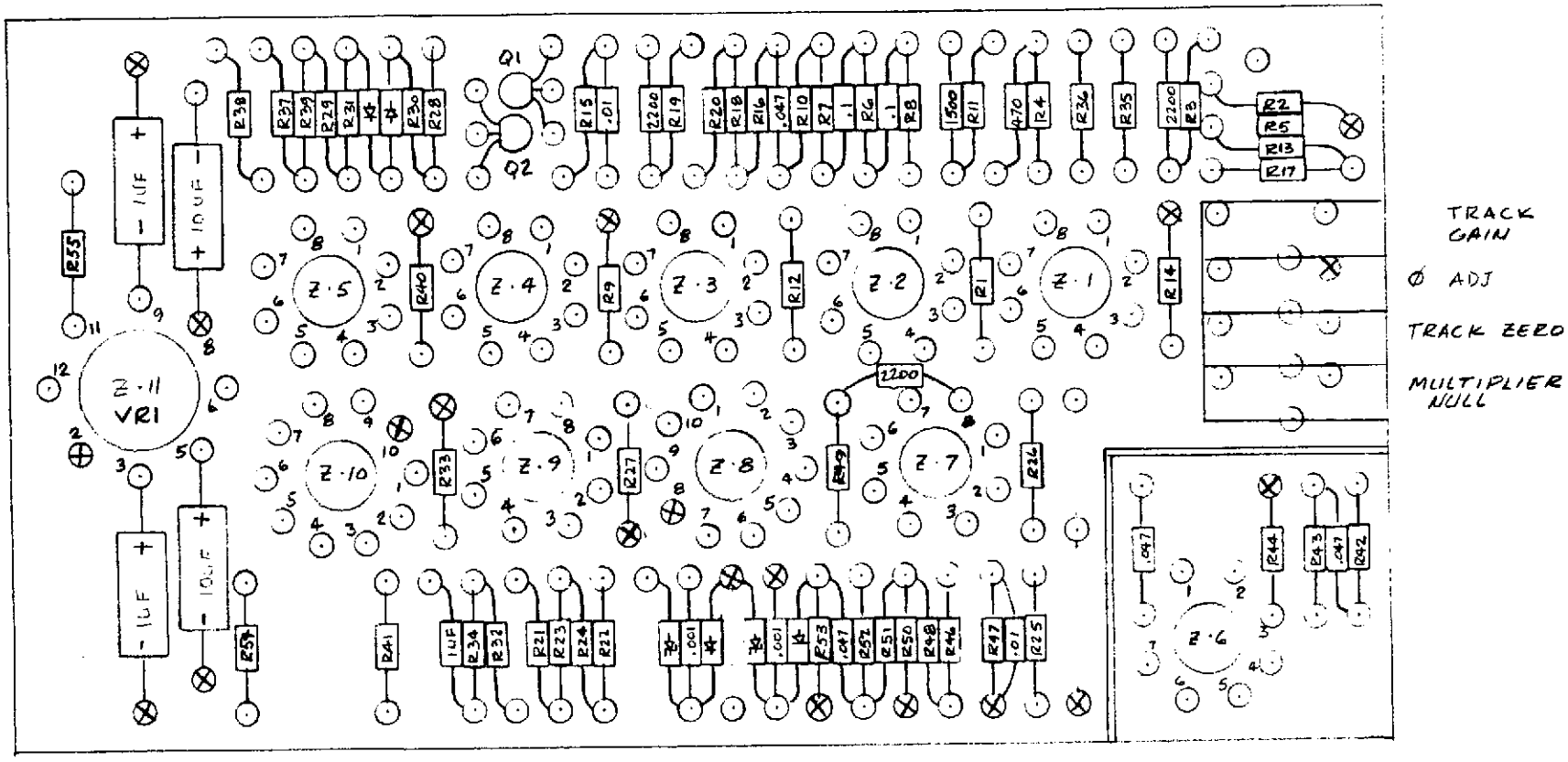

Figure D11. Y Vertical Tracker

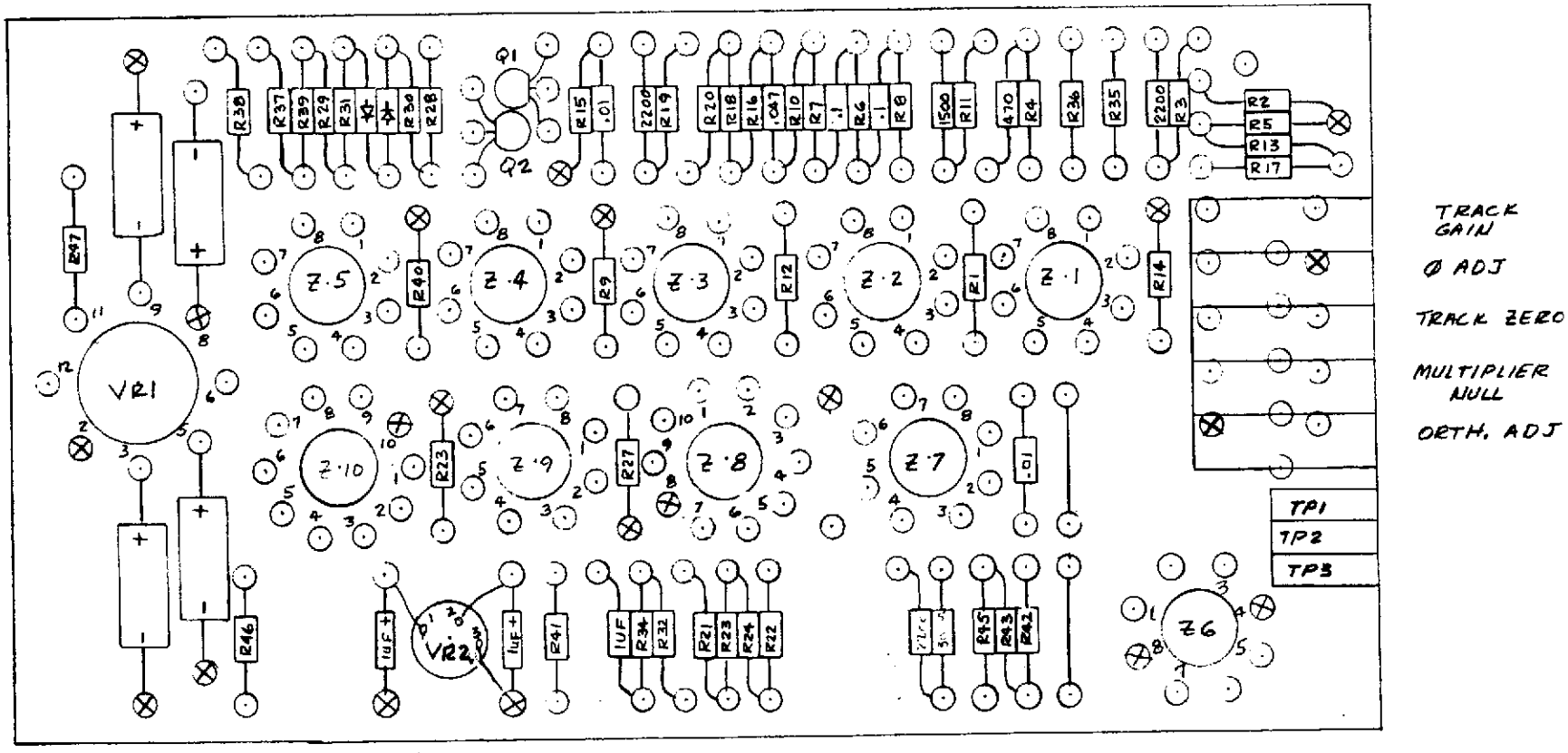

Figure D12. Tracker

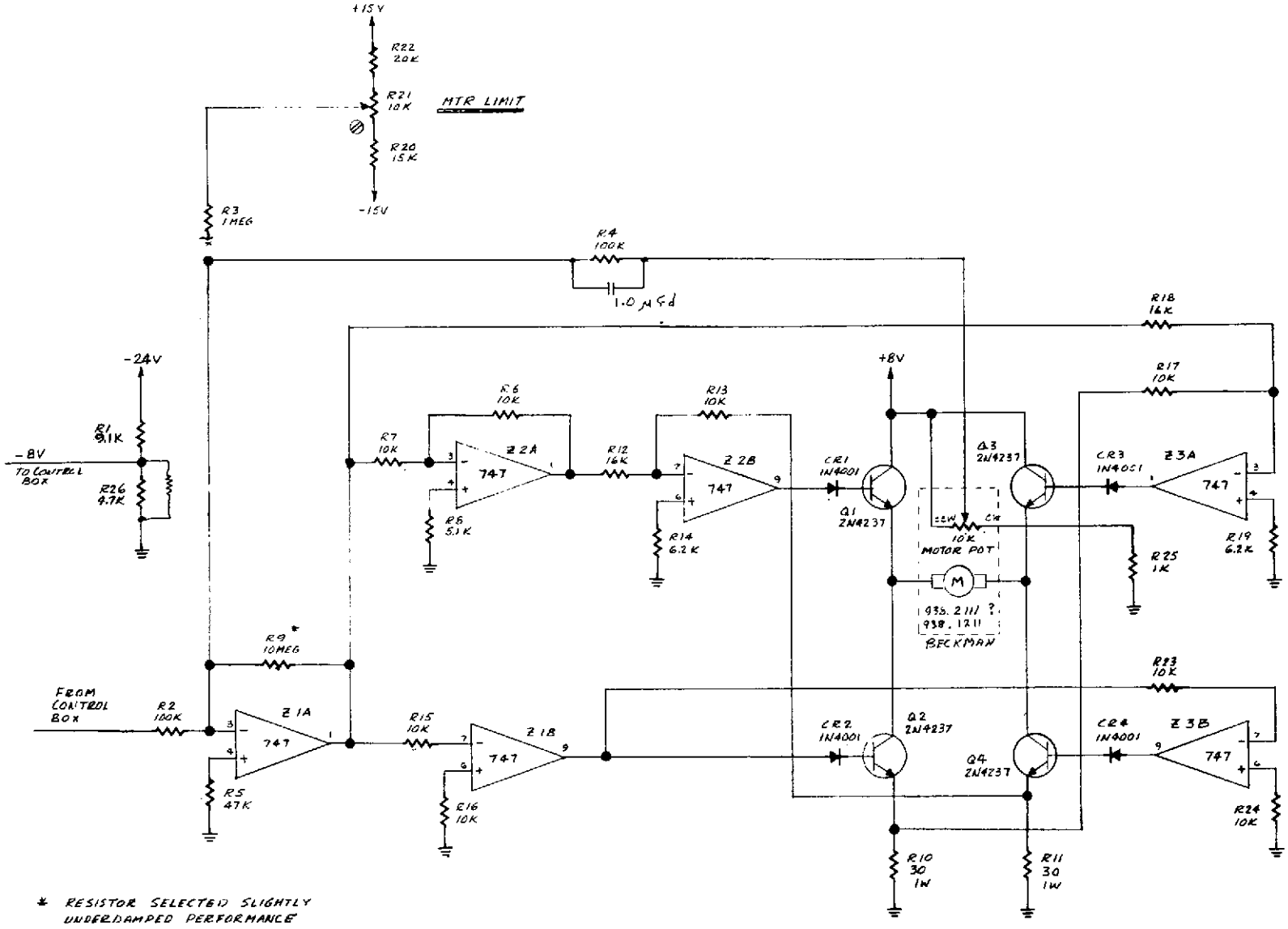

Figure D13. Beam Divergence

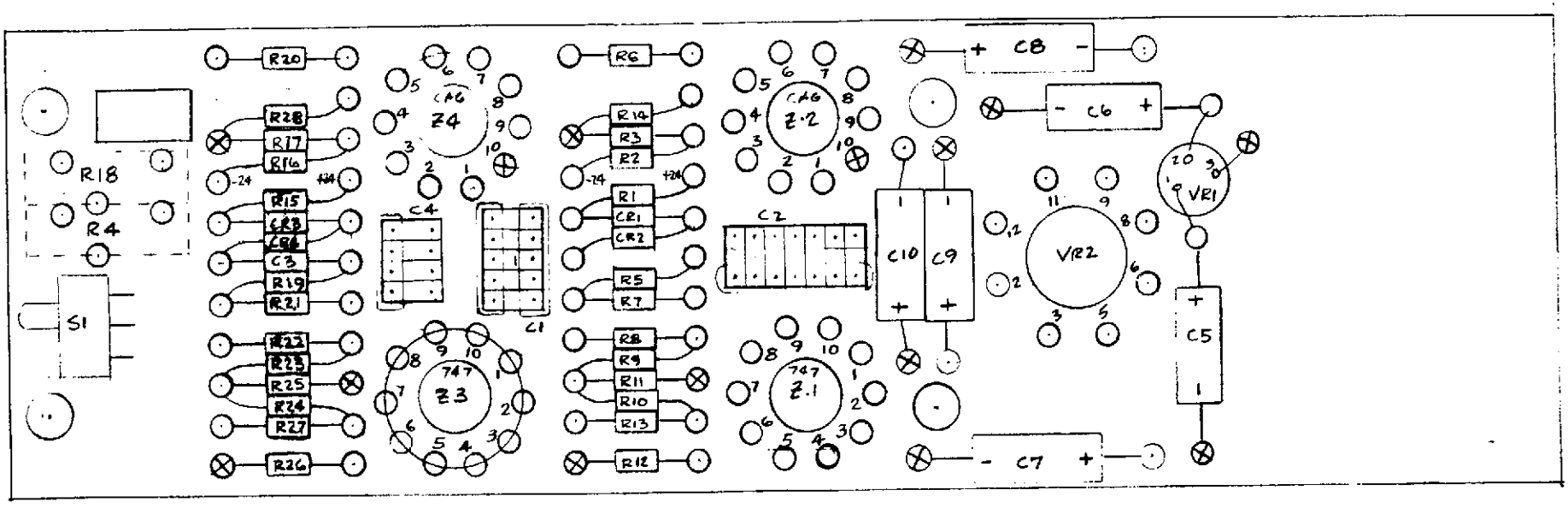

Figure D14. Receiver, Acquisition Scan Generator

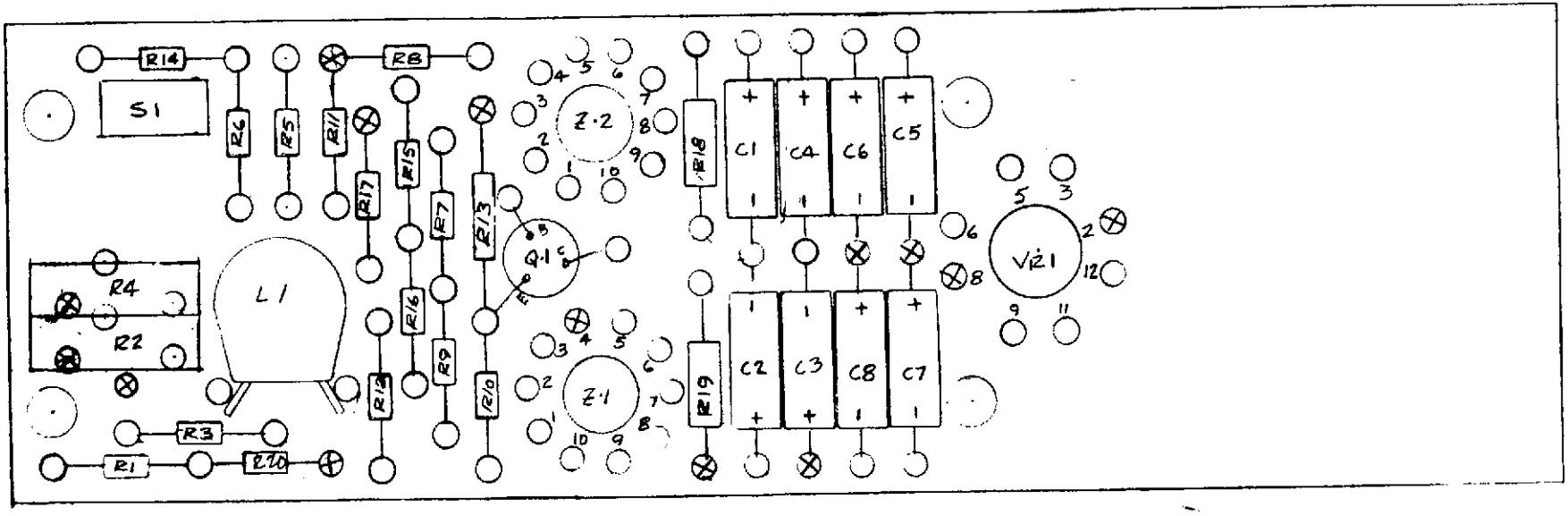

Figure D15. Dynode Gain Control

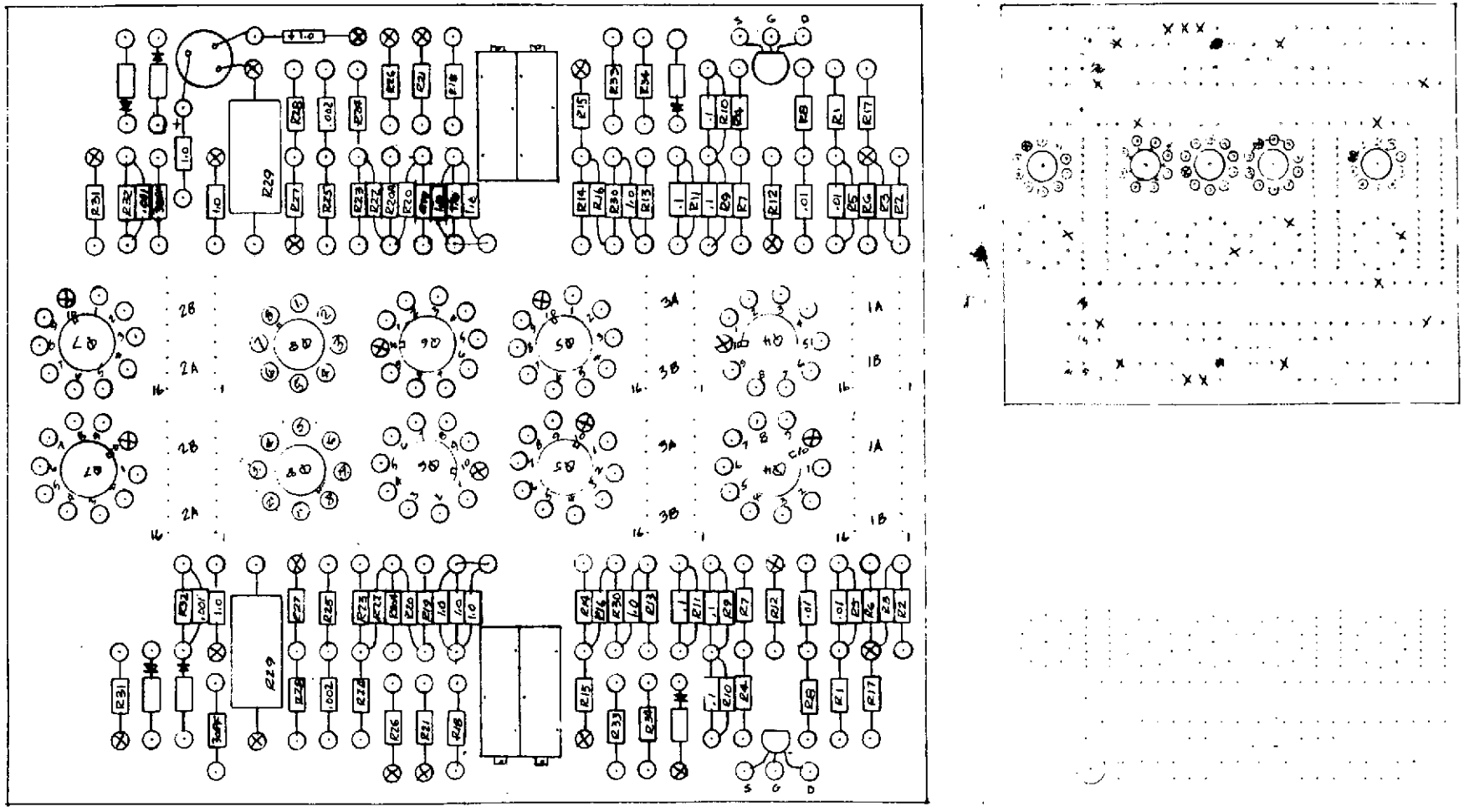

Figure D16. Beam Steerer